



UNIVERSITAT
POLITÈCNICA
DE VALÈNCIA



BRUFACE
BRUSSELS FACULTY
OF ENGINEERING



Influence of the turbulence model formulation on the simulation of flows around buildings

Arantxa Carcelén Sardina

Master thesis submitted under the supervision of
Prof. Alessandro Parente

The co-supervision of
Dr. Riccardo Longo & Ir. Alessandro Gambale

In order to be awarded the Master's Degree in
Electromechanical Engineering – Option Aeronautics

Academic year
2020-2021

Máster Universitario en Ingeniería Aeronáutica
Universitat Politècnica de València

*Exemplaire à apposer sur le mémoire ou travail de fin
d'études,
au verso de la première page de couverture.*

Fait en deux exemplaires, **Bruxelles, le 28/05/2021**

Signature



Réservé au secrétariat : Mémoire réussi*	OUI
NON	

**CONSULTATION DU MEMOIRE/TRAVAIL DE FIN
D'ETUDES**

Je soussigné

NOM :

CARCELÉN SARDINA

PRENOM :

ARANTXA

TITRE du travail :

**INFLUENCE OF THE TURBULENCE MODEL
FORMULATION ON THE SIMULATION OF
FLOWS AROUND BUILDINGS**

AUTORISE

la consultation du présent mémoire/travail de fin
d'études par les utilisateurs des bibliothèques de
l'Université libre de Bruxelles.

Si la consultation est autorisée, le soussigné concède
par la présente à l'Université libre de Bruxelles, pour
toute la durée légale de protection de l'œuvre, une
licence gratuite et non exclusive de reproduction et de
communication au public de son œuvre précisée ci-
dessus, sur supports graphiques ou électroniques, afin
d'en permettre la consultation par les utilisateurs des
bibliothèques de l'ULB et d'autres institutions dans les
limites du prêt inter-bibliothèques.

Abstract

“Influence of the turbulence model formulation on the simulation of flows around buildings”, by Arantxa Carcelén Sardina. Université Libre de Bruxelles, Master’s Degree in Electromechanical Engineering -specialised in aeronautics, 2020-2021. Erasmus programme from Universitat Politècnica de València, Máster en Ingeniería Aeronáutica.

The population tends to concentrate on big cities, leading to a problem of land for housing. High-rise buildings can host many people in little ground, but these structures present different challenges, an important factor for their design is the wind. The aerodynamic loads can cause strong vibrations on the upper side, and the air may flow to the lower part and cause disturbance to pedestrians. In this thesis different analysis of the flow field around buildings are conducted. A simple structure is studied to test different models used in Computational Fluid Dynamics (CFD) simulations since experimental data is available. The numerical solution is obtained with the steady Reynolds-Averaged Navier-Stokes (RANS) method and the unsteady approach (URANS), since this case is intrinsically steady both results are analogous. About the turbulence, the standard k-epsilon model is chosen in a version improved by the comprehensive approach which addresses two inconsistencies generated by the RANS approximations. For the good implementation of this model, the Building Influence Area (BIA) concept is integrated to apply the Non-Linear Eddy Viscosity (NLEV) model within it. The improvements of this model will be shown by comparing its results with traditional turbulence models as the k- ϵ and the SST k- ω . Once the comprehensive approach is validated, it is implemented in another simple geometry and later in a high-rise building in order to analyse the flow behaviour. The separation bubble at the top, the wake, the base vortex and the corner streams are visualized. The comprehensive approach provides accurate results, but the simulation time is also higher. Moreover, the steady simulations require a lower computational cost, however, an unsteady simulation is advisable for the skyscraper to study dynamic phenomenons that could induce harmful vibrations and fatigue.

Keywords: CFD, wind simulation, Reynolds-Averaged Navier-Stokes (RANS), turbulence, comprehensive approach, high-rise building.

Resumen

La población tiende a concentrarse en las grandes ciudades, lo que genera un problema de suelo para vivienda. Los rascacielos pueden hospedar muchas personas en poco terreno, pero estas estructuras presentan diferentes desafíos, un factor importante para su diseño es el viento. Las cargas aerodinámicas pueden provocar fuertes vibraciones en la parte superior, y el aire puede fluir hacia la parte inferior y causar molestias a los transeúntes.

En esta tesis se realizan diferentes análisis del flujo alrededor de edificios. Se estudia una estructura simple para probar diferentes modelos utilizados en simulaciones de Dinámica de Fluidos Computacional (CFD), ya que se dispone de datos experimentales. La solución numérica se obtiene con el método estacionario de las ecuaciones de Navier-Stokes promediadas por Reynolds (RANS) y el enfoque transitorio (URANS), ya que este caso es intrínsecamente estacionario, ambos resultados son análogos. Sobre la turbulencia, se elige el modelo k-epsilon estándar en una versión mejorada por el enfoque integral (comprehensive approach) que aborda dos inconsistencias generadas por las aproximaciones RANS. Para la buena implementación de este modelo, se integra el concepto de área de influencia del edificio (BIA) para aplicar dentro del mismo el modelo de viscosidad de vórtice no lineal (NLEV). Las mejoras de este modelo se mostrarán comparando sus resultados con modelos de turbulencia tradicionales como el k- ϵ y el SST k- ω . Una vez validado el enfoque integral, se implementa en otra geometría simple y luego en un edificio de gran altura para analizar el comportamiento del flujo. Se visualiza la burbuja de separación en la parte superior, la estela, el vórtice de la base y las corrientes de las esquinas.

El enfoque integral proporciona resultados precisos, pero el tiempo de simulación también es mayor. Además, las simulaciones estacionarias requieren un menor coste computacional, sin embargo, una simulación transitoria es aconsejable para el rascacielos con el fin de estudiar fenómenos dinámicos que podrían inducir vibraciones dañinas y fatiga.

Acknowledgement

This Master thesis would not have been possible to conduct without the support of several great people and enterprises. First of all, I am really grateful to my supervisor Prof. Alessandro Parente for the opportunity to work in such an interesting topic as building's aerodynamics. As this project was done in cooperation with the company BuildWind, I would also like to thank Mr. Alessandro Gambale and Mr. Gabriele Mosca personally for their technical expertise and knowledge sharing. I would like to give special thanks to Dr. Riccardo Longo for his involvement, support and availability. I deeply appreciate his kindness in these times of social distancing.

More in general, I would like to thank all the teachers who throughout my degree and my master studies have encouraged my interest in science, and have contributed to my personal and academic development.

I am also grateful to all the people involved in the universities exchange programmes for their commitment with Erasmus students in this tough year. This international experience has been very rewarding for many reasons, I have gained a new perspective on life, I have seen what I am capable of and I have overcome various obstacles developing new skills that I will make use of in the future. A part of Brussels will stay with me forever.

On the other hand, I would like to thank my family for their support since the beginning of my studies and for inspiring me to be the person I am today. To my friends with whom I shared many experiences, most of them of joy but also through hard times, in Valencia and in Belgium. Truly thankful to finalise my stage as a student with all the amazing people I have encountered along this journey.

Contents

List of Figures	iii
List of Tables	iv
Nomenclature and List of Symbols	v
1 Introduction	1
1.1 Motivation	1
1.2 Background	2
1.3 Objectives	2
1.4 Methodology	2
1.5 Structure of the thesis	3
2 CFD simulations	4
2.1 Introduction	4
2.2 Simulation of the ABL	4
2.2.1 RANS formulation	6
2.2.2 Turbulence models	6
2.2.3 Wall treatment	9
2.2.4 Inlet configuration	11
2.3 Comprehensive approach	11
2.3.1 Equations for the inlet conditions	12
2.3.2 Building Influence Area	15
2.3.3 Non Linear Eddy Viscosity Model	16
2.4 Steady vs Unsteady	17
2.5 Convergence schemes	18
3 Wind flow around an isolated building	19
4 Case studies	22
4.1 Validation of the comprehensive approach	22
4.1.1 Geometry	22
4.1.2 Mesh	23
4.1.3 Physical configuration	25
4.1.4 Numerical configuration and solver	26
4.1.5 Results	26
4.1.6 Conclusions	34

4.2	Comparison of turbulence models	34
4.2.1	Results	34
4.2.2	Conclusions	43
4.3	Geometry analysis	43
4.3.1	Geometry and Mesh	43
4.3.2	Results	44
4.3.3	Conclusions	50
4.4	Application to a high-rise building	50
4.4.1	Geometry and Mesh	50
4.4.2	Configuration	51
4.4.3	Results	52
4.4.4	Conclusions	58
5	Conclusion and perspectives	59
	References	61
	ANNEX I	65
	Validation of the comprehensive approach	65
	Comparison of turbulence models	70
	Geometry analysis	78
	Application to a high-rise building	84

List of Figures

2.1	Pure and Hybrid BIA for simple geometries.	16
3.1	Representation of wind flow pattern around a building.	21
4.1	Geometry of the Building 1:4:4.	23
4.2	Computational domain for the Building 1:4:4.	23
4.3	View of the mesh for the Building 1:4:4.	24
4.4	Horizontal view of the mesh for the Building 1:4:4 at $z=0.1m$	24
4.5	Vertical view of the mesh for the Building 1:4:4 at $y=0m$	24
4.6	BIA building 1:4:4 steady.	26
4.7	Velocity contour for the building 1:4:4 steady and unsteady.	27
4.8	Streamlines for the building 1:4:4 steady and unsteady.	28
4.9	Velocity in vertical lines. Building 1:4:4 experimental and CFD	30
4.10	TKE in vertical lines. Building 1:4:4 experimental and CFD	31
4.11	Velocity in horizontal lines. Building 1:4:4 experimental and CFD	32
4.12	TKE in horizontal lines. Building 1:4:4 experimental and CFD	33
4.13	Velocity in vertical lines. Building 1:4:4 effect of turbulence model	37
4.14	TKE in vertical lines. Building 1:4:4 effect of turbulence model	38
4.15	Velocity in horizontal lines. Building 1:4:4 effect of turbulence model	39
4.16	TKE in horizontal lines. Building 1:4:4 effect of turbulence model	40
4.17	Velocity contour for the building 1:4:4 with the comprehensive approach and SST k-omega.	41
4.18	TKE contour for the building 1:4:4 with the comprehensive approach and SST k-omega.	42
4.19	Streamlines for the building 1:4:4 with the comprehensive ap- proach and SST k-omega.	42
4.20	BIA buildings 1:4:4 and 1:2:4.	44
4.21	Velocity around the buildings 1:4:4 and 1:2:4.	45
4.22	TKE contour for the buildings 1:4:4 and 1:2:4.	45
4.23	Streamlines for the buildings 1:4:4 and 1:2:4.	46
4.24	Velocity in vertical lines. Buildings 1:4:4 and 1:2:4	48
4.25	TKE in vertical lines. Buildings 1:4:4 and 1:2:4	49
4.26	Geometry and view of the mesh of the high-rise building.	51
4.27	Building influence area for the high-rise building.	52

LIST OF FIGURES

4.28	Stagnation point of the high-rise building.	53
4.29	TKE around the high-rise building, horizontal view.	54
4.30	Close-up of velocity around the high-rise building.	54
4.31	Streamlines around the high-rise building.	55
4.32	Close-up of streamlines around the high-rise building.	56
4.33	Close-up of velocity on the front facade of the high-rise building.	57
4.34	Close-up of velocity on the lateral facade of the high-rise building.	57
5.1	Residuals of the steady case of the building 1:4:4 with the comprehensive approach.	65
5.2	Residuals of the unsteady case of the building 1:4:4 with the comprehensive approach.	65
5.3	BIA building 1:4:4 steady and unsteady.	66
5.4	Velocity contour for the building 1:4:4 steady and unsteady.	67
5.5	TKE contour for the building 1:4:4 steady and unsteady.	68
5.6	Comparison inlet and outlet of CFD Building 1:4:4	69
5.7	Residuals of the steady case of the building 1:4:4 with the SST k-omega model.	70
5.8	Residuals of the steady case of the building 1:4:4 with the k-epsilon model.	71
5.9	Residuals of the steady case of the building 1:4:4 with the k-omega model.	71
5.10	Vertical, velocity contour for the building 1:4:4 with the different turbulence models.	72
5.11	Horizontal, velocity contour for the building 1:4:4 with the different turbulence models.	73
5.12	Vertical, TKE contour for the building 1:4:4 with the different turbulence models.	74
5.13	Horizontal, TKE contour for the building 1:4:4 with the different turbulence models.	75
5.14	Vertical, streamlines for the building 1:4:4 with the different turbulence models.	76
5.15	Horizontal, streamlines for the building 1:4:4 with the different turbulence models.	77
5.16	View of the mesh for the Building 1:2:4.	78
5.17	BIA buildings 1:4:4 and 1:2:4.	79
5.18	Velocity contour for the buildings 1:4:4 and 1:2:4.	80
5.19	TKE contour for the buildings 1:4:4 and 1:2:4.	81

LIST OF FIGURES

5.20	Velocity in horizontal lines. Buildings 1:4:4 and 1:2:4	82
5.21	TKE in horizontal lines. Buildings 1:4:4 and 1:2:4	83
5.22	Residuals of the steady case of the high-rise building.	84
5.23	Building influence area for the high-rise building.	85
5.24	Pressure distribution on the faces of the building	86
5.25	Pressure around the high-rise building.	87
5.26	Turbulent kinetic energy around the high-rise building.	88
5.27	Velocity around the high-rise building.	89
5.28	Streamlines around the high-rise building.	90

List of Tables

3.1	Components of the wind-flow around an isolated building. . .	21
4.1	Setting configuration of the ABL model for the simple cases. .	25
4.2	Setting configuration of the ABL model for the high-rise building.	52

Nomenclature

ABL	Atmospheric Boundary Layer
BIA	Building Influence Area
CAD	Computer-Aided Design
CFD	Computational Fluid Dynamics
LEV	Linear Eddy Viscosity
NLEV	Non Linear Eddy Viscosity Model
NS	Navier-Stokes
OpenFoam	Open-source Field Operation And Manipulation
RANS	Reynolds-Averaged Navier-Stokes
SI	International System of Units
TKE	Turbulent Kinetic Energy
URANS	Unsteady Reynolds-Averaged Navier-Stokes

List of Symbols

α_i	Orientation of the gravity vector
ϵ	Turbulent dissipation
δ_{ij}	Kronecker delta
κ	Von Karman constant
ν	Kinematic viscosity
ν_t	Turbulent kinetic viscosity
$\mu_T,$	Eddy or turbulent viscosity
ρ	Density
ω	Specific turbulent dissipation
τ_{ij}	Viscous stress tensor
τ_{ij}^R	Reynolds stress tensor
τ_w	Wall shear stress tensor
Ω_{ij}	Vorticity tensor
E	Wall function constant
g	Gravitational acceleration
h	Height
I	Turbulence intensity
k	Turbulent Kinetic Energy
k_s^+	Dimensionless roughness height
p	Instantaneous pressure
P	Kinematic pressure (divided by the density)
S_{ij}	Strain-rate tensor
t	Time
u	Velocity
u_i, u_j	Components of fluid velocity
u^*	Friction velocity
u^+	Dimensionless wall velocity
x_i, x_j	Components of position
y^+	Dimensionless wall distance
z_0	Aerodynamic roughness length

1 Introduction

1.1 Motivation

The current trend regarding the distribution of people is the concentration in large cities to the detriment of the population of large rural areas. In this way, the position of cities as neurological centres of the economy is strengthened, which in turn motivates more people to live there. However, space is limited and therefore high-rise buildings have gradually increased in number since the last century.

These imposing buildings present specific architectural challenges. On the one hand, they suffer stronger winds which can cause oscillations. They can also be more affected by earthquakes and other meteorological phenomena because the foundations must support a great weight and the moments produced by the horizontal loads reach great values.

It is also necessary to consider how the structure affects the wind, when the flow hits the building it is diverted to the sides, up and down. In this way, a downdraught is created that increases the wind in the lower part, a phenomenon that could cause annoyance to pedestrians. This effect of acceleration is increased if the building has completely square corners, and also if there is a wind tunnel effect.

Another big problem is the wake that originates in the rear, since there is a recirculating flow zone, very turbulent and with low pressures that also affects the structure and the surroundings. All this loads are not to be considered static but also dynamic since the wind is highly variable in large scales of time, but also in short scales (minutes).

Different solutions have been implemented, such as corner softening, tapering and twisted designs, alternating building's profile with height, porosity, damping and twist, etc. Therefore, an aerodynamic analysis of the flow around these buildings is essential.

1.2 Background

This Master Thesis follows the study of P. Van Muylders [1], who conducted simulations of buildings applying the comprehensive approach. She analysed with steady simulations the effect of the twist in a high-rise building.

The comprehensive approach developed by A. Parente, R. Longo and M. Ferrarotti [2] has been proven to show advantages in this type of studies. It is also important to highlight the PhD Thesis of R. Longo [3] to have a better understanding of this analysis.

In fact, in his PhD Thesis he conducted simulations of the same simple case treated in this thesis with the standard k-epsilon turbulence model and the comprehensive approach. However, he only showed the results for vertical profiles. It would be also interesting to analyse another standard turbulence model as it is the SST k- ω .

1.3 Objectives

In this project the flow field around buildings will be studied. Schematically the following objectives can be mentioned:

- Analysis of the flow field in the Atmospheric Boundary Layer and its influence on buildings.
- Study of the improvements of the comprehensive approach comparing with standard turbulence models.
- Analysis of the cost-effectiveness of unsteady simulations for buildings.

1.4 Methodology

To meet the proposed objectives, a CFD software is used, specifically the open code OpenFoam in its version 2.3.0. A simple case will be used to check the results when using the comprehensive approach since experimental data is available. Later, this model is applied to a high-rise building. All the geometries come from different studies prior conducted by the Aero-thermo-mechanics department (ATM) of the Université Libre de Bruxelles. It may be remarked that due to the characteristics of the simulations all the CADs are 3D.

1.5 Structure of the thesis

The structure of this document is described below.

In Chapter 1 an introduction is made, explaining the interest in the study that is carried out, as well as the works that precede it. In addition, the methodology followed in the study is mentioned and different objectives are established to orient the procedure and the results.

In Chapter 2 the different models and equations that are applied in this thesis are exposed. The Atmospheric Boundary Layer and the Comprehensive approach are explained. Moreover, the differences between steady and unsteady simulations in this type of cases are addressed.

In Chapter 3 the main characteristics of the flow around an isolated building are enumerated. This will allow to gain more knowledge and help understand the results that will be later obtained.

In Chapter 4 the different cases analysed are exposed. Their geometry, mesh, physical and numerical configuration and the solver used. In addition, the results obtained are presented and explained.

In Chapter 5 the most interesting conclusions of the study are collected, and possible future works that start and continue from the present are established.

2 CFD simulations

2.1 Introduction

The analysis of the flow around buildings, especially in skyscrapers, is of vital importance since its design greatly affects the loads on it, but it also modifies the flow around it and even pedestrians can be affected.

To determine the air flow, measurements can be made in situ after the building construction. This is expensive and difficult to obtain as many points at different altitudes around the building need to be measured, and then an extrapolation of those results is necessary. This is also not very useful in the design phase, which is why scale models in a wind tunnel are used. This has the disadvantage of not reproducing the exact conditions.

In this situation, Computational Fluid Dynamics (CFD) has been proven to be a useful tool to simulate any flow conditions and obtain a continuous map of it (not point-to-point). On the other hand, this method includes various sources of uncertainty, especially related to turbulence modelling.

The engineer is required to have a certain level of experience in this tool. The geometry does not include small features that would increase the computational cost without improving the results, and the size of the computational domain needs to be large enough to not disturb the solution without increasing too much the time of resolution. The mesh needs to reach a compromise between the accuracy of the results and the computational cost. The user needs to understand the models used, as for turbulence, and their limitations. Furthermore, the initial and the boundary conditions must be properly selected. Finally, the results need to be analysed since in some cases the software provides an unreal solution.

2.2 Simulation of the ABL

In order to define all the previous features it is necessary to understand the type of flow that will be analysed so the right options can be implemented. First, the characteristics of the Atmospheric Boundary Layer need to be defined.

The flow around buildings is usually treated as an incompressible gas since low Mach numbers predominate in the domain. Moreover, due to the interference of the building the flow acquires great turbulence. On the other hand, the flow has a three-dimensional nature and air is a Newtonian fluid.

The Navier–Stokes equations describe the motion of the type of flows previously exposed. These equations do not have an analytical solution, so different numerical models have been developed. The main problem is the calculation of the turbulence, the only model that numerically solves it is the DNS (Direct Numerical Simulation), but its computational cost is very high so it does not correspond to the character of the present study.

The LES (Large Eddy Simulation), solves only the large turbulent scales and models the small ones. The DES (Detached Eddy Simulation) model could be considered a hybrid between RANS and LES which saves computation time, but increases the accuracy relative to RANS.

For stationary simulations, the RANS (Reynolds-Averaged Navier-Stokes) model can be used. This models all scales of turbulence, in this way, the variables are divided into an average value plus a fluctuation, and an average of the fluctuations is calculated. This model reduces the computational cost to a great extent.

However, these equations are not closed, that is, they cannot be solved because new terms have appeared, the Reynolds stresses. Additional equations are needed to model turbulence and close the transport equations, which will be explained later.

The number of cells in typical domains of ABL simulations greatly increases the computational cost. In addition, the nature of this thesis justifies seeking a balance between cost and precision, which is why the RANS approach is chosen. For the unsteady simulations, the equations are adapted in the URANS model.

2.2.1 RANS formulation

The flow of a 3D, viscous, incompressible, Newtonian fluid with constant properties is governed by the Navier–Stokes equations:

$$\frac{\partial \rho}{\partial t} + \frac{\partial \rho u_j}{\partial x_j} = 0 \quad (1)$$

$$\frac{\partial \rho u_i}{\partial t} + \frac{\partial \rho u_i u_j}{\partial x_j} = \rho g \alpha_i + \frac{\partial \tau_{ji}}{\partial x_j} - \frac{\partial p}{\partial x_i} \quad (2)$$

While the Reynolds decomposition is defined as a mean value and a fluctuating part [5]:

$$u_i = \bar{u}_i + u'_i; \quad P = \bar{P} + P' \quad (3)$$

Therefore, the Reynolds-Averaged Navier-Stokes are defined as:

$$\frac{\partial \bar{u}_i}{\partial t} + \frac{\partial \overline{u_i u_j}}{\partial x_j} = -\frac{\partial \bar{P}}{\partial x_i} + \frac{\partial (\nu \frac{\partial \bar{u}_i}{\partial x_j} - \overline{u'_i u'_j})}{\partial x_j} \quad (4)$$

$$\frac{\partial \bar{u}_j}{\partial x_j} = 0 \quad (5)$$

Where the Reynolds stress tensor $\tau_{ij}^R = \overline{\rho u'_i u'_j}$ appears comparing with the Navier-Stokes equations. This term incorporates the effects of turbulent motions on the mean stresses and adds additional unknown variables.

Because of this term, the system of Equations 4 and 5 is not closed. The problem of the closure of the Reynolds-averaged Navier–Stokes equations is solved by expressing the Reynolds-stress tensor as a function of the mean field or other variables. The modelling of such behaviour in a simple way, instead of solving it directly, will reduce the precision of the calculations and their universality, but will greatly reduce the cost.

2.2.2 Turbulence models

The methods for calculating the Reynolds stress tensor fall into two main categories: the turbulent viscosity hypothesis and the Reynolds stress equation model.

The simplest approach, a first-order closure, is the Boussinesq eddy-viscosity hypothesis which corresponds to an alignment between the Reynolds stress and mean strain tensors (Linear Eddy Viscosity model) [6].

$$\frac{\partial \overline{u'_i u'_j}}{\partial x_j} = \frac{2}{3} \cdot k \cdot \delta_{ij} - \nu_T \cdot \left(\frac{\partial \overline{u_j}}{\partial x_i} + \frac{\partial \overline{u_i}}{\partial x_j} - \frac{2}{3} \cdot \frac{\partial u_k}{\partial x_k} \cdot \delta_{ij} \right) \quad (6)$$

Where ν_T is the eddy viscosity, δ_{ij} is the Kronecker delta, and k is the turbulent kinetic energy:

$$k = \frac{1}{2} \overline{u'_k u'_k} \quad (7)$$

The eddy viscosity still needs to be determined whether being solved algebraically or being modelled, and for this there are several models.

The Spalart-Allmaras model transports the eddy viscosity with a single transport equation, with lower computational cost than the two-equation models, but it does not give information about the turbulence. Regarding the two-equations models, the most common options are the k - ϵ and k - ω .

k - ϵ model

For solving ABL cases, the k - ϵ model is widely used [8]. This method assumes that the turbulent viscosity is isotropic, and that the mixing length is $l_m = k^{3/2}/\epsilon$. It uses two extra transport equations: one for the turbulent kinetic energy, k , and another for the turbulence dissipation, ϵ , with several empirically selected adjustment constants and valid for many types of flows. The equation for k is obtained by a rigorous development of the equations, while for ϵ an empirical approximation is done [7].

The general model equations are expressed as:

$$\frac{\partial}{\partial t}(\rho k) + \frac{\partial}{\partial x_j}(\rho k u_j) = \frac{\partial}{\partial x_j} \left[\left(\mu + \frac{\mu_t}{\sigma_k} \right) \frac{\partial k}{\partial x_j} \right] + G_k - \rho \epsilon \quad (8)$$

$$\frac{\partial}{\partial t}(\rho \epsilon) + \frac{\partial}{\partial x_j}(\rho \epsilon u_j) = \frac{\partial}{\partial x_j} \left[\left(\mu + \frac{\mu_t}{\sigma_\epsilon} \right) \frac{\partial \epsilon}{\partial x_j} \right] + C_{\epsilon 1} \frac{\epsilon}{k} G_k - C_{\epsilon 2} \rho \frac{\epsilon^2}{k} \quad (9)$$

Where $C_{\epsilon 1}$ and $C_{\epsilon 2}$ are model constants, σ_k is the Prandtl number of turbulent kinetic energy and σ_ϵ is the Prandtl number of turbulence dissipation.

G_k is the generation of turbulent kinetic energy due to the mean velocity gradients.

The equations that describe a two-dimensional ABL with the standard k - ϵ model, considering: zero vertical velocity, constant pressure along vertical and stream-wise directions, and constant shear stress, are the following [9]:

$$\frac{\partial}{\partial z} \left(\frac{\mu_t}{\sigma_k} \frac{\partial k}{\partial z} \right) + G_k - p\epsilon = 0 \quad (10)$$

$$\frac{\partial}{\partial z} \left(\frac{\mu_t}{\sigma_\epsilon} \frac{\partial \epsilon}{\partial z} \right) + C_{\epsilon 1} C_k \frac{\epsilon}{k} - C_{\epsilon 2} \rho \frac{\epsilon^2}{k} = 0 \quad (11)$$

Where the dynamic viscosity is neglected with respect to the turbulent viscosity, while σ_k , σ_ϵ , $C_{\epsilon 1}$ and $C_{\epsilon 2}$ are constants of this turbulence model. And the production of turbulent kinetic energy and the turbulent viscosity are respectively given by:

$$G_k = \mu_t \left(\frac{\partial u}{\partial z} \right)^2; \quad \mu_t = \rho C_\mu \frac{k^2}{\epsilon} \quad (12)$$

The k - ϵ model does not represent well problems with boundary layers with significant adverse pressure gradients, secondary flow, highly rotational, etc. However, it is easy to implement, it does not require a huge computational cost and it is robust for regions away from the wall.

SST k - ω model

The model k - ω uses the specific turbulence dissipation rate ($\omega = \epsilon/k$) as the second transport equation. This model works better than k - ϵ for the regions close to the walls, but fails in the free-flow zones. This model is for instance used in turbomachinery simulations.

The governing equations are the following, where B^* , σ^* , σ , σ_d , α and β , are closure coefficients:

$$\frac{\partial}{\partial t}(\rho k) + \frac{\partial}{\partial x_j}(\rho u_j k) = \rho \tau_{ij} \frac{\partial u_i}{\partial x_j} - \beta^* \rho k \omega + \frac{\partial}{\partial x_j} \left[\left(\mu + \sigma^* \frac{\rho k}{\omega} \right) \frac{\partial k}{\partial x_j} \right] \quad (13)$$

$$\frac{\partial}{\partial t}(\rho\omega) + \frac{\partial}{\partial x_j}(\rho u_j \omega) = \alpha \frac{\Omega}{k} \rho \tau_{ij} \frac{\partial u_i}{\partial x_j} - \beta \rho \omega^2 + \sigma_d \frac{\rho}{\omega} \frac{\partial k}{\partial x_j} \frac{\partial \omega}{\partial x_j} + \frac{\partial}{\partial x_j} \left[\left(\mu + \sigma \frac{\rho k}{\omega} \right) \frac{\partial \omega}{\partial x_j} \right] \quad (14)$$

The Shear Stress Transport (SST) k - ω is a hybrid model which combines the k - ω and the k - ϵ models. A blending function activates the k - ω model near the wall and the k - ϵ model in the free stream. The SST models presents less sensitivity to free stream conditions (flow outside the boundary layer) than many other turbulence models. And the shear stress limiter helps the k - ω model avoid a build-up of excessive turbulent kinetic energy near stagnation points [10].

Others models

The previous models are of first-order, however, second-order models can also be used. This is the case of the Reynolds stress equation model, RSM, which solves the components of τ_{ij} and the dissipation ϵ . This method adds new equations, but it allows a better computation of flows with a high rotation or with quick variations in the mean flow.

On the other hand, Non-Linear Eddy Viscosity (NLEV) models have also been developed. This will be explained in a following section.

2.2.3 Wall treatment

Many of the turbulence models present problems very close to the walls. To solve this, wall functions are used that assume a certain behaviour of the boundary layer in cells in contact with the wall.

The boundary layer is the region closest to the wall in which the flow is conditioned to a high gradient since in the wall the no slip conditions determines that the velocity of the flow on it must be zero.

For CFD to solve this correctly, extremely fine cells would be required with the following increase of computational cost. A solution is the use of non-linear functions in these zones. The stability and convergence of the computation is also enhanced since cells with a huge aspect ratio are avoided.

When the flow encounters a wall, it presents a laminar behaviour that will transform into a turbulent one. In this last zone, three regions can be distinguished by their value of y^+ . If y^+ is lower than 5 then the viscous stresses predominate in the called viscous sub-layer, so the Reynolds shear stress is negligible. If the value is between 30 and 300 the effect of viscosity is negligible in the named log-law region. Between those two region there is the buffer layer which is recommended to avoid in CFD studies.

It is necessary to remind the expression of y^+ . Where u^* is the friction velocity, y is the distance to the nearest wall and τ_w is the wall shear stress.

$$y^+ = \frac{u^* y}{\nu}; \quad u^* = \sqrt{\frac{\tau_w}{\rho}} \quad (15)$$

The expression for the viscous sub-layer (or laminar law) is $u^+ = y^+$ and for the logarithmic law region:

$$u^+ = \frac{U}{u^*} = \frac{1}{\kappa} \ln(y^+) + B \quad (16)$$

Where κ is the Von Karman constant and B is an integration constant

To be able to calculate with wall functions, a certain value of y^+ is needed, which is obtained after running the simulation. Normally an estimation is made before meshing and after the calculation the mesh can be corrected if necessary.

Rough wall

On ABL flows the surface is usually not smooth, therefore an additional function is used to consider the effect of the roughness. The logarithmic law for a rough wall can be expressed as [11]:

$$\frac{U_p}{u^*} = \frac{1}{\kappa} \ln(Ey^+) - \Delta B(k_s^+) \quad (17)$$

$$\frac{U_p}{u^*} = \frac{1}{\kappa} \ln\left(\frac{Ey^+}{C_s k_s^+}\right) \quad (18)$$

Equation 17 corresponds to the standard smooth law and is used when $k_s^+ \leq 90$. While Equation 18 is used when $k_s^+ \geq 90$, being k_s^+ the dimensionless roughness height.

U_p is the mean tangential velocity at $y = z_p$, what is the same, at the first cell centroid. E and C_s are constants, and $\Delta B(k_s^+)$ is a function that depends on the dimensionless roughness height.

2.2.4 Inlet configuration

The inlet is one the boundaries conditions to be set, in ABL flows it is really important to try to achieve the maximum grade of realism. The following expressions are usually used in these simulations:

$$u = \frac{u^*}{\kappa} \ln \left(\frac{z + z_0}{z_0} \right) \quad (19)$$

$$\kappa = \frac{u_*^2}{\sqrt{C_\mu}} \quad (20)$$

$$\epsilon = \frac{u_*^3}{\kappa(z + z_0)} \quad (21)$$

Where z_0 is the aerodynamic roughness length, which is the height at which the velocity of the wind is zero. This model was proposed by P. Richards and R. Hoxey [12].

2.3 Comprehensive approach

As mentioned before, many ABL simulations are carried out with the RANS equations and the k- ϵ model. Nevertheless, the ABL inlet profile defined by Richards and Hoxey [12] presented some inconsistencies. For example, it assumes that the TKE is constant although in reality it decreases with height.

Several authors worked to improve this methodology, for example, Parente et al. developed the comprehensive approach for numerical simulations of the neutral ABL [13]. This method consists in a new inlet condition for turbulent kinetic energy, the turbulence model constant C_μ was generalized as a location-dependent parameter, and a source term in the equation of the turbulent dissipation rate was included. Furthermore, the implementation of an algorithm allows the automatically switch of the turbulence model formulation in the region directly affected by a building (Building Influence Area, BIA).

In addition, a modified version of the Richards and Hoxey rough-wall boundary condition was implemented. On the other hand, inside the BIA Longo et al. implemented Non-Linear Eddy-Viscosity models (NLEV) [14], which has also been continuously improved by other authors as Nicastro who proposed an improvement of the hybrid BIA [21].

On the other hand, the traditional approach presented another inconsistency too. Near a wall the velocity profile obtained by the ABL inlet profile (Equation 19) and the one obtained by the rough wall function (Equation 18) are not consistent.

This was also addressed by A. Parente [22] [23], who developed a new implementation to handle both smooth-wall and rough-wall treatments in the same simulation, and an algorithm automatically selects the suitable formulation.

2.3.1 Equations for the inlet conditions

As it was said before, the fully developed inlet profiles of mean longitudinal velocity, turbulent kinetic energy and dissipation rate under neutral stratification conditions specified by Richards and Hoxey [12] assume a constant value for the inlet turbulent kinetic energy, k .

Yang et al. [26] developed an alternative inlet condition for k obtained as a solution of the turbulent kinetic energy transport equation, under the assumption of constant value for C_μ and local equilibrium between production and dissipation of k . Gorlé et al. [27] generalized the expression of C_μ as a function of z .

Following that methodology and integrating the expression, the general solution for turbulent kinetic energy profile is achieved (Equation 23). The inlet conditions and turbulence model formulation of the comprehensive approach are the following [2]:

$$U = \frac{u^*}{\kappa} \ln \left(\frac{z + z_0}{z_0} \right) \quad (22)$$

$$k(z) = C_1 \ln(z + z_0) + C_2 \quad (23)$$

$$\epsilon = \frac{u_*^3}{\kappa(z + z_0)} \quad (24)$$

Regarding the turbulence model, the formulation is the next:

$$\mu_t = \rho C_\mu \frac{k^2}{\epsilon} \quad (25)$$

$$S_\epsilon(z) = \frac{\rho u_*^4}{(z + z_0)^2} \left(\frac{(C_{\epsilon 2} - C_{\epsilon 1}) \sqrt{C_\mu}}{\kappa^2} - \frac{1}{\sigma_\epsilon} \right) \quad (26)$$

$$C_\mu = \frac{u_*^4}{k^2} \quad (27)$$

In the case of an increasing-decreasing behaviour of the turbulent kinetic energy with height, a four parameter profile has been formulated:

$$k(z) = C_1 \ln \left(\frac{z + z_0}{z_0} \right) + C_2 \ln \left(\frac{z + z_0}{z_0} \right)^2 + C_3 \left(\frac{z + z_0}{z_0} \right) + C_4 \quad (28)$$

This formulation implies the addition of the following source term to the k transport equation:

$$S_k = -\frac{\partial}{\partial z} \left(\nu_t \frac{k}{z} \right) = -\frac{u_* \kappa}{z_0} \left(4B \frac{z + z_0}{z_0} + C \right) \quad (29)$$

The previously profiles require experimental data to determine the parameters C_1 , C_2 , A , B , C and D . However, this data may not be available, therefore a semi-empirical parametrization can be applied for the turbulent quantities, provided these expressions for the mean squared fluctuation velocity components [2]:

$$\frac{\langle u'^2 \rangle}{u_*^2} = 5 - 4 \frac{z}{h} \quad (30)$$

$$\frac{\langle v'^2 \rangle}{u_*^2} = 2 - \frac{z}{h} \quad (31)$$

$$\frac{\langle w'^2 \rangle}{u_*^2} = 1.7 - \frac{z}{h} \quad (32)$$

Where h is the ABL height, and hence the variation of turbulent kinetic energy with height can be expressed as:

$$k(z) = \frac{1}{2} (\langle u'^2 \rangle + \langle v'^2 \rangle + \langle w'^2 \rangle) = \frac{u_*^2}{2} \left(8.7 - 6 \frac{z}{h} \right) \quad (33)$$

Wall treatment

As many authors have appointed due to the significant dimensions of the domain and the high Reynolds number associated with ABL flows, the use of wall functions is generally required for near-wall modelling [2].

Parente et al. [2] proposed an implementation of the rough wall function which preserves the form of the universal law of the wall, with the introduction of a new wall function constant and a non-dimensional wall distance:

$$\frac{U_p}{u_*} = \frac{1}{\kappa} \ln(\tilde{E} \tilde{y}^+) \quad (34)$$

Where the non-dimensional distance, \tilde{y}^+ , is simply a y^+ shifted by the aerodynamic roughness, and the new wall function constant, \tilde{E} , depends on the roughness characteristics of the surface. The friction velocity is computed as $u_* = C_\mu^{0.25} k^{0.5}$.

This approach can be extended to mixed rough and smooth surfaces through a redefinition of the law of the wall constants. The implementation of screening algorithm allows the automatic switch between the smooth wall equations (Equation 35) and the rough wall ones (Equation 36), depending on the boundary surface properties. Moreover, this approach permits associating different aerodynamic roughness values to different surfaces within the same simulation [9].

$$\tilde{y}^+ = y^+; \quad \tilde{E} = E \quad (35)$$

$$\tilde{y}^+ = \frac{u^*(z + z_0)}{\nu}; \quad \tilde{E} = \frac{\nu}{z_0 u^*} \quad (36)$$

2.3.2 Building Influence Area

The comprehensive approach is only valid in those regions with an homogeneous ABL. With the employment of an algorithm which automatically detects obstacles (as buildings or hills) the equations can be used in the case of disturbed flow field. This way the comprehensive approach is gradually blended into a turbulence model appropriate for the region around the obstacle.

A. Parente defined the Building Influence Area according to the local turbulence properties deviation [24] to achieve a gradual transition of the formulation outside and inside the BIA, and also for the BIA to have an adaptive shape so it changes according to the obstacle.

Two different blending formulations were developed. On the one hand, the Pure blending consists of analysing the deviations of turbulent ABL parameters individually. Parente et al. took into account the relative velocity difference between the disturbed flow regions and the homogenous ABL [24]. Later, Longo et al. introduced a blending formulation related to the turbulent kinetic energy relative difference [14].

On the other hand, the Hybrid blending combines the formulas of the pure blending approach. Both u and k are considered and the new deviation term, δ_h , is computed by selecting the maximum value of both deviations (Equation 37). Figure 2.1 shows the formulation and the visualization of both approaches.

$$\delta_h = \max[\delta_u, \delta : k, \delta_\epsilon] \quad (37)$$

For a generic turbulent variable x , the deviation reads:

$$\delta_x = \min \left[A_x \left| \frac{x_{wake} - x_{ABL}}{x_{ABL}} \right|, 1 \right] \quad (38)$$

Where A_x is an attenuation parameter, aimed to limit the unnecessary over-extent of the BIA. If the flow field is undisturbed, the resulting deviation is zero: $\delta_x = 0$. While, a fully perturbed region would bring to a maximum deviation: $\delta_h = 1$.


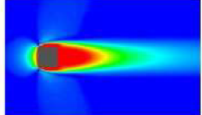
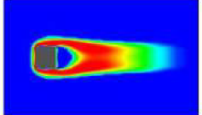
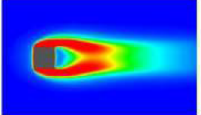
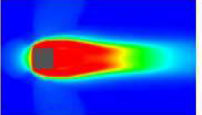

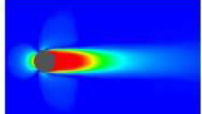
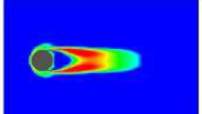
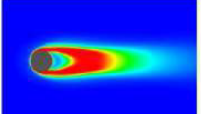
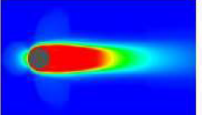
	Pure BIA			Hybrid BIA
Primitives	$\delta_u = \min \left[* \frac{u_{ABL}}{u_{ABL}}, 1 \right]$	$\delta_k = \min \left[* \frac{k_{ABL}}{k_{ABL}}, 1 \right]$	$\delta_\epsilon = \min \left[* \frac{\epsilon_{ABL}}{\epsilon_{ABL}}, 1 \right]$	$\delta_h = \max[\delta_u, \delta_k, \delta_\epsilon]$
				
				

Figure 2.1: Formulation and visualization of the BIA for the pure and hybrid blending for two simple geometries. Obtained from [3], adapted from [24].

2.3.3 Non Linear Eddy Viscosity Model

Inside the BIA, Non-Linear Eddy Viscosity models (NLEV) can be implemented to gain better predictions in disturbed regions. These models consist in extending the Boussinesq hypothesis to higher order terms [14].

Parente et al. [2] expressed the general stress-strain relation including cubic terms in the mean velocity gradients as:

$$\begin{aligned}
 \overline{u'_i u'_j} = & -2\nu_t S_{ij} + \frac{2}{3}k\delta_{ij} + C_1\nu_t \frac{k}{\epsilon} \left(S_{ik}S_{jk} - \frac{1}{3}S_{kl}S_{kl}\delta_{ij} \right) + C_2\nu_t \frac{k}{\epsilon} (\Omega_{ik}S_{kj} + \Omega_{jk}S_{ki}) + \\
 & + C_3\nu_t \frac{k}{\epsilon} \left(\Omega_{ik}\Omega_{jk} - \frac{1}{3}\Omega_{lk}\Omega_{lk}\delta_{ij} \right) + C_4\nu_t \frac{k^2}{\epsilon^2} (S_{ki}\Omega_{lj} + S_{kj}\Omega_{li})S_{kl} + \\
 & + C_5\nu_t \frac{k^2}{\epsilon^2} \left(\Omega_{il}\Omega_{lm}S_{mj} + S_{il}\Omega_{lm}\Omega_{mj} - \frac{2}{3}S_{lm}\Omega_{mn}\Omega_{nl}\delta_{ij} \right) + \\
 & + C_6\nu_t \frac{k^2}{\epsilon^2} S_{ij}S_{kl}S_{kl} + C_7\nu_t \frac{k^2}{\epsilon^2} S_{ij}\Omega_{kl}\Omega_{kl} \quad (39)
 \end{aligned}$$

Where S_{ij} and Ω_{ij} are the strain-rate tensor and the vorticity tensor respectively. The definition of C_μ and the values for the coefficients C_i depend on the NLEV model used. For this project, the next expression is applied:

$$C_\mu = \min \left(0.15, \frac{1}{0.9S^{1.4} + 0.4\Omega^{1.4} + 3.5} \right) \quad (40)$$

That equation is implemented inside the BIA, while outside that region Equation 27 is used. Regarding the values of the different C_i , they are considered to be null since, according to Merci et al. [25], in the absence of swirl the infinitesimal terms can be neglected.

The present thesis will then make use of the comprehensive approach, as the Hybrid BIA formulation in which Non-Linear Eddy Viscosity equations are also employed.

2.4 Steady vs Unsteady

Every phenomenon of the nature is unsteady, however, depending of the scale of time considered different steady approaches can be applied in order to decrease the computational time of resolution. Regarding the flow around buildings, it can be considered steady only when the wind is constant (in magnitude and direction), the temperature, the humidity... and the building has a symmetrical configuration oriented with the incident building. It is then clear that unsteady simulations are necessary to study the flow around real buildings.

Nevertheless, steady simulations provide a quick solution that can be used as a first estimation and also as the initialization for unsteady simulations. For the cases that will be analysed in this document, the RANS and URANS equations will be applied.

The unsteady simulations provide better results at the expense of more consuming computer resources. On the other hand, regarding the user configuration of the case the time step of computation or the number of time steps, among others, need to be defined.

For this project, the steady simulations were run on OpenFOAM 2.3.0, employing the steady-state solver for incompressible turbulent flows *simpleFoam*. While the unsteady cases used the transient solver for incompressible fluids *pimpleFoam*. Both solvers are implemented on the software by default.

2.5 Convergence schemes

Regarding the convergence schemes, for the simple case 2nd order schemes are used with the function *Gauss linearUpwind* of the program for the variables U, k, epsilon and nuEff . While the 1st order scheme *Gauss Upwind* are implemented in the variables R and nuTilda. For cases in which the stability of the case is more difficult to achieve, the simulations can be initialized with 1st order schemes for all the variables except nuEff, and the relaxation factors are set to really low values.

It needs to be said that the Upwind schemes are conservative, transportive, bounded, and they take into account the direction of propagation. The value of the nOuterCorrectors can also be increased to solve more corrections (momentum - pressure coupling) for each time step and therefore the computational effort increases, but the stability is enhanced. After a time, the calculation will exit the loop to speed-up the computation.

3 Wind flow around an isolated building

This chapter presents the main characteristics of the flow around an isolated building in order to facilitate the understanding of the future results. Figure 3.1 represents the flow around a high-rise building, the name of the different flows are shown in Table 3.1.

It is interesting to describe the behaviour of those components of the wind. The incoming flow is divided in three components: the flow which is directed towards the building (2), the flow which goes over the building (1), and the flow which passes through the sides at ground level (9).

The stagnation point is known to be located around $2/3$ or $3/4$ of the windward face height [18] [20], which is shown as the origin of different flows in the Figure. Part of the flow goes over the building (3), but as the flow encounters the sharp edge it detaches from the surface. Separation of the flow occurs around the sides and top of the building's edges originating low pressure recirculation zones, named separation bubbles. The size of these regions depend on the surface roughness, wind velocity and turbulence intensities. The flow may reattach if the building is long enough, but it will separate again at the back edges of the structure [20].

Other part of flow goes to the sides (4) and part runs down towards the ground (5). This last component is a reason of annoyance to pedestrians, since wind speed increases with height the downdraught results in a large mass of air at high velocity. In fact, the amplification factor of the wind speed at ground level can be above 1.4 [19].

Once this flow reaches the ground the standing vortex (6) are originated. There is another stagnation point at ground level (7) due to the interaction of the incoming flow and downdraught. On the other hand, the standing vortex which run at the sides of the building are named corner streams (8). These streams are usually accelerated, especially in buildings with square corners.

Behind the building there is a wake, in which several recirculation phenomena occur. These regions are generally associated with lower wind speed values and so they are of less concern to pedestrians [17].

There is a stagnation region (11), since part of the flow recirculates (10), but other goes downwind (12) and it will tend to recover the original ABL wind profile. It must be said that the recirculation region is not scaled in the Figure since it can have a great extension.

Another component of the wind correspond to the large vortices behind the building (13) and there are also small vortices (16) located between the large ones and the corner streams. This region is denominated as the shear layer since there are high velocity gradients in it.

Finally, it may be mentioned that the characteristics of each of the described components of the flow pattern depend on the building. The orientation of the building or its size will affect the wind interaction. For example, if the building has a passage the wind will accelerate inside it.

The presence of other buildings and/or obstacles will also vary the wind flow pattern. Passages between buildings can also lead to amplifications factors of 2 [17].

Regarding the behaviour of the flow it must be treated with an unsteady approach. The wake presents high turbulence, but also the separation bubble on top of the building will change in size and even collapse over time.

3 WIND FLOW AROUND AN ISOLATED BUILDING

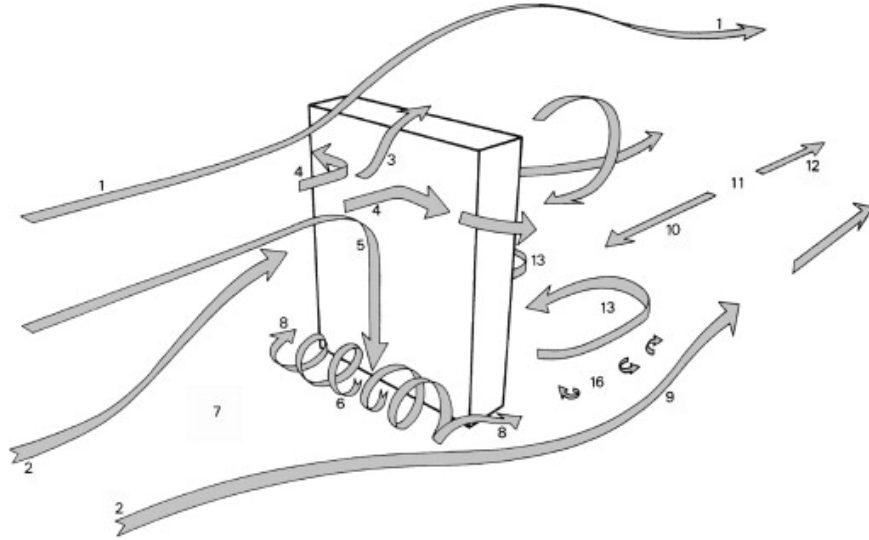


Figure 3.1: Schematic representation of wind flow pattern around a high-rise building [15].

1	Flow over building
2	Incoming flow
3	Flow from stagnation point over building
4	Flow from stagnation point around vertical building edges
5	Downflow from stagnation point
6	Standing vortex / Base vortex / Horseshoe vortex
7	Stagnation point in front of building near ground level
8	Corner streams (vortex wrapping around corners)
9	Flow around building sides at ground level (Adding to corner streams)
10	Recirculation flow
11	Stagnation region behind building at ground level
12	Restored flow direction
13	Large vortices behind building
16	Small vortices in shear layer

Table 3.1: Components of the wind-flow around an isolated building [16].

4 Case studies

This chapter discusses the configurations and results of the CFD simulations. The simple case treated allows to validate the results of the comprehensive approach with experimental data, as well as to obtain more knowledge of the program. The differences between a stationary and a transient, or unsteady, simulation are also studied. The comprehensive approach is also compared with other turbulence models.

With this done, another geometry of the simple case is analysed in order to study the differences, especially in the wake. And finally, the flow around a high-rise building is simulated with the comprehensive approach in order to identify its main characteristics.

It needs to be said that all the contour plots are represented in SI units, so the velocity in $[m/s]$ and the turbulent kinetic energy in $[m^2/s^2]$. Regarding the convergence of the computations, the residuals plots can be observed at the ANNEX I. The simulations run until a stable low value of the parameters was achieved.

4.1 Validation of the comprehensive approach

The Architectural Institute of Japan published a guidebook for CFD Predictions of Urban Wind Environment [4]. The results of different wind tunnel experiments are public, specifically the case B 1:4:4 shape building model is used to validate the comprehensive approach and gain experience in the configuration of a building flow field simulation.

4.1.1 Geometry

The building is straight shaped and doesn't have any facade elements. Its dimensions are 0.05x0.2x0.2 m, and it can be seen in Figure 4.1, the shorter dimension correspond to the x direction. The width direction is the y axis, and z is related to the height.

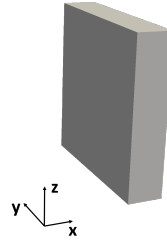


Figure 4.1: Geometry of the Building 1:4:4.

Regarding the domain, a straight box is defined around the building with a size that ensures that the boundary conditions do not affect the internal flow ($7 \times 1.55 \times 1.6$ m). In Figure 4.2 the domain for this case is shown, also a plane at $x=0.55$ m to clarify the future post-processing.

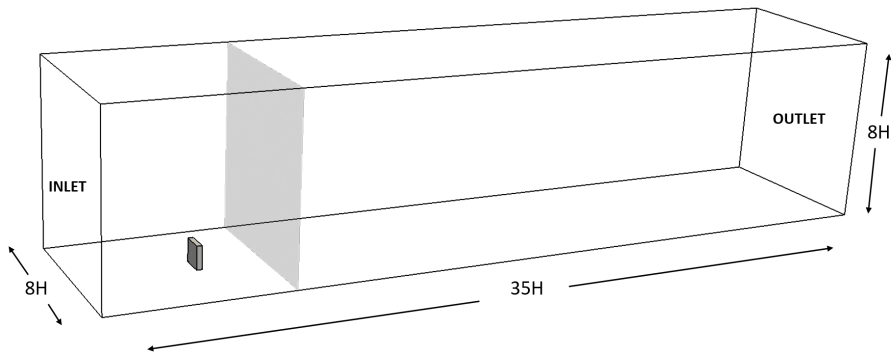


Figure 4.2: Computational domain for the Building 1:4:4. Dimensions regarding the height of the building. In grey, plane at $x=0.55$ m.

Since experimental results are compared, the boundary conditions reproduce the conditions of the experiment. For this, in addition to the ground, the side walls are defined as walls to reproduce the wind tunnel.

4.1.2 Mesh

The computational domain is divided in 4 blocks which collide at the centre of the building (origin of the coordinate system). In all of the blocks there is a refinement progression directed to the building in all the three directions.

4 CASE STUDIES

On the other hand, a structured mesh with hexahedral cells is configured since this type of mesh provides good results in cases of external aerodynamics in which there is a predominant flow direction. Moreover, an additional refinement box is set around the building to improve the quality of the mesh in the region where there are bigger gradients.

In Figure 4.3 a view of the mesh is shown in which only half of the domain has been clipped. In Figure 4.4 and Figure 4.5 different views can be seen.

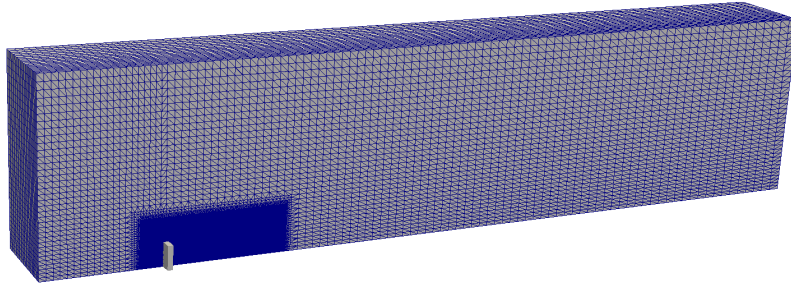


Figure 4.3: View of the mesh for the Building 1:4:4.

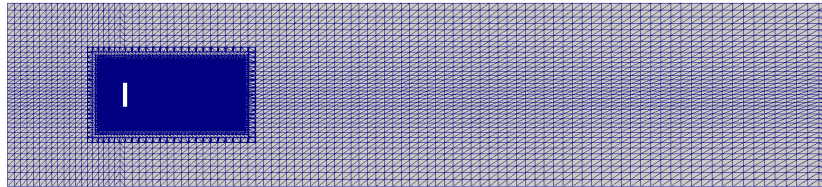


Figure 4.4: Horizontal view of the mesh for the Building 1:4:4 at $z=0.1\text{m}$.

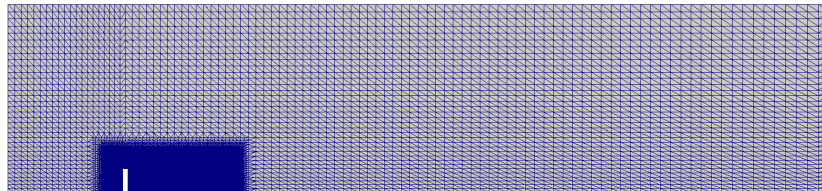


Figure 4.5: Vertical view of the mesh for the Building 1:4:4 at $y=0\text{m}$.

The final mesh has around 2.2 million of cells. On the other hand, an important parameter in the creation of a mesh is the y^+ value in the walls, this depends on the mesh refinement and the velocity and viscosity conditions of the flow in that area. In order to apply the wall functions, this value should be between 30 and 300. Checking the mean values on the building and on the ground, these values are 84.2 and 101.9 respectively.

4.1.3 Physical configuration

The mainly parameters of the configuration are the next:

- All the simulations are three-dimensional.
- The outlet and the top surfaces are defined as a patch boundary.
- The building, the ground and the side walls are defined as walls with the condition of zero velocity (as a wind tunnel).
- The inlet boundary is defined as a patch with the ABL model configured. The reference conditions of the ABL model are shown in Table 4.1.
- The experimental data show an increase-decrease TKE inlet profile with height. Therefore, Equation 28 considers the 4 parameters.

ABL configuration	
Parameter	Value
Reference velocity	5.133 m/s
Reference height	0.2 m
ABL height	1.6 m
Roughness length	0.000096 m
Von Karman constant	0.41

Table 4.1: Setting configuration of the ABL model for the simple cases.

4.1.4 Numerical configuration and solver

The SIMPLE algorithm of OpenFoam is used for the steady cases, and the PIMPLE algorithm for the unsteady ones. The SIMPLE algorithm solves the continuity and the momentum equations considering zero the elements with the derivate of time. For the unsteady configuration the time step is set on $1e-6$ s ($1\mu s$), and two functions are defined to compute the mean value of velocity and TKE.

Regarding the solvers, the pressure uses the GAMG while all the other variables use a smooth solver. A Gauss linear scheme is also implemented. Under-relaxation factors are configured to enhance the stability and convergence of the case, this is 0.4 in the case of the velocity and a little more conservative, 0.3, for the other variables. These values are 0.3 and 0.2 respectively in the unsteady case.

4.1.5 Results

First, the Building Influence Area should be checked. Figure 4.6 shows that the BIA is correctly defined around the building, this area is the same on both simulations (Figure 5.3 in the ANNEX I).

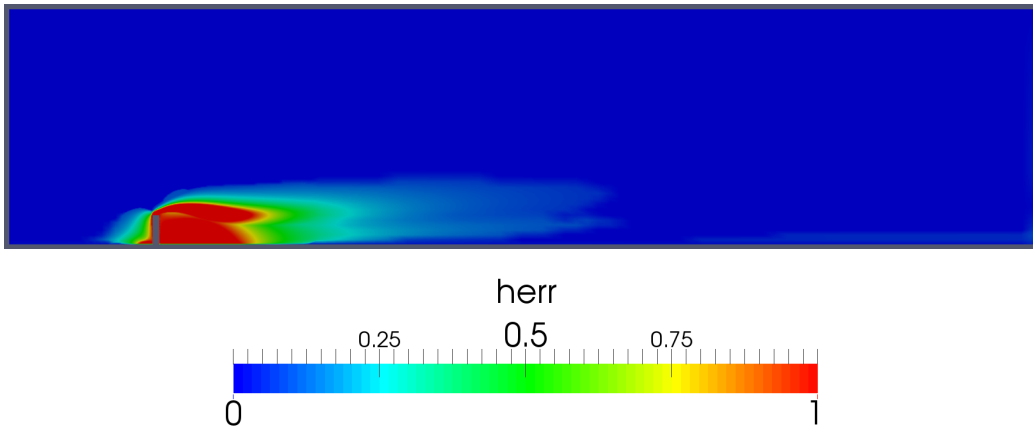


Figure 4.6: BIA of the building 1:4:4 shown with the variable herr for the steady case. Vertical view at $y=0$ (symmetry plane).

CFD steady and unsteady comparison

The experimental data available correspond to the velocity and the turbulent kinetic energy (TKE), so these two variables are analysed. In Figure 4.7 practically no difference can be detected between the steady and unsteady cases for the contour plot of mean velocity in the vertical plane $y=0$. The same trend is true for the horizontal plane $z=0.1\text{m}$ (half of the building), and for the turbulent kinetic energy (Figures 5.4 and 5.5 at the ANNEX I).

In Figure 4.8 the streamlines around the building show the flow behaviour in the close wake. The differences between both cases are small, the size of the recirculation region is really similar. Furthermore, the features seen in Figure 3.1 can be appreciated. As the standing vortex at the ground in front of the building, the detachment of the flow at the top of the building, and the accelerated corner streams.

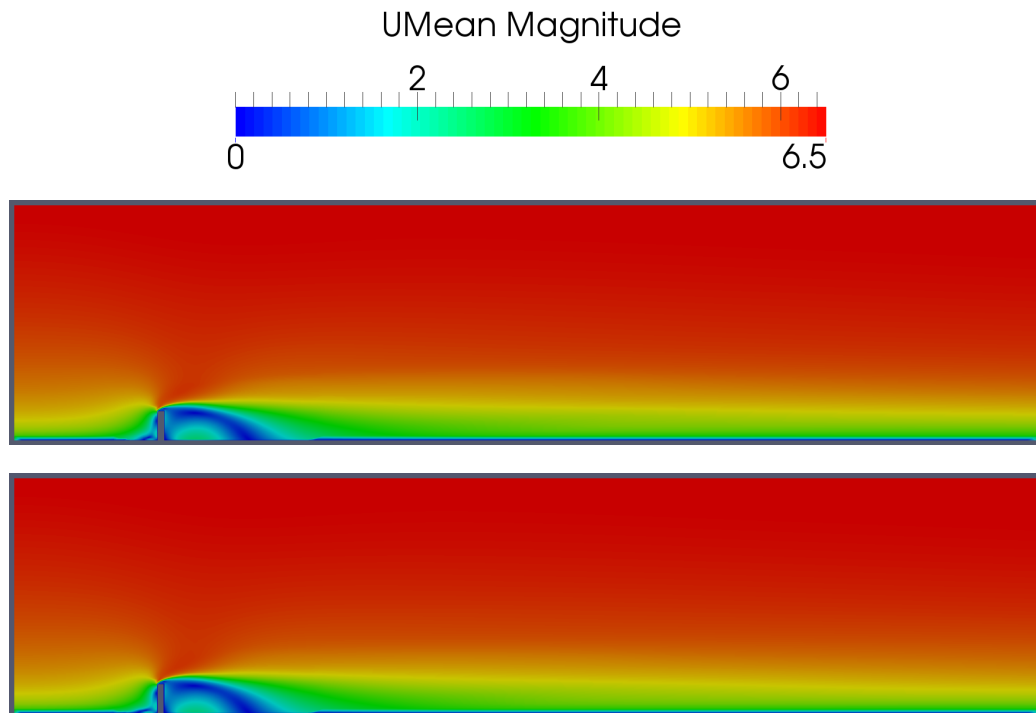


Figure 4.7: Velocity contour for the building 1:4:4. Vertical view at $y=0$, in the upper part the steady case and the lower one is the unsteady.

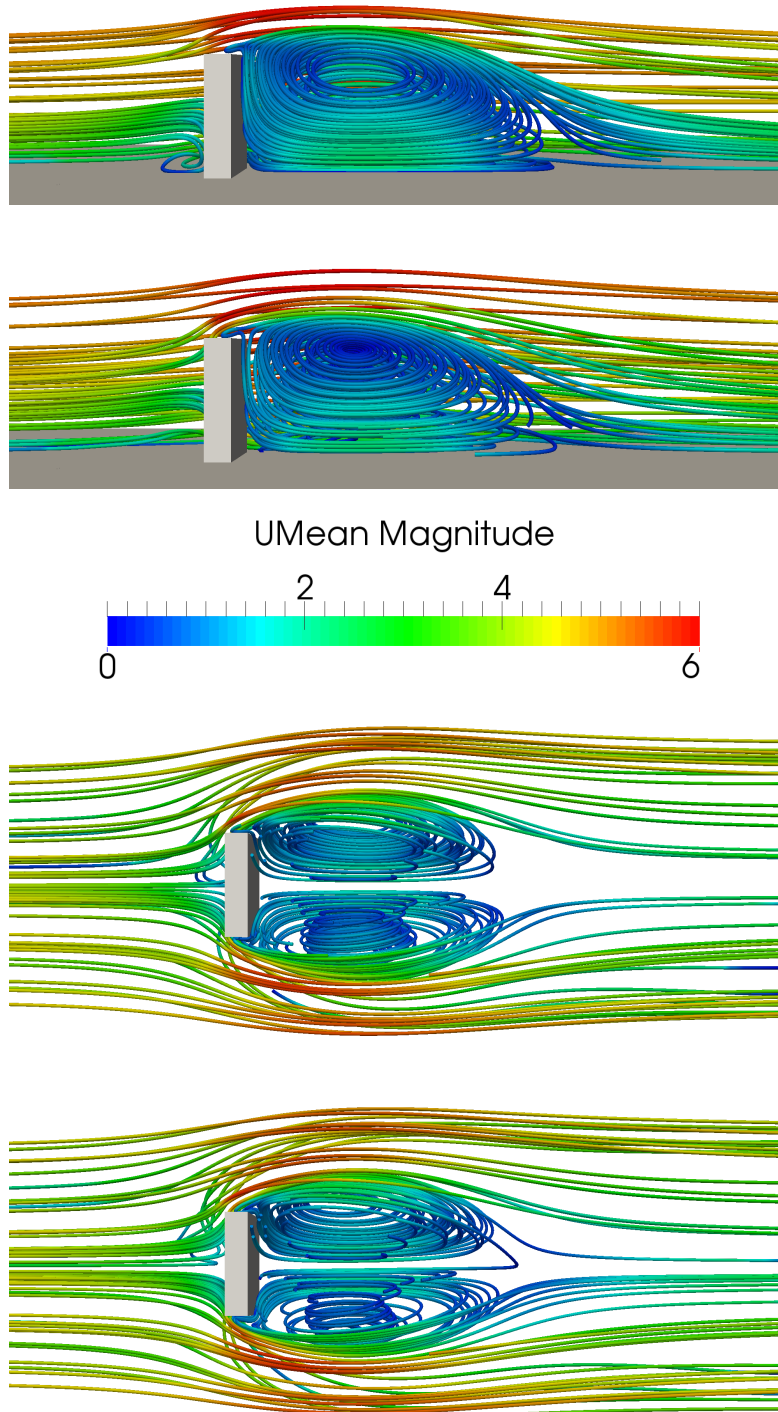


Figure 4.8: Streamlines for the building ²⁸1:4:4. In the upper part, the vertical view, and in the lower part the horizontal view. In both views the up image is the steady case and the lower one is the unsteady.

Vertical lines measurements

The experiment measured different locations of the wind tunnel at different constant x positions, at $y=0$ and from $z=0$ to $z=0.35\text{m}$. It needs to be remembered that the centre of the building at ground level is the point $x=0$, $y=0$, $z=0$. The graphs of velocity and TKE can be seen in Figure 4.9 and Figure 4.10. The steady and the unsteady data matches for almost every point, for the lower heights of $x=-0.075\text{m}$ there are small differences, probably due to the base vortex.

Regarding the experimental data, the CFD simulations provide good results. However, for the lower heights of $x=-0.075\text{m}$ there is a bigger difference. For the locations $x=0\text{m}$ and $x=0.05\text{m}$ the TKE presents also some error, while the velocity is quite similar. This may be due to the recirculation region at ground in front of the building and the separation bubble at the top. Moreover, for the position $x=0.55\text{m}$, in the wake, the velocity presents some remarkable differences. Longo showed in his PhD [3] similar graphs, and the results of the present thesis are consistent with his. However, he did not analyse the horizontal lines.

Horizontal lines measurements

The experiment also measured different locations of the wind tunnel at different constant x positions, at $z=12.5\text{mm}$ and from $y=0$ to $y=-0.35\text{m}$. Both the velocity and the turbulent kinetic energy were obtained. Figure 4.11 and Figure 4.12 show that the results for the TKE present bigger differences with the experimental data than the velocity results. In addition, for this variable there are some differences between the steady and the unsteady CFD case. As was said before, the values for the locations of the recirculation regions on ground don't fit.

The results for the horizontal measurements are worst than the vertical ones, this can also be affected due to measuring really close to the ground ($z=0.0125\text{m}$). And usually more attention is paid to the vertical results, but the experiment doesn't give information about the measurement technique.

4 CASE STUDIES

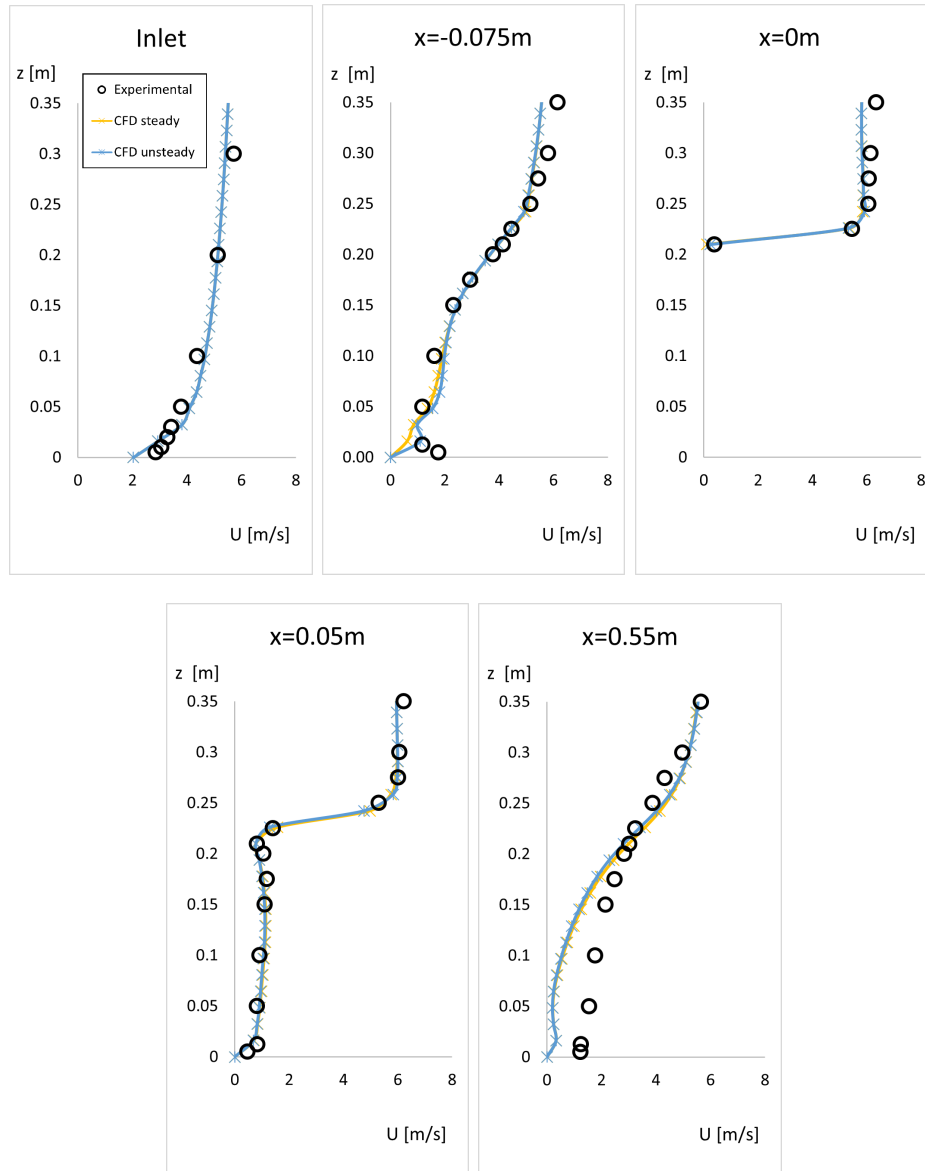


Figure 4.9: Velocity in vertical lines, at different longitudinal positions. Experimental data and CFD simulations of the steady and unsteady case of the building 1:4:4.

4 CASE STUDIES

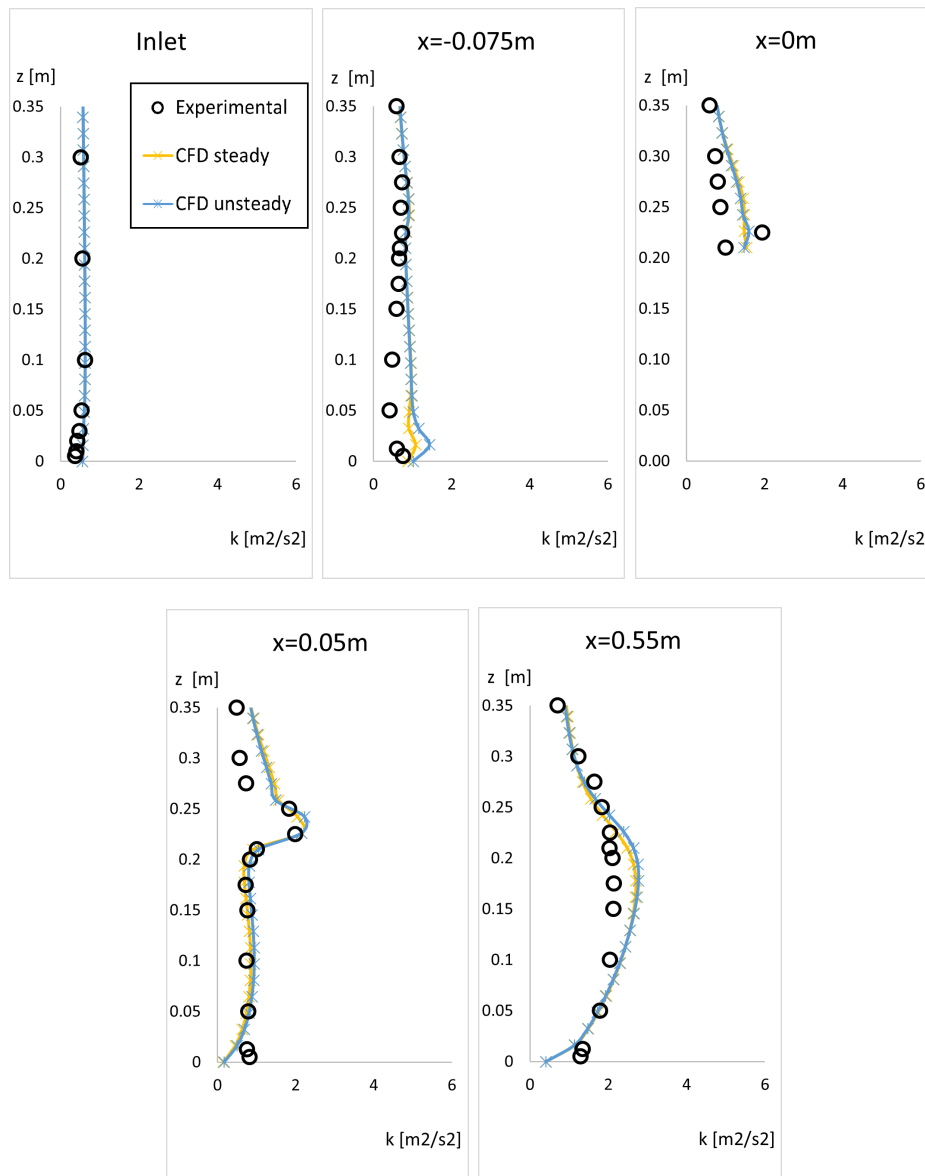


Figure 4.10: Turbulent kinetic energy in vertical lines, at different longitudinal positions. Experimental data and CFD simulations of the steady and unsteady case of the building 1:4:4.

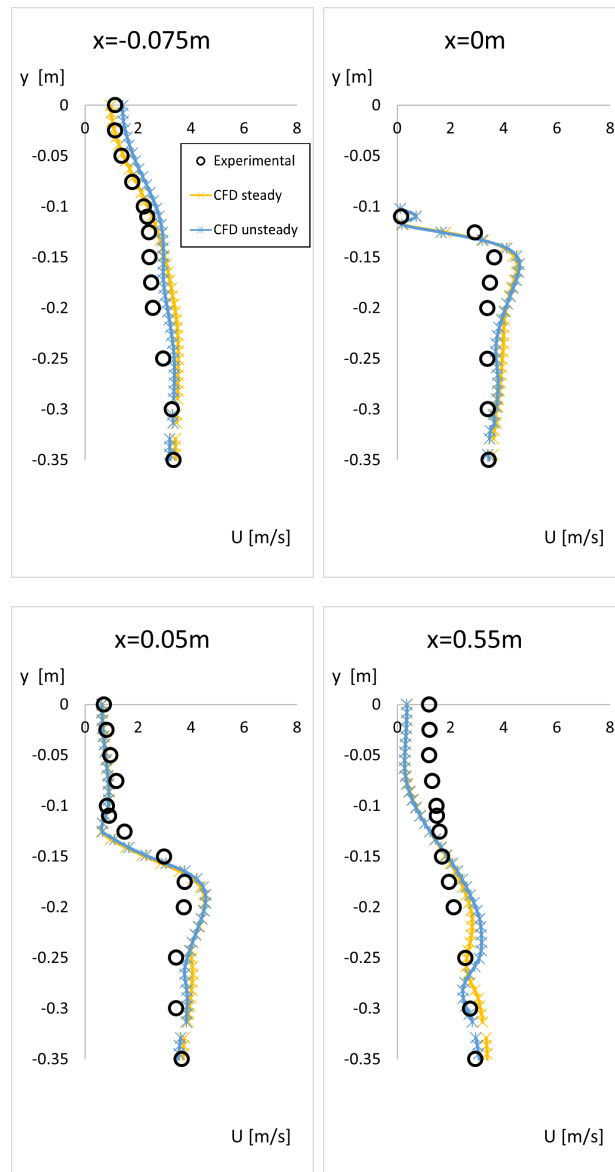


Figure 4.11: Velocity in horizontal lines, at different longitudinal positions. Experimental data and CFD simulations of the steady and unsteady case of the building 1:4:4

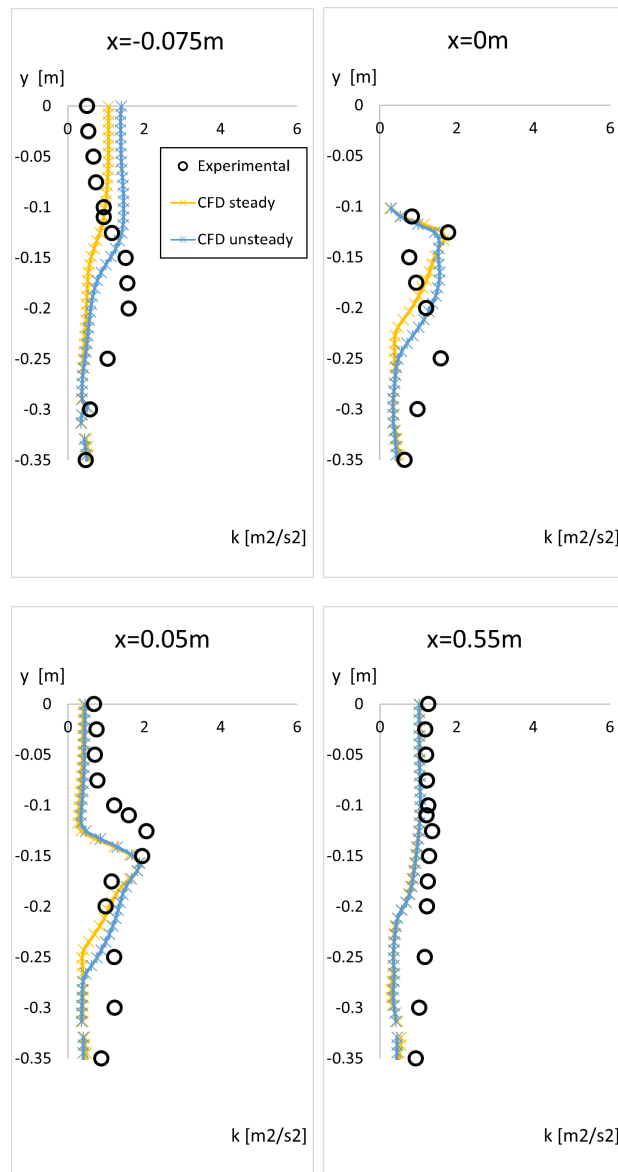


Figure 4.12: Turbulent kinetic energy in horizontal lines, at different longitudinal positions. Experimental data and CFD simulations of the steady and unsteady case of the building 1:4:4.

4.1.6 Conclusions

The comprehensive approach provides good results for this kind of cases. However, there are some discrepancies in the separation bubbles zones, especially for the turbulent kinetic energy. The differences are more remarkable in zones with recirculation, e.g. the velocity in the wake is underestimated. The bigger differences in the horizontal measurements can also be due to their low height. It is also interesting to compare the results with those obtained by Longo [3]. The trends of the vertical curves obtained are really similar to his, and the velocity at the last position presents the same profile. On the other hand, the case analysed is intrinsically steady, so few differences between the steady and the unsteady cases are observed. Some low frequency recirculation zones may be the responsible for these discrepancies.

4.2 Comparison of turbulence models

In the previous study it was seen that the results obtained implementing the comprehensive approach were really similar to the experimental data. However, it is necessary to analyse if indeed it provides more accurate results than standard models as the $k-\epsilon$ and the SST $k-\omega$.

Since the unsteady results are not highly differentiated from the steady ones, this study will be done by the comparisons of the steady state for the different turbulence models. The geometry, mesh and configuration of all the cases are the same, and the inlet boundary condition is also the ABL model.

4.2.1 Results

The different turbulence models can be compared by observing their respective differences respected to the experimental data.

Vertical lines measurements

Some locations are analysed, at constant x positions, at $y=0$ and from $z=0$ to $z=0.35\text{m}$. Being the centre of the building at ground ($x=0, y=0, z=0$).

The velocity is shown in Figure 4.13, and the TKE in Figure 4.14. It can easily be seen that the k-omega model is the worst of all the models implemented. However, the SST k-omega model provides really good results.

Regarding the velocity, the differences between the models are not remarkable upstream the building. At $x=0.05\text{m}$ the comprehensive approach fits perfectly the experimental data while the rest of the models present differences. For $x=0.55\text{m}$ any of the models completely represent the experimental data, the best results come from the comprehensive approach (which underestimates the velocity for low heights) and the k-epsilon model.

For the turbulent kinetic energy (TKE), the differences are more striking. At $x=-0.075\text{m}$ the k-omega model highly overestimates the value (maximum around $11\text{ m}^2/\text{s}^2$), also the k-epsilon doesn't fit the data. This trend is visible in other locations, although for $x=0.55\text{m}$ the k- ϵ model provides good results since this model usually works better away from the walls.

Comparing the comprehensive approach with the SST k-omega model, both models have a similar accuracy. At $x=0\text{m}$ the SST k- ω reproduces better the profile, but it underestimates the maximum k, something similar occurs at $x=0.05\text{m}$. While for $x=0.55\text{m}$ the comprehensive approach overestimates some values of TKE.

Horizontal lines measurements

It is interesting to analyse the horizontal profiles, at different x positions, at $z=12.5\text{mm}$ and from $y=0$ to $y=-0.35\text{m}$. Figure 4.15 shows the velocity, while Figure 4.16 the TKE.

The k-omega model still differs considerably from the experimental data. The comprehensive approach fits better the data, especially at $x=0.55\text{m}$, where all the rest of models overestimate the velocity far away from the building. Even the k-epsilon has considerable discrepancies, this may be due to the presence of recirculation, which is higher just behind the building so the k-omega models do solve it correctly.

The comprehensive approach also underestimates the velocity behind the building. Focusing on the TKE, the k-epsilon model differs a lot from the data for $x=-0.075\text{m}$ and $x=0\text{m}$ (close to the building). The SST k-omega model reproduces the profile better, but it underestimates the values behind the building in these locations while the comprehensive approach doesn't.

On the other hand, it must be pointed that the SST k-omega model doesn't behave as the k-epsilon away from the building and neither as the k-omega close to it. Compared to the standard k-omega model, the SST k-omega model can include improvements, such as adding a special cross-diffusion in the ω equation and the constants in both models are different [28]. Moreover, the k-omega model implemented in OpenFoam is a Standard high Reynolds-number turbulence model. While the SST k- ω model can be used as a Low-Re turbulence model without any extra damping functions [30].

The SST model exhibits less sensitivity to free streams conditions than many other turbulence models, and the shear stress limiters avoids the k-omega model to build-up an excessive turbulent kinetic energy near stagnation points [29]. In addition, the SST model switches automatically between the two formulations, however, it doesn't provide information about the limit of both regions. To understand this, the topology of the flow, which is the same, the shear flows should be identified but this is not easily realizable.

Considering the computational cost, if resources are limited then the k-epsilon model is advisable for velocity results, but not for turbulent kinetic energy. While the SST k-omega model and the comprehensive approach are more accurate for both variables, depending on the region one or other may be more interesting. For example, at regions really close to the building the comprehensive approach fits better the experimental data.

4 CASE STUDIES

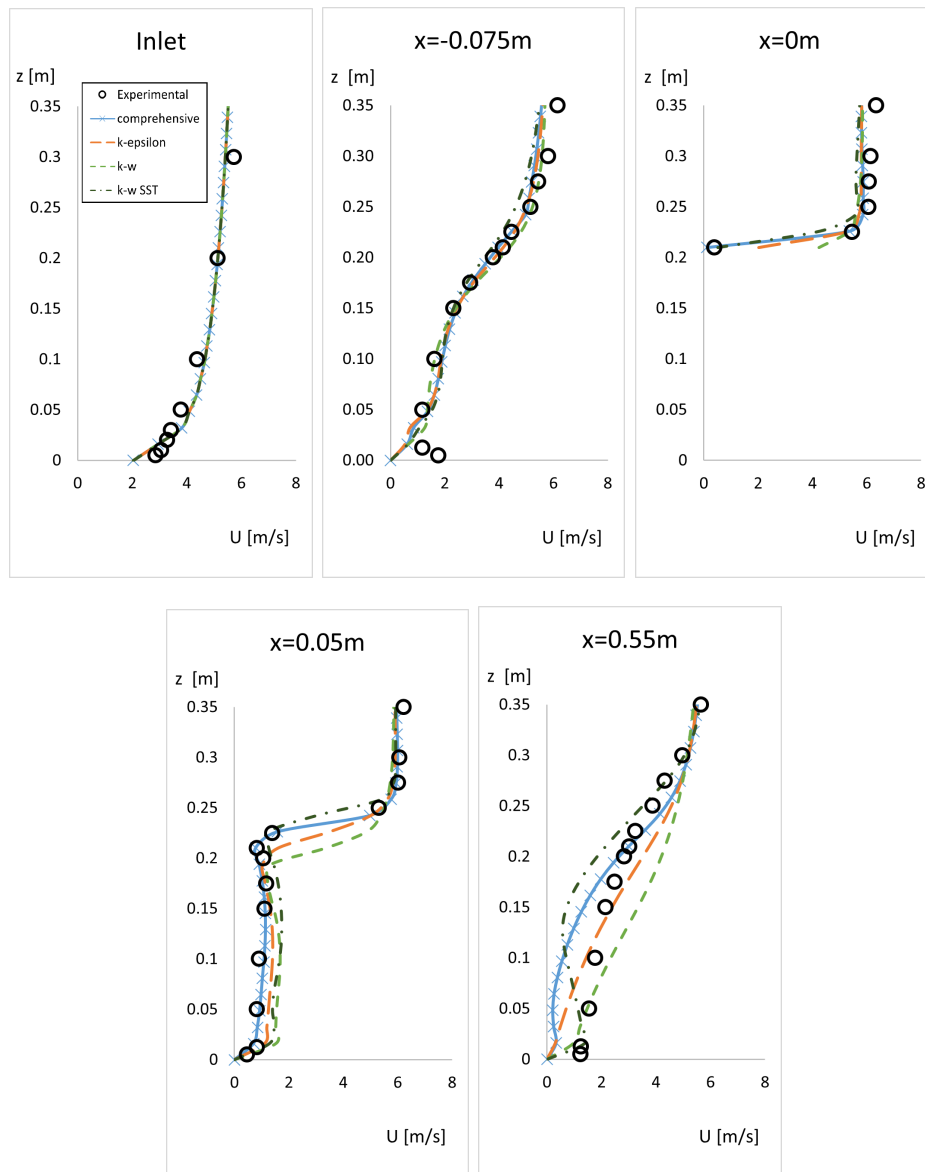


Figure 4.13: Velocity in vertical lines, at different longitudinal positions. Experimental data and CFD simulations with different turbulence models of the steady case of the building 1:4:4.

4 CASE STUDIES

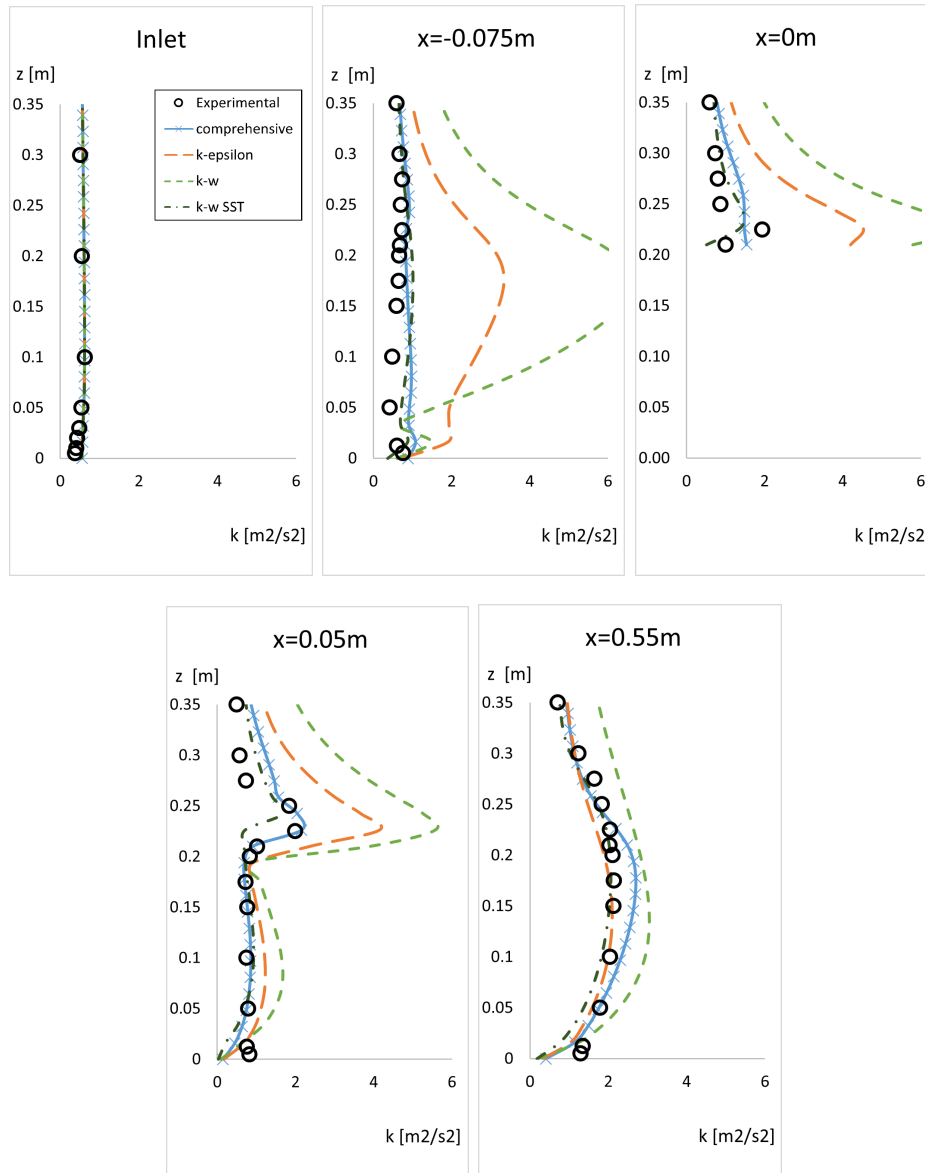


Figure 4.14: Turbulent kinetic energy in vertical lines, at different longitudinal positions. Experimental data and CFD simulations with different turbulence models of the steady case of the building 1:4:4.

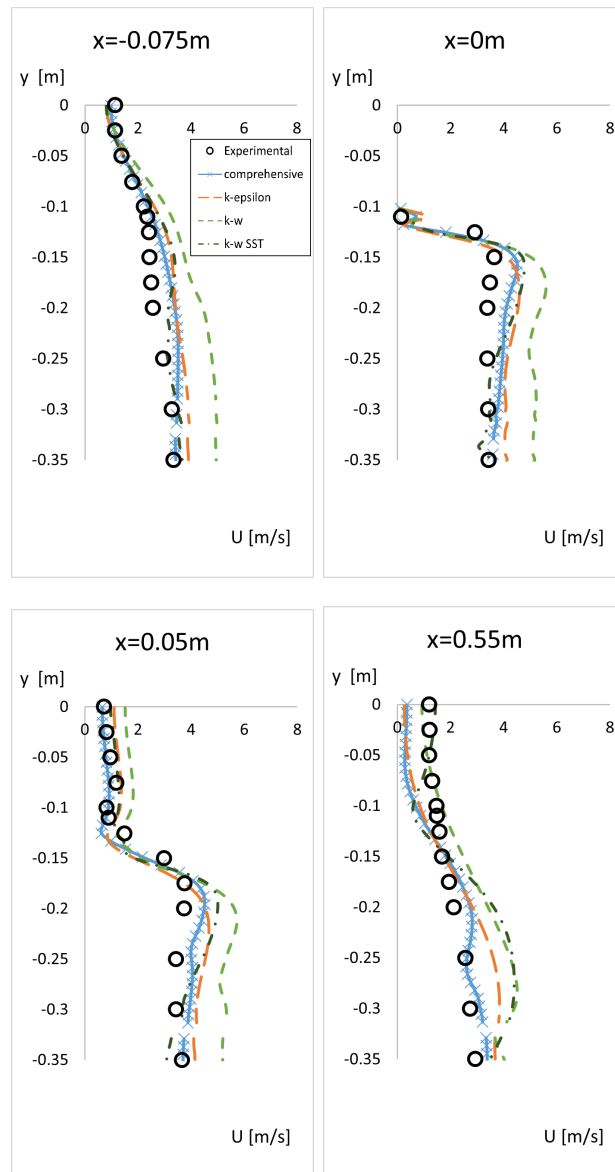


Figure 4.15: Velocity in horizontal lines, at different longitudinal positions. Experimental data and CFD simulations with different turbulence models of the steady case of the building 1:4:4.

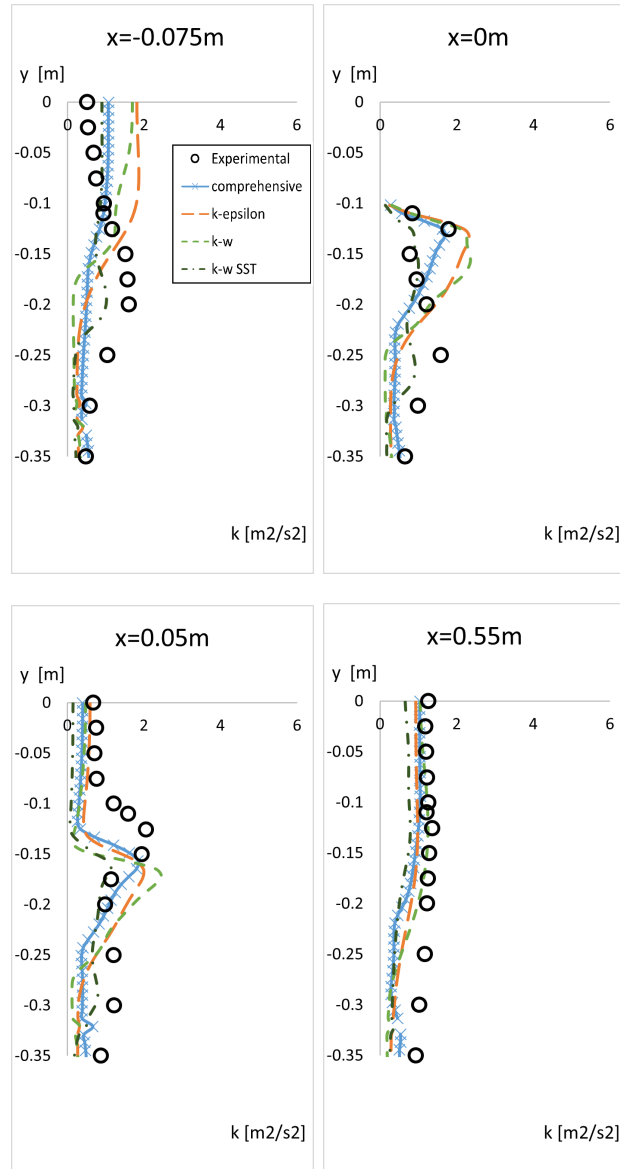


Figure 4.16: Turbulent kinetic energy in horizontal lines, at different longitudinal positions. Experimental data and CFD simulations with different turbulence models of the steady case of the building 1:4:4.

Contour plots

Different contour plots that show the comparison of the turbulence models can be seen at the ANNEX I, in Figure 5.10, Figure 5.11, Figure 5.12, Figure 5.13, Figure 5.14 and Figure 5.15. Since the k-omega model and the k-epsilon present considerable differences from the experimental data, it is more interesting to focus on the comparison between the comprehensive approach and the SST k-omega model.

Figure 4.17 shows that the SST k-omega case presents higher velocities at both sides of the building, it is important to mention that the velocity is zero at the walls since the simulations correspond to a wind tunnel. The recirculation region behind the building is larger for the SST k- ω . This is also seen in Figure 4.19, where the flow is visualized with streamlines. Regarding the TKE, in Figure 4.18 this model presents much lower values in the wake.

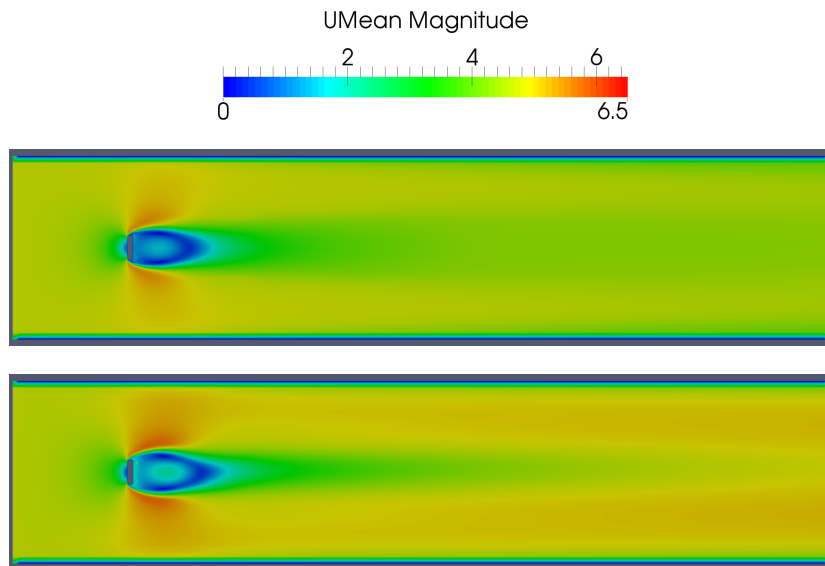


Figure 4.17: Velocity contour of the steady cases, horizontal view at $z=0.1\text{m}$. Building 1:4:4 case, comprehensive approach above and SST k-omega model below.

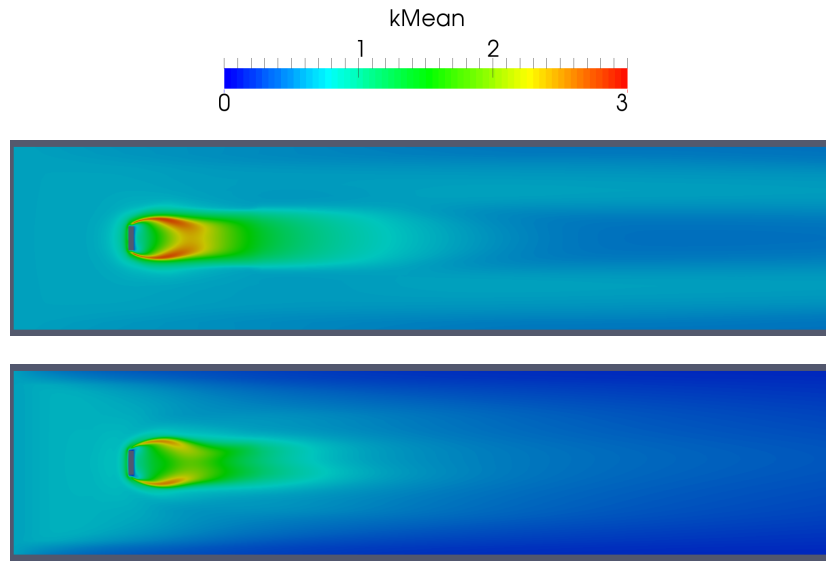


Figure 4.18: TKE contour, steady cases, horizontal view at $z=0.1\text{m}$. Building 1:4:4, comprehensive approach above and SST k-omega model below.

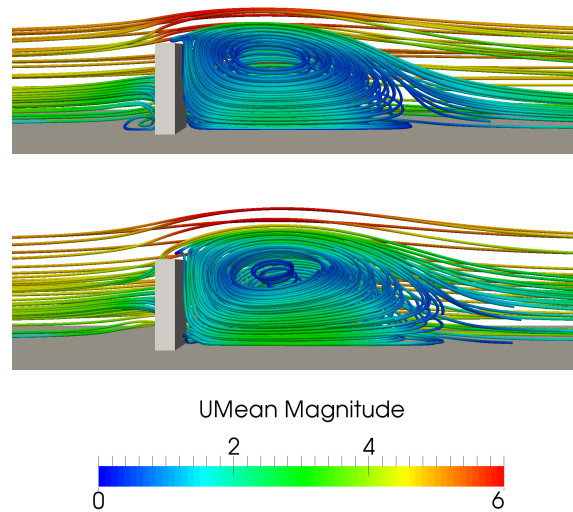


Figure 4.19: Streamlines, steady cases, vertical view. Building 1:4:4, comprehensive approach above and SST k-omega model below.

4.2.2 Conclusions

The k-omega model is not usually used for these studies, and indeed, it doesn't provide good results. While the k-epsilon reproduces quite well the velocity, but presents considerable differences for the TKE. The SST k-omega, which switches between these models in an improved version depending on the region, provides really good results, comparable to the comprehensive approach.

In the wake, the SST k-omega model underestimates the velocity at medium heights, and overestimates it in the horizontal plane far away from the building. Regarding the TKE, it underestimates some values although it reproduces quite well the profile. The comprehensive approach also presents some differences from the experimental data, it underestimates the velocity at low heights in the wake, and overestimates the TKE at medium heights. For the horizontal measurements, it is accurate for the far wake, but it underestimates the velocity behind the building. It also underestimates the TKE for some positions. Nevertheless, for positions really close to the building, the comprehensive approach provides the best results.

4.3 Geometry analysis

Once the comprehensive approach has been validated, another geometries can be studied. For example, a straight shaped building of ratio 1:2:4 in a wind tunnel, so it has half the width of the previous case. The physical and numerical configuration are the same as for the previous case.

4.3.1 Geometry and Mesh

The dimensions of this building are 0.05x0.1x0.2 m. The characteristics of the mesh are the same as for the Building 1:4:4, the refinement box is shorter since the wake is expected to be smaller.

There are around 1.8 million cells in this case, and the mean y^+ for the ground and the building both are in the range 30-300. The domain, which is the same, with the mesh can be seen in [Figure 5.16](#) at the ANNEX.

4.3.2 Results

For this case, the steady and the unsteady simulation are exactly, the same as it is shown later. For this reason, just the unsteady case of both buildings are compared with contour plots.

The Building Influence Area (BIA) of both cases are shown in Figure 4.20, and in Figure 5.17 at the ANNEX I. The width of the building affects the size of the BIA considerably.

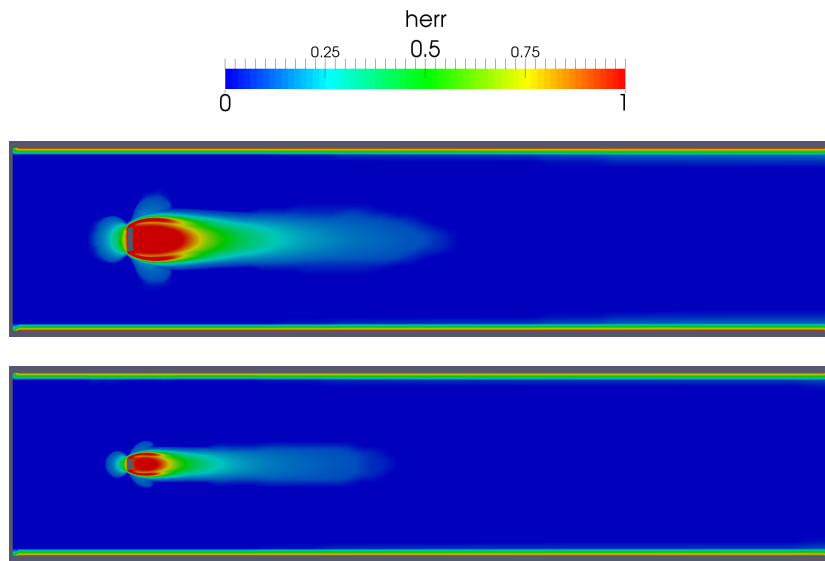


Figure 4.20: BIA of unsteady cases shown with the variable $herr$. Horizontal view at $z=0.1m$, building 1:4:4 up and Building 1:2:4 down.

In Figure 4.21, it can be seen that the effect of the wider building is higher in front of it, at the sides and in the wake. In wider buildings, the vortex standing is more visible and the corner streams are wider [1]. The Figure 5.19 shows that the biggest effect of the width of the building is on the wake. This can also be seen in Figures 5.18 and 5.19 at the ANNEX I.

In Figure 4.23 the streamlines around both buildings also show how the wake is larger, not only in length but also in height, and obviously in width.

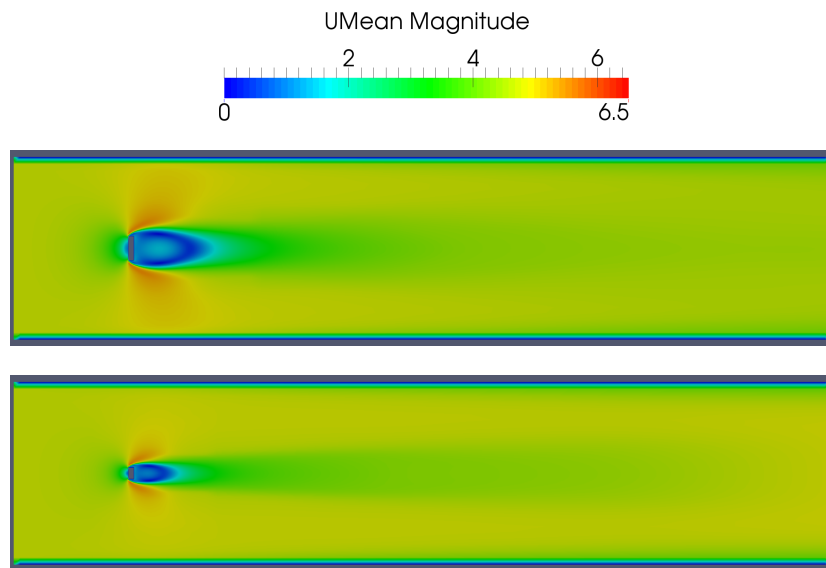


Figure 4.21: Velocity around the Building 1:4:4 (up) and Building 1:2:4 (down), horizontal view at $z=0.1\text{m}$.

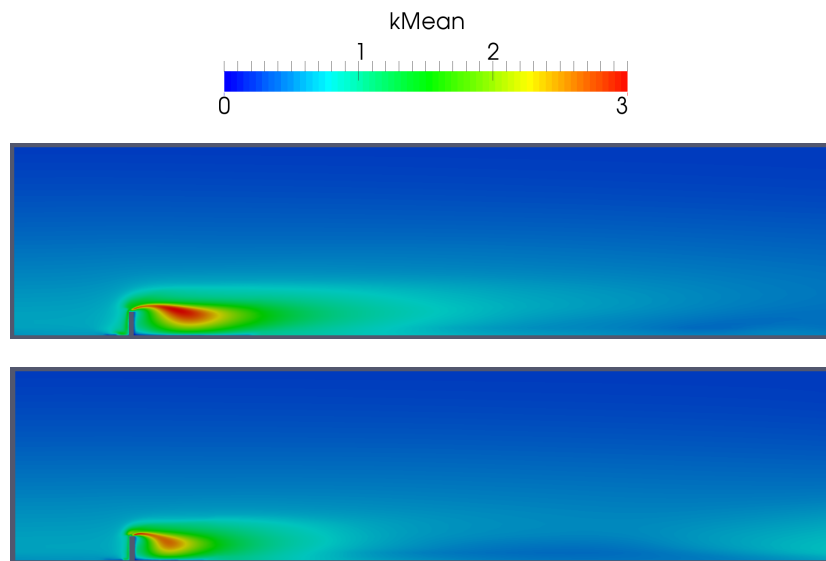


Figure 4.22: Turbulent Kinetic Energy around the Building 1:4:4 (up) and Building 1:2:4 (down), vertical view at $y=0$.

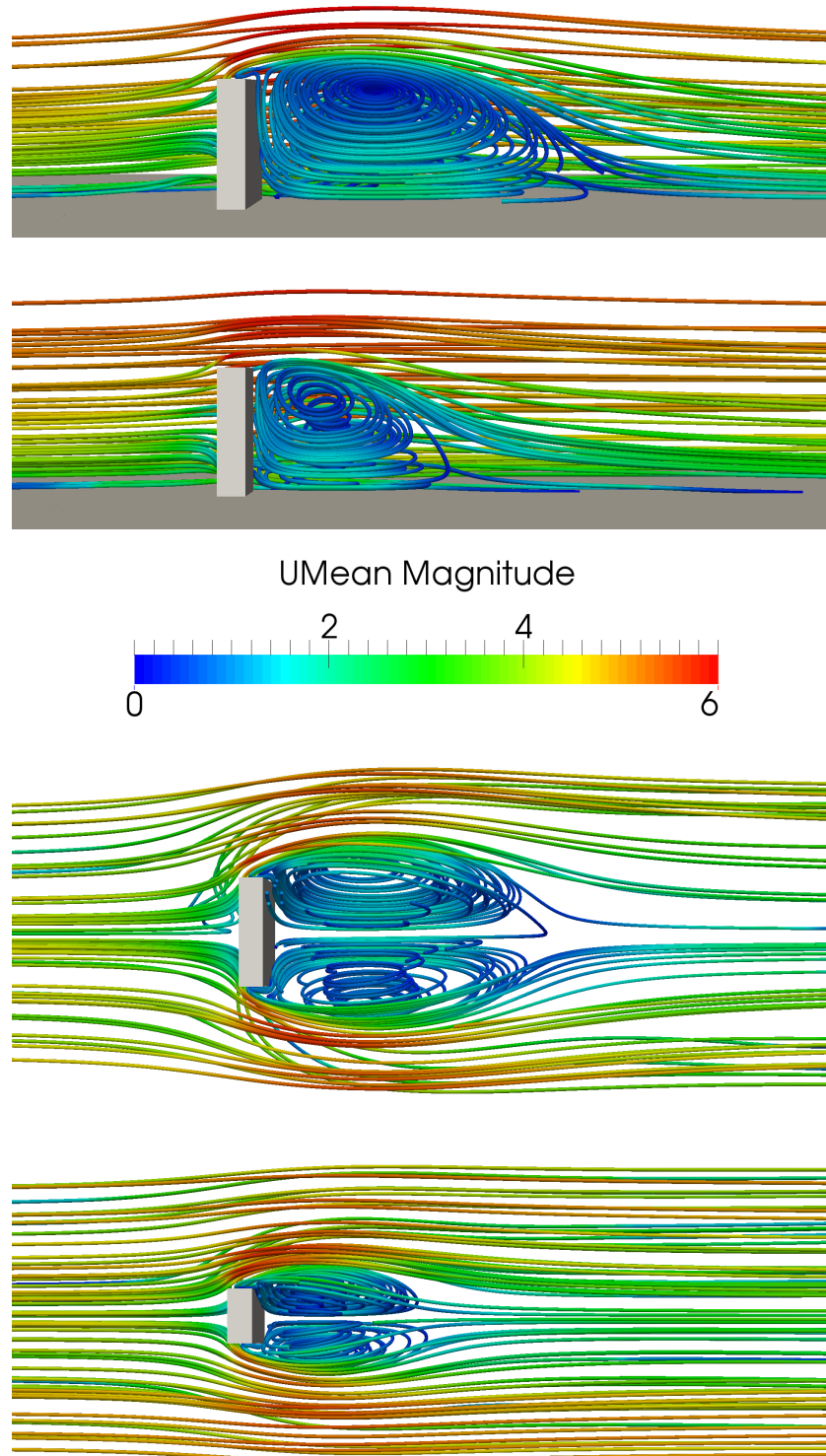


Figure 4.23: Streamlines of the unsteady cases. In the upper part, the vertical view, and in the lower part the horizontal view. In both views the up image is the Building 1:4:4 and the lower one is the Building 1:2:4.

Vertical lines measurements

Since different lines were obtained in the case before, it is interesting to compare them with the new geometry. These lines at different constant longitudinal positions of the wind tunnel, at $y=0$ and from $z=0$ to $z=0.35\text{m}$. It needs to be remembered that the centre of the building at ground level is the point $x=0$, $y=0$, $z=0$.

Both the velocity and the turbulent kinetic energy are represented in Figure 4.24 and Figure 4.25. For the Building 1:2:4, the steady and the unsteady data matches perfectly, probably because the recirculation regions are of less importance (lower values of k at ground level).

Comparing both buildings, the flow is similar for these vertical lines until the wake. At the last position of $x=0.55\text{m}$ there is a big difference for lower heights. The velocity profile presents lower values for the wider building, while higher for the TKE. What is the same, the wider building disturbs more the flow.

Horizontal lines measurements

Figure 5.20 and Figure 5.21 at the ANNEX I show the same trends. And for the horizontal profile of TKE before the building the smaller building also presents lower values. It is also interesting to remark that at $x=0.05\text{m}$ it can be seen how the profile of both cases is really similar but it is displaced in space according to the width of the building.

4 CASE STUDIES

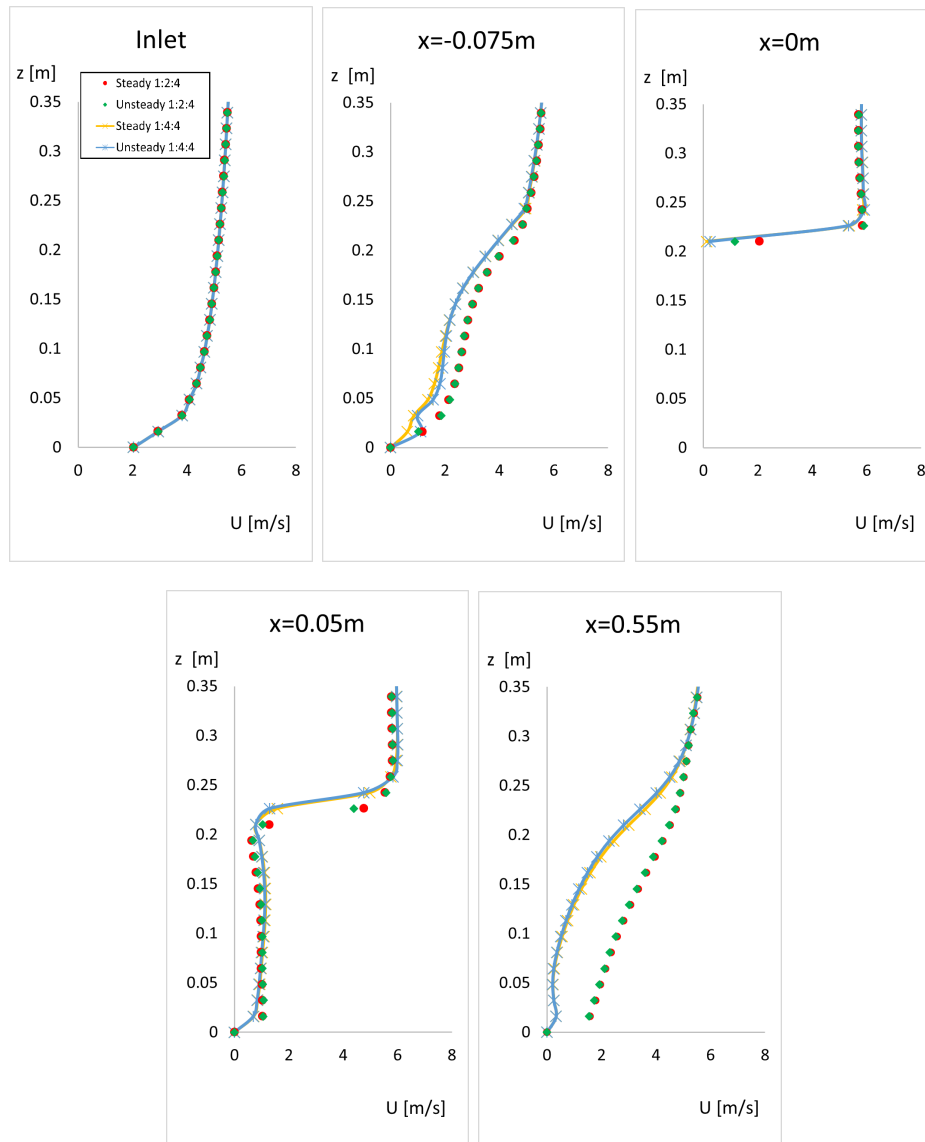


Figure 4.24: Velocity in vertical lines, at different longitudinal positions. CFD simulations of the steady and unsteady case of the buildings 1:4:4 and 1:2:4.

4 CASE STUDIES

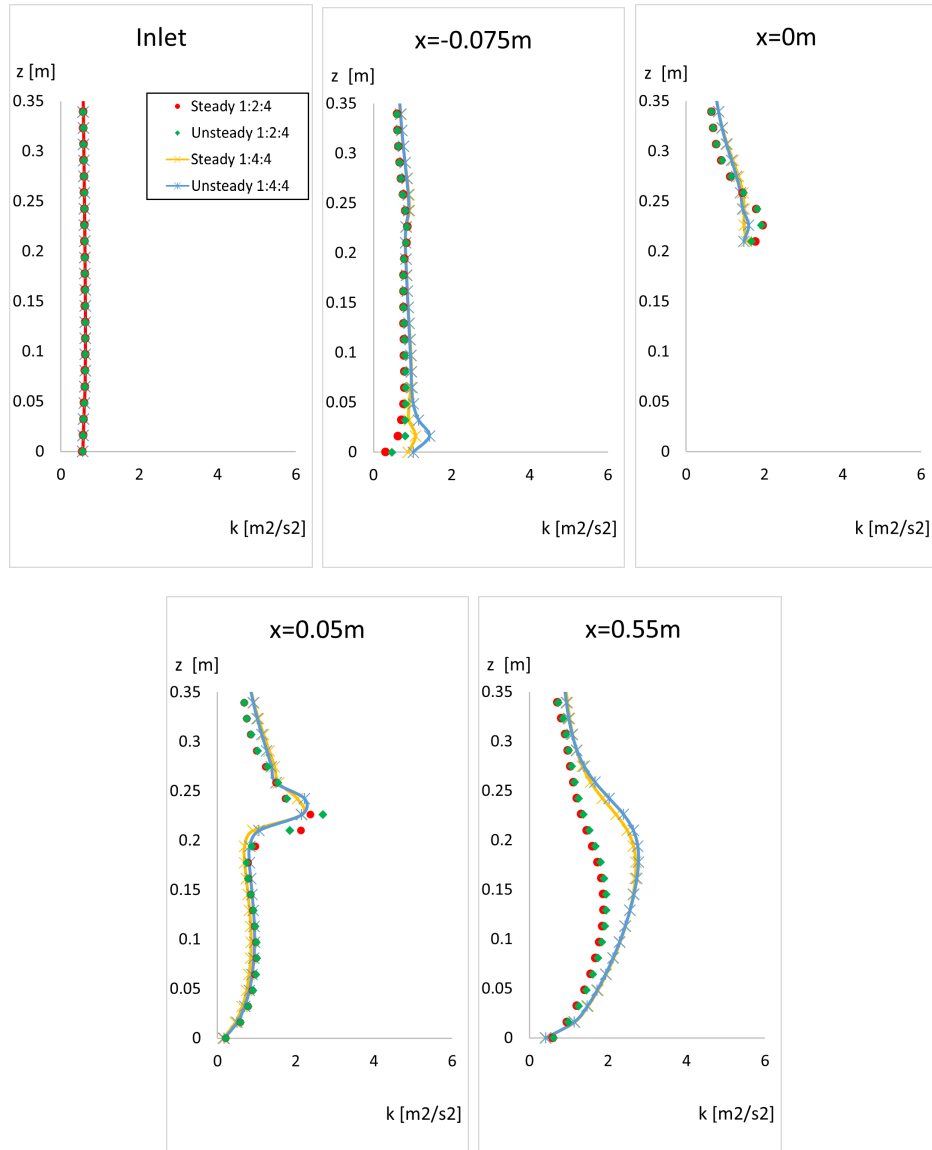


Figure 4.25: Turbulent Kinetic Energy in vertical lines, at different longitudinal positions. CFD simulations of the steady and unsteady case of the buildings 1:4:4 and 1:2:4.

4.3.3 Conclusions

The comprehensive approach can be applied to different geometries once it has been validated with experimental data. In the case of a building with half the width the BIA is reduced as expected.

The width of the building has a great influence in the perturbation of the flow, as was seen in the contour plots. The streamlines figures showed that the recirculation region downstream the building is around $2/3$ of the wider building case in length and width. However, the influence of the building downstream is still considerable far away from it in both cases studied.

The last can also be checked with the graphs of lines at different positions. The curves of velocity and TKE are quite similar near the building, although the recirculation zone at ground level is smaller for the building with less width. However the biggest differences are present at the last location ($x=0.55m$), where the velocity of the flow for the 1:2:4 case is higher than for the wider case. However, comparing the profile with the unperturbed flow there are remarkable differences, especially for low heights at the wake.

4.4 Application to a high-rise building

The comprehensive approach can also be implemented for a high-rise building, for which an aerodynamic study is essential. The configuration of this case is similar as the previous, regarding e.g. the type of mesh cell.

4.4.1 Geometry and Mesh

The geometry analysed was used in another master thesis [1], and it can be seen in Figure 4.26. This structure is a version of the Cayan Tower in Dubai. The geometry conserves the 306m height and the cross section of around 30x30m, but it was “straighten”, a special feature is the V-shape on the front face.

The total dimensions of the domain are 4210x2200x1250m, being this around 14Hx7Hx4H. The mesh was more refined in the region of interest around the building, obtaining a total of 16.9 million cells. The value of y^+ was beyond 300 for the ground and the building, but the minimum value at the building is 11. Therefore, considering the balance precision-computational cost this mesh was accepted.

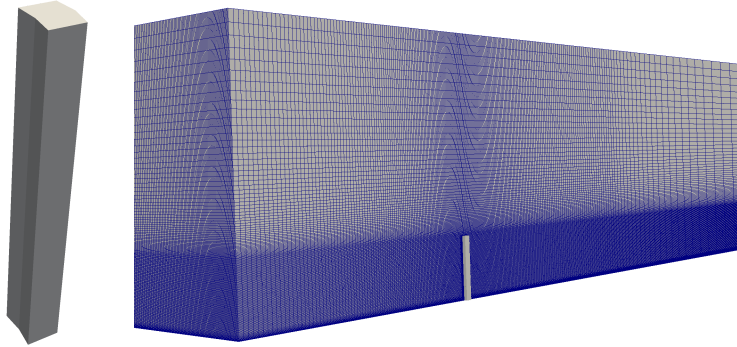


Figure 4.26: Geometry and view of the half mesh (section at $y=0$) of the high-rise building.

4.4.2 Configuration

Comparing with the previous simulations, this case represents real conditions, e.g. the walls of the domain are not defined as walls (wind tunnel) but as patch boundary with slip condition.

The ABL conditions are shown in Table 4.2. Moreover, the TKE profile presents a decreasing shape with height, so instead of the 4 parameters it only uses 2 ($C_2=C_3=0$ in Equation 28).

SimpleFoam is used to compute the steady simulation since the flow can still be consider incompressible. The stability of this case can be enhanced by starting with first order schemes and low relaxation factors.

ABL configuration	
Parameter	Value
Reference velocity	30 m/s
Reference height	10 m
Ground roughness height	0.03 m
ABL height	1810 m
Roughness length	0.003 m
Von Karman constant	0.41

Table 4.2: Setting configuration of the ABL model for the high-rise building, as in [1].

4.4.3 Results

A study of the advantages of the twist of the tower was already conducted by Van Muylders [1], however, it is interesting as an user to configure this case and analyse the characteristics of the flow in a skyscraper. First, the Building Influence Area can be seen in Figure 4.27 (and in Figure 5.23 at the ANNEX I). It can be pointed out that the BIA extends until the end of the domain.

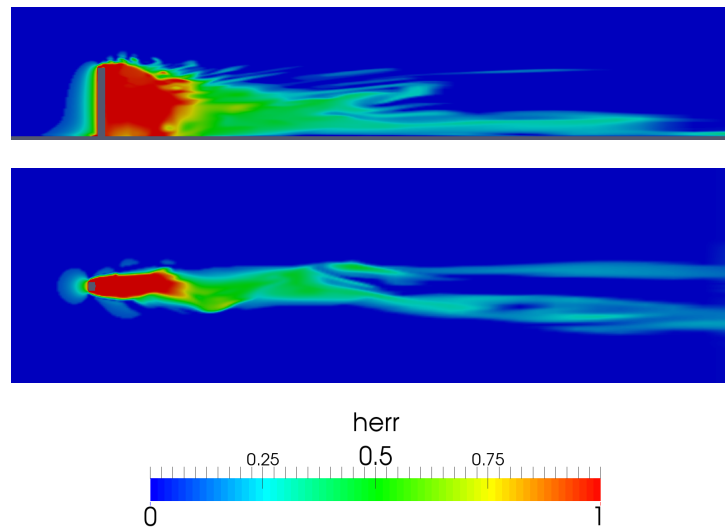


Figure 4.27: Building influence area for the high-rise building, vertical view at $y=0$ (above) and horizontal view at $z=150\text{m}$ (below).

The pressure distribution on the faces of the building is shown in Figure 5.24 and Figure 5.25 at the ANNEX I, this is directly proportional to the loads. The front face is under positive pressure while the other are under negative pressure. It should be remembered that OpenFoam provides information of pressure divided by density.

The stagnation point can be located by reducing the pressure range in the contour plot, it can be seen in Figure 4.28 around 3/4 of the windward face height, as it was commented in Chapter 3.

In Figure 4.29 (and in Figure 5.26 at the ANNEX I), different views of the TKE around the building are shown. It is interesting to point out that indeed there is turbulence at both sides of the building at ground level, these are the corner streams.

Furthermore, the vortex shedding phenomenon seems to be present, although it is not possible to assure with a steady simulation. This is defined as vortices shed across the wake alternately from one side to the other which generates a series of alternating low-pressure zones on the downwind side of the structure resulting in a fluctuating force perpendicular to the wind direction [31]. This phenomenon can induced harmful vibrations on the building, and introduce a turbulent character in the wake which is undesirable for neighbour structures.

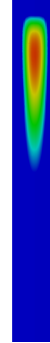


Figure 4.28: Stagnation point of the high-rise building.

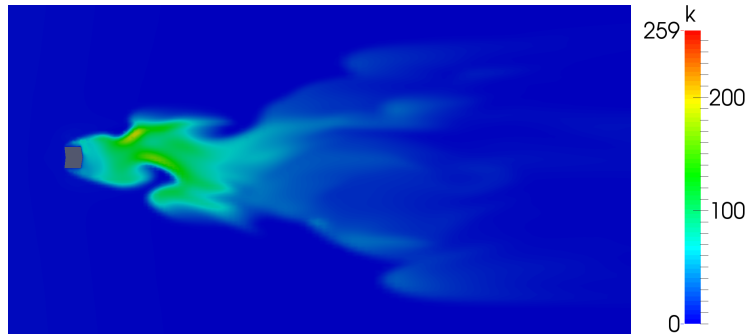


Figure 4.29: Turbulent kinetic energy around the high-rise building. Horizontal view at $z=150\text{m}$ (half building height).

In Figure 4.30 (and in Figure 5.27 at the ANNEX I) different views of the velocity around the building are shown. The influence of the building extends over 2900m (end of the computational domain), although the region with higher turbulence of the wake is limited at a length around 350m, with a width of 90m. Moreover, the speed-up of the flow at both sides of the building can be appreciated. The higher velocities, and also the higher values of k , can be found at greater heights due mainly to the logarithmic wind profile.

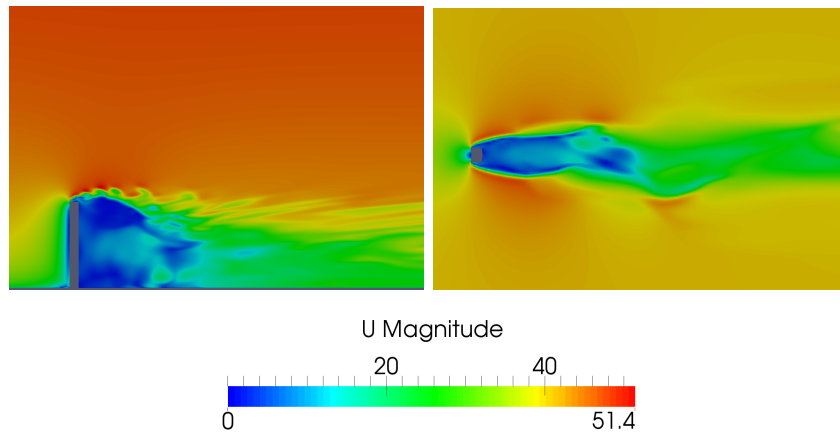


Figure 4.30: Close-up of velocity around the high-rise building. In order: vertical view at $y=0$, horizontal view at $z=150\text{m}$.

A close-up view of the wake can be visualized with streamlines in Figure 4.31 (and in Figure 5.28 at the ANNEX I). The flow is highly turbulent behind the building.

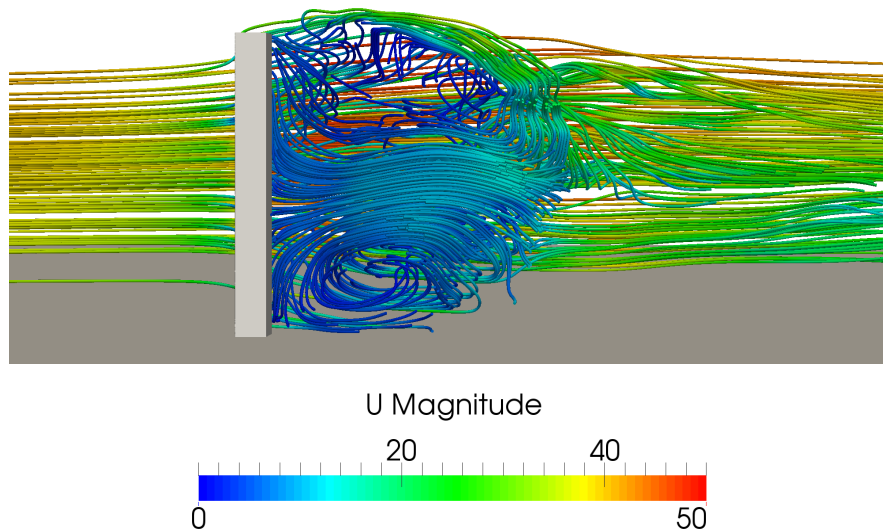


Figure 4.31: Streamlines around the high-rise building, vertical view at $y=0$.

It is also interesting to show streamlines of characteristic parts of the flow, Figure 4.32 shows the detachment once it reaches the corner at the top face (separation bubble and acceleration of the fluid above it), the corner streams at ground level and the base vortex in front of the building, as it was described in Figure 3.1.

Regarding the corner streams, they occur on the lateral facades at all the height of the building as soon as the flow reaches the corners. These recirculation zones (base vortex and corner streams) are extended up to 30m away from the building, and may cause annoyance to pedestrians.

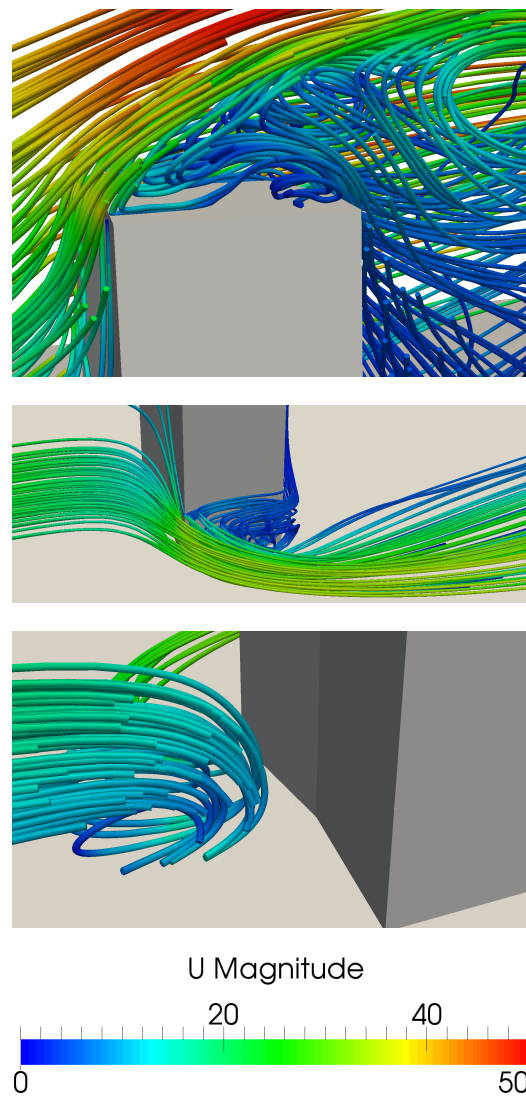


Figure 4.32: Close-up of streamlines around the high-rise building. In order: detachment at the top, corner streams and base vortex.

In addition, it can be seen in Figure 4.33 how the base vortex is concentrated in the centre region of the building. While the flow is accelerated at near the lateral faces due to the corner streams. The pedestrians discomfort can also be analysed with Figure 4.34, the amplification factor is around 1.4 since the velocity is accelerated from around 22 m/s to 31m/s (and beyond).

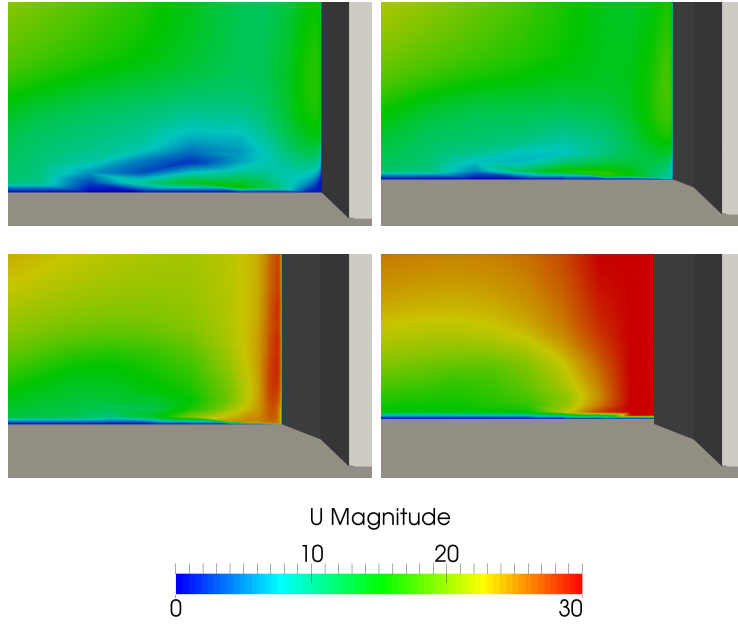


Figure 4.33: Close-up of velocity on the front facade of the high-rise building, for different vertical planes in order: $y=0$ (half of the building), $y=10\text{m}$, $y=20\text{m}$ (lateral face) and $y=30\text{m}$ (corner stream).

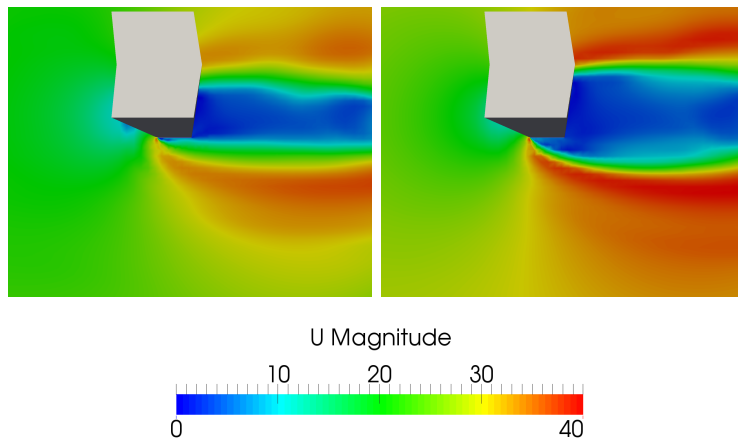


Figure 4.34: Close-up of velocity on the lateral facade of the high-rise building, corner streams view from the top of it, for $z=2\text{m}$ (left) and $z=10\text{m}$ (right).

4.4.4 Conclusions

The comprehensive approach can be implemented in high-rise buildings, it was seen that the aerodynamics of the case treated, of 306m height, is similar to the general case explained in the previous Chapter 3. The stagnation point was indeed found around 3/4 of the front face height, which is the only facade under positive pressure.

Furthermore, the vortex shedding was encountered, these alternating turbulent region on the wake can be harmful to the producing building and its surroundings. However, this is an unsteady phenomenon which can't be completely analysed with the present simulation. The skyscraper disturbs the flow over 2900m long, and the main turbulent wake is around 350m long and 90m width all the height of the building.

On top of the building, the flow is detached once it reaches the corner of the front face creating a separation bubble, and it doesn't re-attach again. On the base of the building, the base vortex was found, and his eye was located around more than 30m far from the front facade. The corner streams are present in both lateral faces of the structure, and along with the previous recirculation, they may disturb nearby pedestrians due to an amplification factor of the wind velocity of around 1.4. Moreover, these separation bubbles change in size with time and even explode, therefore, unsteady simulations would be required for their complete analysis.

5 Conclusion and perspectives

Computational Fluid Dynamics is a tool that is increasingly being used in aerodynamic studies, it is specially interesting for big geometries simulations with real conditions, which are usually very expensive or directly impossible to do in a wind tunnel. In addition, it provides information of the whole field. However, a highly experienced user is required in order to set up the simulation since the programme will provide data but this may not have a physical meaning if the configuration is wrong. In addition, the equations are solved numerically, which introduces the need of validate the results through experiments. Nevertheless, this tool is still being improved, the comprehensive approach described in this thesis is a good example of this.

First, this method was compared with available experimental data from a simple case of an isolated building in a wind tunnel. This model was proven really accurate for both velocity and turbulent kinetic energy in different locations. With some discrepancies due to the recirculation bubbles and in the wake. Moreover, the steady and the unsteady solutions were compared, and it was seen that for the treated case both results were really similar while the steady case had also the advantage of a much reduced simulation time.

Later, different turbulence models were implemented in the same case to further analyse the behaviour of the comprehensive approach. These cases were conducted with steady simulations since as it was seen this case is intrinsically steady. The k-omega model is not used in ABL simulations, and indeed it provided the worst results, the k-epsilon also failed in some locations, especially for the TKE. Nevertheless, this model may be interesting for obtaining velocity results since its requires less computational cost. The comprehensive approach was the most accurate along with the SST k-omega model. However, as it was visualized with contour plots, these two models present several differences. The SST k-omega overestimates the velocity at the sides of the building, and underestimates the TKE.

Once the comprehensive approach has been validated and compared with other models, it can be implemented in other geometries. A building of half the width was analysed, and it was seen that this measure influences in great proportion the wake, being this 2/3 in length and width for the smaller building.

The wider structure's wake also presents lower velocity values and higher TKE, since this building perturbs more the flow. Moreover, it was interesting to analyse that in the horizontal plane, the profiles were the same but displaced the width of the building.

Lastly, a high-rise building was studied since the aerodynamics in this structures are essential in their design. The stagnation point was found at $3/4$ of the windward face height. Moreover, the vortex shedding phenomenon might be present, this may be harmful since it can induce vibrations. The separation bubble at the top was also visualized, as the base vortex and the corner streams, these last both with their eye at 30m far away from the building, which may cause annoyance to pedestrians since the velocity is amplified in a factor of 1.4.

For future studies, the simulation of the comprehensive approach with more accurate models as DES or LES would be interesting to further study the discrepancies with the experimental data encountered in different recirculation zones. Furthermore, the implementation of the comprehensive approach in unsteady simulations for high-rise buildings is advisable, especially due to the transient behaviour of phenomena as the vortex shedding in the wake, the change of the separation bubbles, and also for the determination of the dynamic forces related to fatigue.

References

- [1] Philippine Van Muylders. Use of CFD to assess the effectiveness of the twisted shape of the Cayan Tower as an aerodynamically favorable shape. Master Thesis (2020).
- [2] Alessandro Parente, Riccardo Longo, Marco Ferrarotti. Turbulence model formulation and dispersion modelling for the CFD simulation of flows around obstacles and on complex terrains. Research work (2019).
- [3] Riccardo Longo. Advanced turbulence models for the simulation of air pollutants dispersion in urban area. Phd Thesis (2020).
- [4] Architectural Institute of Japan. Guidebook for CFD Predictions of Urban Wind Environment. Retrieved from: https://www.aij.or.jp/jpn/publish/cfdguide/index_e.htm.
- [5] Giancarlo Alfonsi. Reynolds-Averaged Navier–Stokes Equations for Turbulence Modeling. Retrieved from: https://www.researchgate.net/publication/245371007_Reynolds-Averaged_Navier-Stokes_Equations_for_Turbulence_Modeling.
- [6] François G. Schmitt. About Boussinesq’s turbulent viscosity hypothesis: historical remarks and a direct evaluation of its validity. Retrieved from: <https://www.sciencedirect.com/science/article/pii/S1631072107001386>.
- [7] Universitat Politècnica de València. Syllabuls for the course Computational Fluid Mechanics.
- [8] Zhang, Xiaodong. CFD simulation of neutral ABL flows (2009). Retrieved from: <https://core.ac.uk/download/pdf/13721578.pdf>.
- [9] A. Parente, C. Gorié, J. van Beeck, C. Benocci. Improved $k-\epsilon$ model and wall function formulation for the RANS simulation of ABL flows. Retrieved from: <https://doi.org/10.1016/j.jweia.2010.12.017>
- [10] Autodesk. SST K-Omega Turbulence Models. Retrieved from: <https://knowledge.autodesk.com/support/cfd/learn-explore/caas/CloudHelp/cloudhelp/2014/ENU/SimCFD/files/GUID-0F5C4828-9F91-46B6-A16A-2578D72DCFCC-htm.html>

REFERENCES

- [11] A. Parente. CFD inflow conditions, wall functions and turbulence models for flows around obstacles (2013).
- [12] P. Richards and R. Hoxey. Appropriate boundary conditions for computational wind engineering models using the k-epsilon turbulence model. *Journal of Wind Engineering and Industrial Aerodynamics*, *Journal of Wind Engineering and Industrial Aerodynamics* (1993).
- [13] A. Parente, C. Górlé, J. van Beeck and C. Benocci. A Comprehensive Modelling Approach for the Neutral Atmospheric Boundary Layer: Consistent Inflow Conditions, Wall Function and Turbulence Model. 2011.
- [14] R. Longo, M. Ferrarotti, C. G. Sánchez, M. Deurdi and A. Parente. Advanced turbulence models and boundary conditions for flows around different configurations of ground-mounted buildings. *Journal of Wind Engineering and Industrial Aerodynamics*.
- [15] 2. Beranek, W.J. and Van Koten, H. (1979). *Beperken van windhinder om gebouwen, deel 1*, Stichting Bouwresearch no. 65, Kluwer Technische Boeken BV, Deventer (in Dutch).
- [16] Blocken, B. *Sports building aerodynamics: Building aerodynamics*.
- [17] Peter Moonen, Thij sDefraeye, Viktor Dorer, Bert Blockend, Jan Carmelieta. *Urban Physics: Effect of the micro-climate on comfort, health and energy demand*. Retrieved from: <https://www.sciencedirect.com/science/article/pii/S2095263512000301>
- [18] Z. Luo and J. Hang. *Wind pressure on a single building immersed in a low-jet wind profile* (2013). Retrieved from: <http://centaur.reading.ac.uk/36698/>
- [19] Rheologic. *Wind Assessment for Urban Planning and Architecture*. Retrieved from <https://rheologic.net/en/urban-wind-assessment>
- [20] S.J. Kooiman, S.W. Tullis. *Wind Power Production in the Urban Environment*. Retrieved from: https://www.researchgate.net/publication/228889354_Wind_Power_Production_in_the_Urban_Environment

REFERENCES

- [21] P. Nicastro et al. CFD study for the correct placing and calibration of vertical axis wind turbine in urban environment (2019).
- [22] A. Parente, C. Benocci. On the RANS simulation of neutral ABL flows. Retrieved from: https://www.researchgate.net/publication/247778554_On_the_RANS_simulation_of_ABL_flows
- [23] A. Parente, C. Gorlé, J. van Beeck, C. Benocci. Improved k-epsilon model and wall function formulation for the RANS simulation of ABL flows. Retrieved from: https://www.researchgate.net/publication/229329277_Improved_k-e_model_and_wall_function_formulation_for_the_RANS_simulation_of_ABL_flows
- [24] A. Parente, C. Gorlé, J. van Beeck, C. Benocci. A comprehensive modelling approach for the neutral atmospheric boundary layer: Consistent in flow conditions, wall function and turbulence model. Retrieved from: https://www.researchgate.net/publication/226868790_A_Comprehensive_Modelling_Approach_for_the_Neutral_Atmospheric_Boundary_Layer_Consistent_Inflow_Conditions_Wall_Function_and_Turbulence_Model
- [25] B. Merci, C. D. Langhe, K. Lodefier, E. Dick. Axisymmetric impingement heat transfer with a nonlinear k-e model. Retrieved from: <https://arc.aiaa.org/doi/10.2514/1.1378>
- [26] Yi Yang, Ming Gu, Suqin Chen, and Xinyang Jin. New inflow boundary conditions for modelling the neutral equilibrium atmospheric boundary layer in computational wind engineering. *Journal of Wind Engineering and Industrial Aerodynamics*, 2009.
- [27] C. Gorlé, J. van Beeck, P. Rambaud, and G. Van Tendeloo. Cfd modelling of small particle dispersion: The influence of the turbulence kinetic energy in the atmospheric boundary layer. *Atmospheric Environment*, 2009.
- [28] Shako A. Mohammed1, Saman A. Abdullah. Aerodynamic simulation of windflow around urban regions using different turbulence modeling approaches. Retrieved from: https://www.researchgate.net/publication/327204027_Aerodynamic_simulation_of_windflow

REFERENCES

[aroundurban_regionsusing_different_turbulence_modeling_approaches](#)

- [29] Saurabh Burde. Mixing Tee. Retrieved from: <https://skill-lync.com/projects/week-1-mixing-tee-3>
- [30] CFD online. SST k-omega model. Retrieved from: https://www.cfd-online.com/Wiki/SST_k-omega_model
- [31] Fu, F. Design and Analysis of Tall and Complex Structures. Retrieved from: <https://doi.org/10.1016/C2015-0-06071-3>

ANNEX I

Validation of the comprehensive approach

Convergence

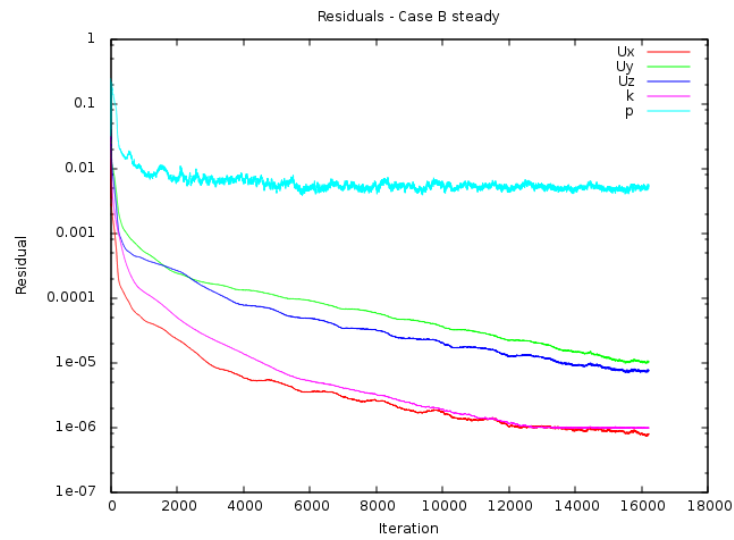


Figure 5.1: Residuals of the steady case of the building 1:4:4 with the comprehensive approach.

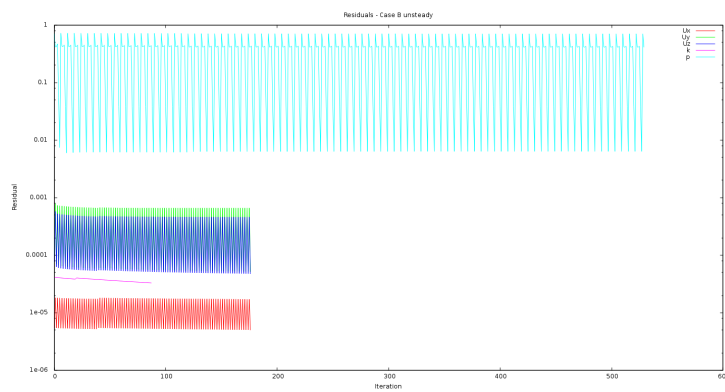


Figure 5.2: Residuals of the unsteady case of the building 1:4:4 with the comprehensive approach.

Post-processing

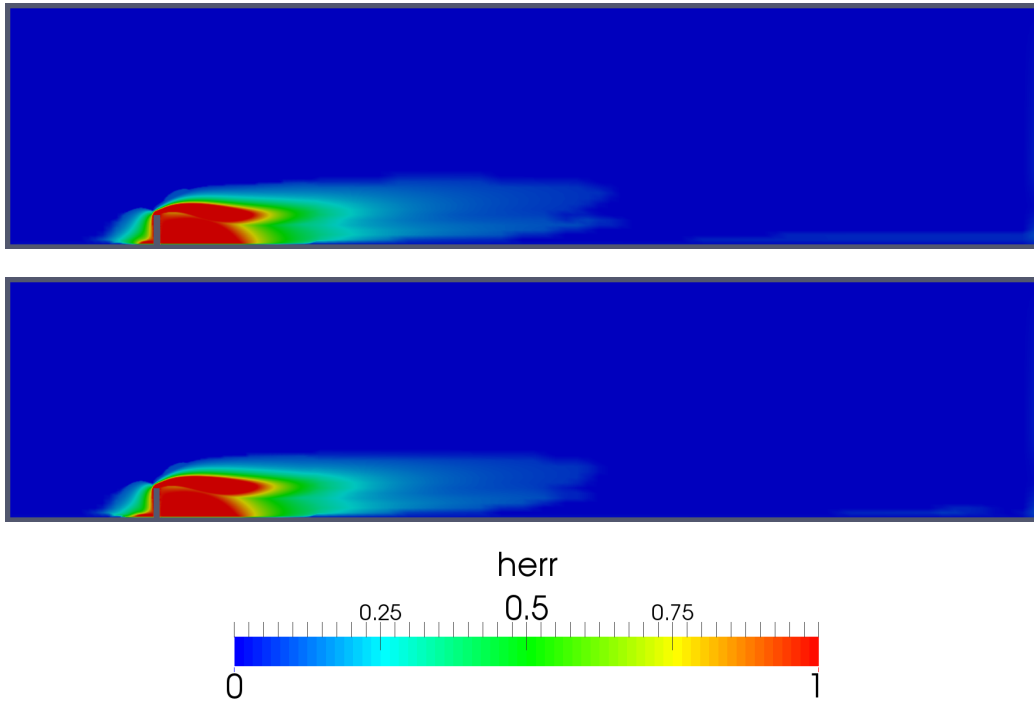


Figure 5.3: BIA of the building 1:4:4 shown with the variable $herr$. Vertical view at $y=0$ (symmetry plane). Steady case up, and unsteady down.

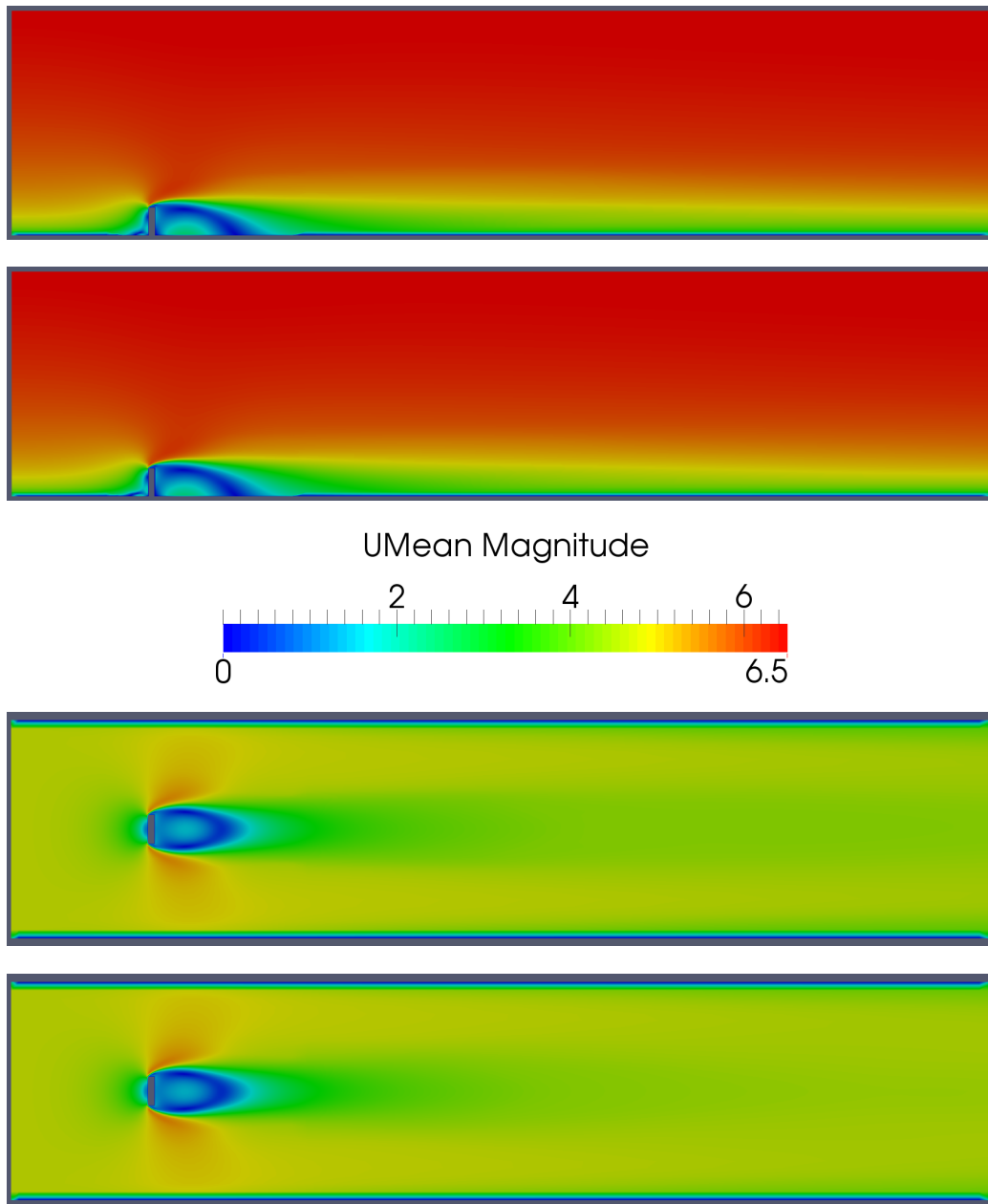


Figure 5.4: Velocity contour for the building 1:4:4. In the upper part, the vertical view at $y=0$, and in the lower part the horizontal view at $z=0.1\text{m}$. In both views the up image is the steady case and the lower one is the unsteady.

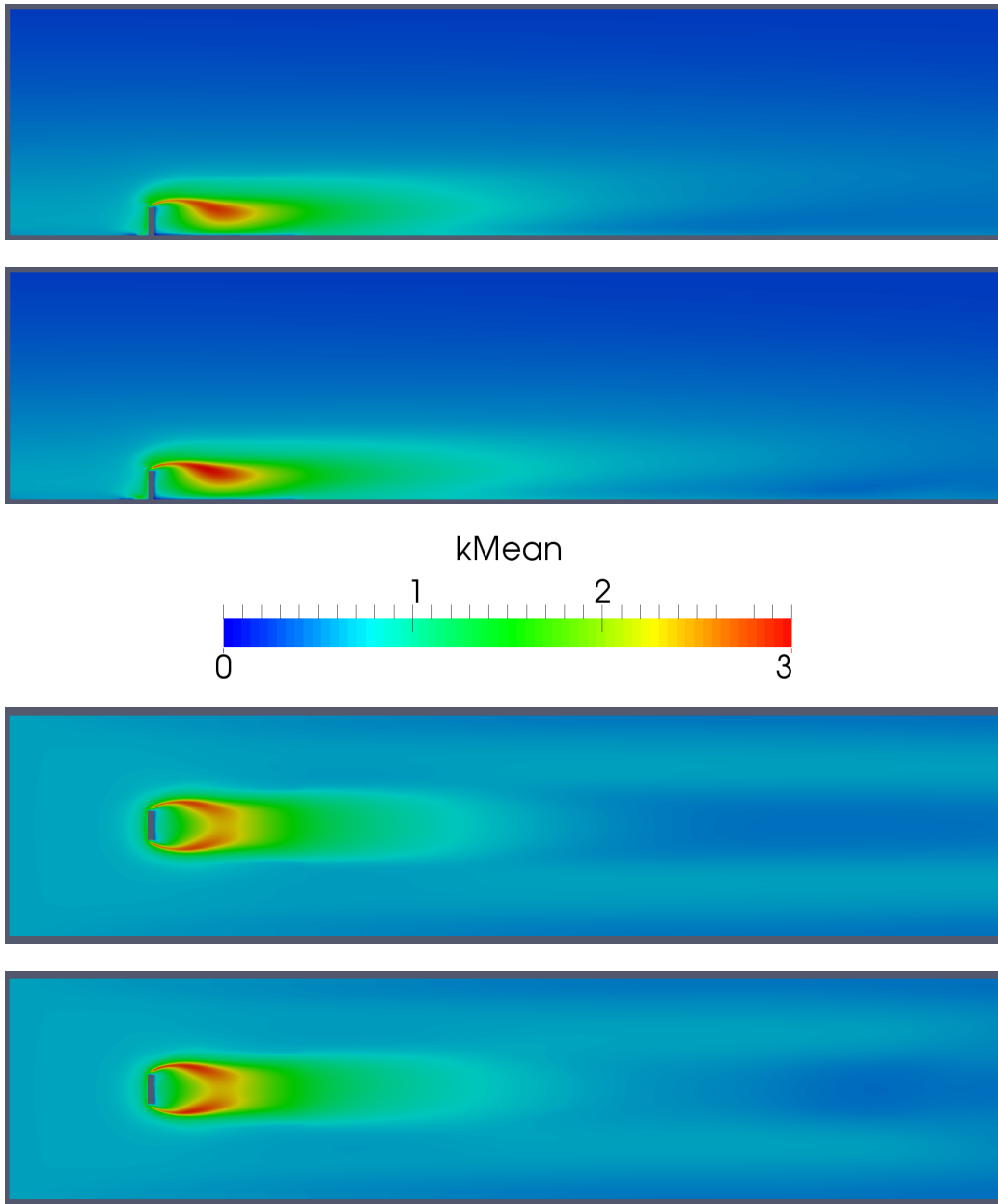


Figure 5.5: Turbulent Kinetic Energy (TKE) contour for the building 1:4:4. In the upper part, the vertical view at $y=0$, and in the lower part the horizontal view at $z=0.1\text{m}$. In both views the up image is the steady case and the lower one is the unsteady.

Inlet-Outlet of the CFD simulations

In Figure 5.6 there is a comparison of the velocity and the TKE vertical profiles for the CFD simulations at the inlet and outlet. The inlets are exactly the same since they are a boundary conditions, and the outlet for the turbulent kinetic energy also matches. However, for the velocity the steady and the unsteady case present differences.

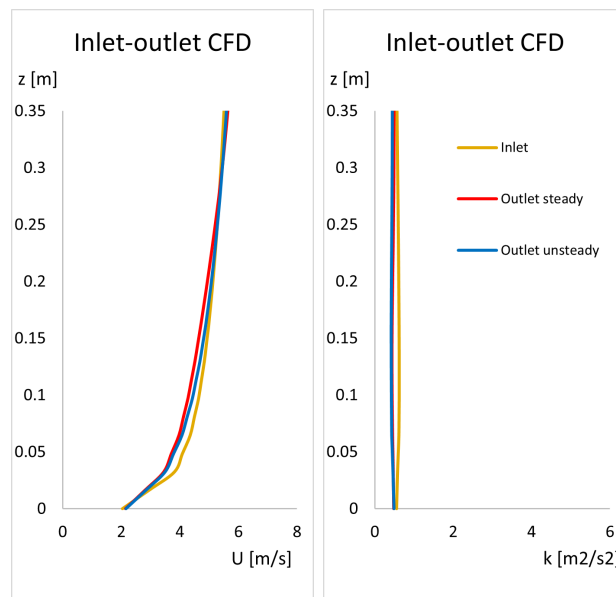


Figure 5.6: Comparison of the inlet and outlet of the steady and unsteady CFD simulations for the building 1:4:4.

Comparison of turbulence models

Convergence

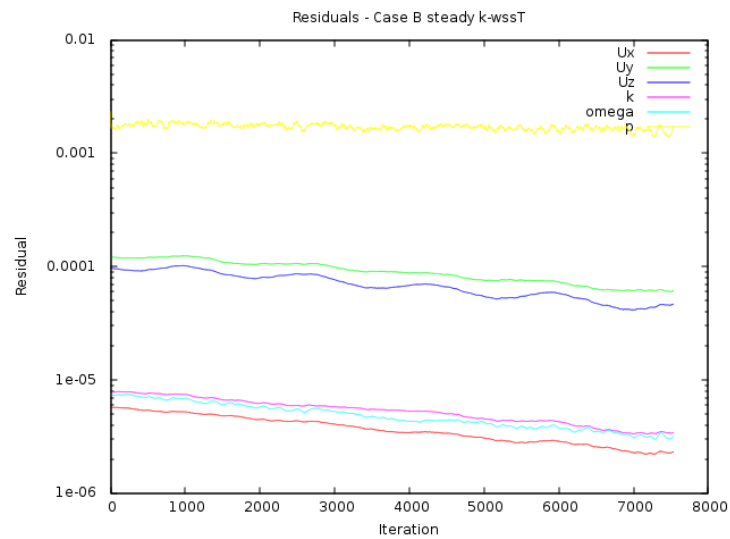


Figure 5.7: Residuals of the steady case of the building 1:4:4 with the SST k-omega model.

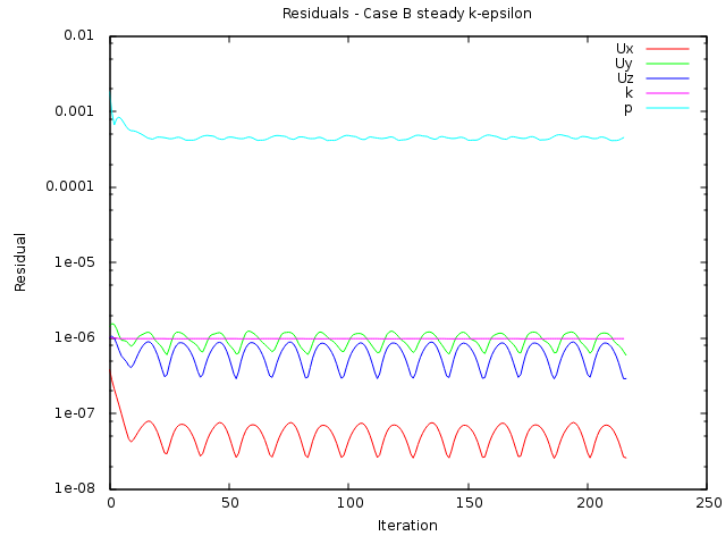


Figure 5.8: Residuals of the steady case of the building 1:4:4 with the k-epsilon model.

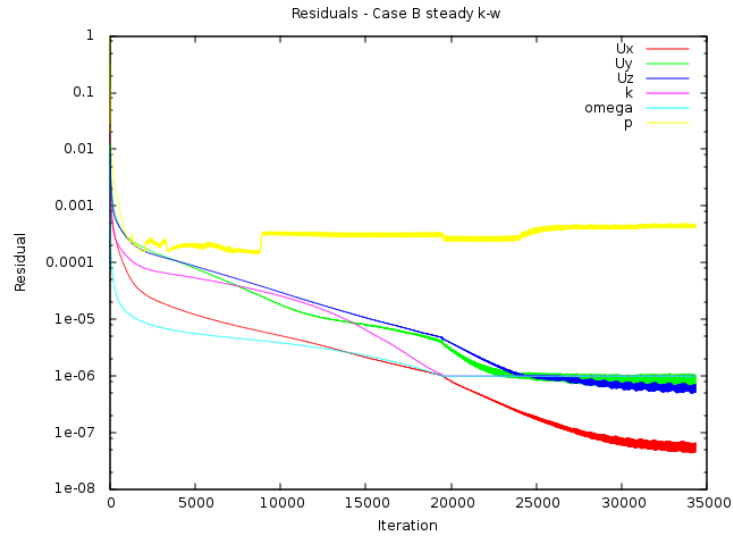


Figure 5.9: Residuals of the steady case of the building 1:4:4 with the k-omega model.

REFERENCES

Post-processing

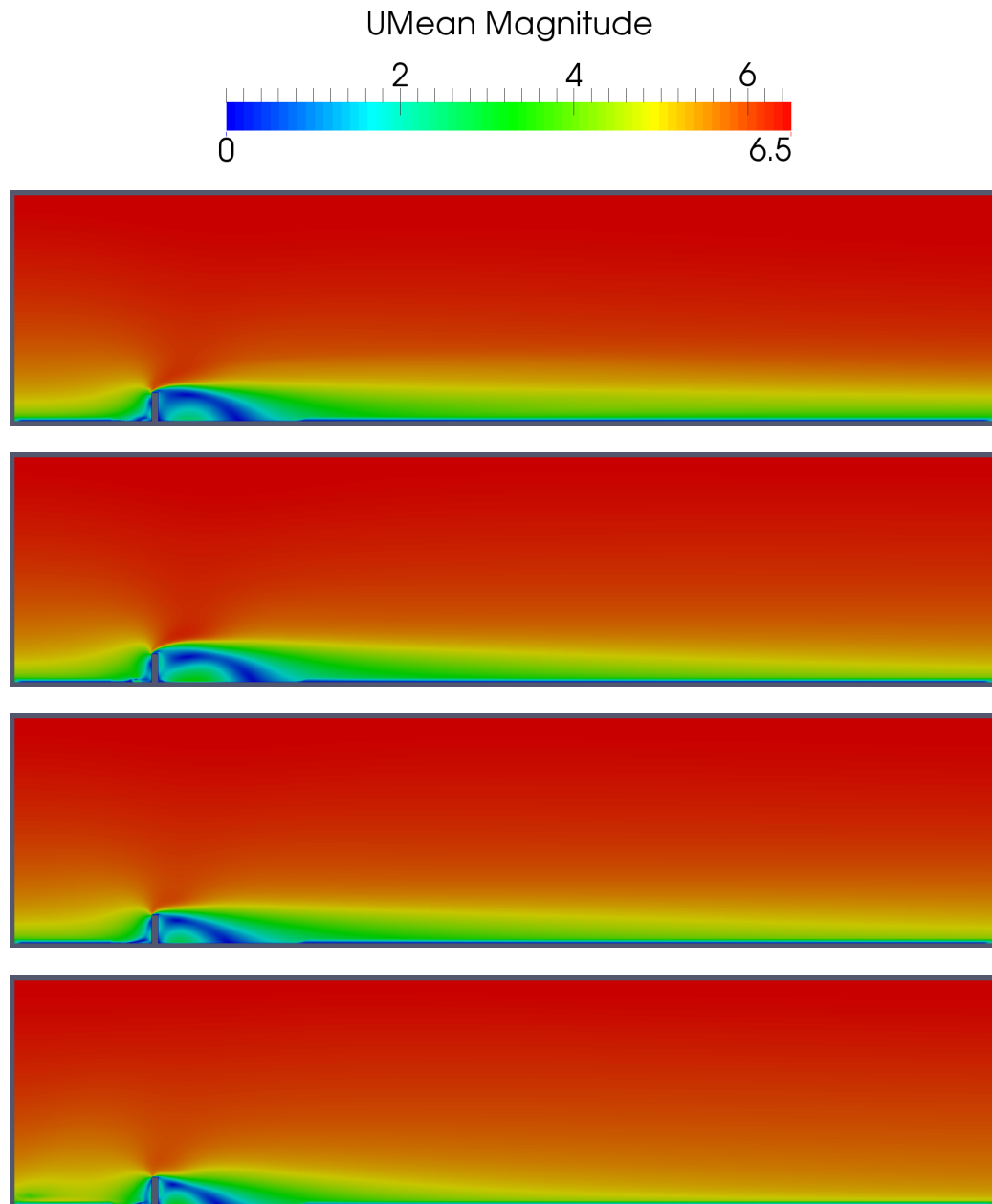


Figure 5.10: Velocity contour of the steady cases, vertical view at $y=0$ for the building 1:4:4. In order: comprehensive approach, SST k-omega model, k-epsilon model, k-omega model.

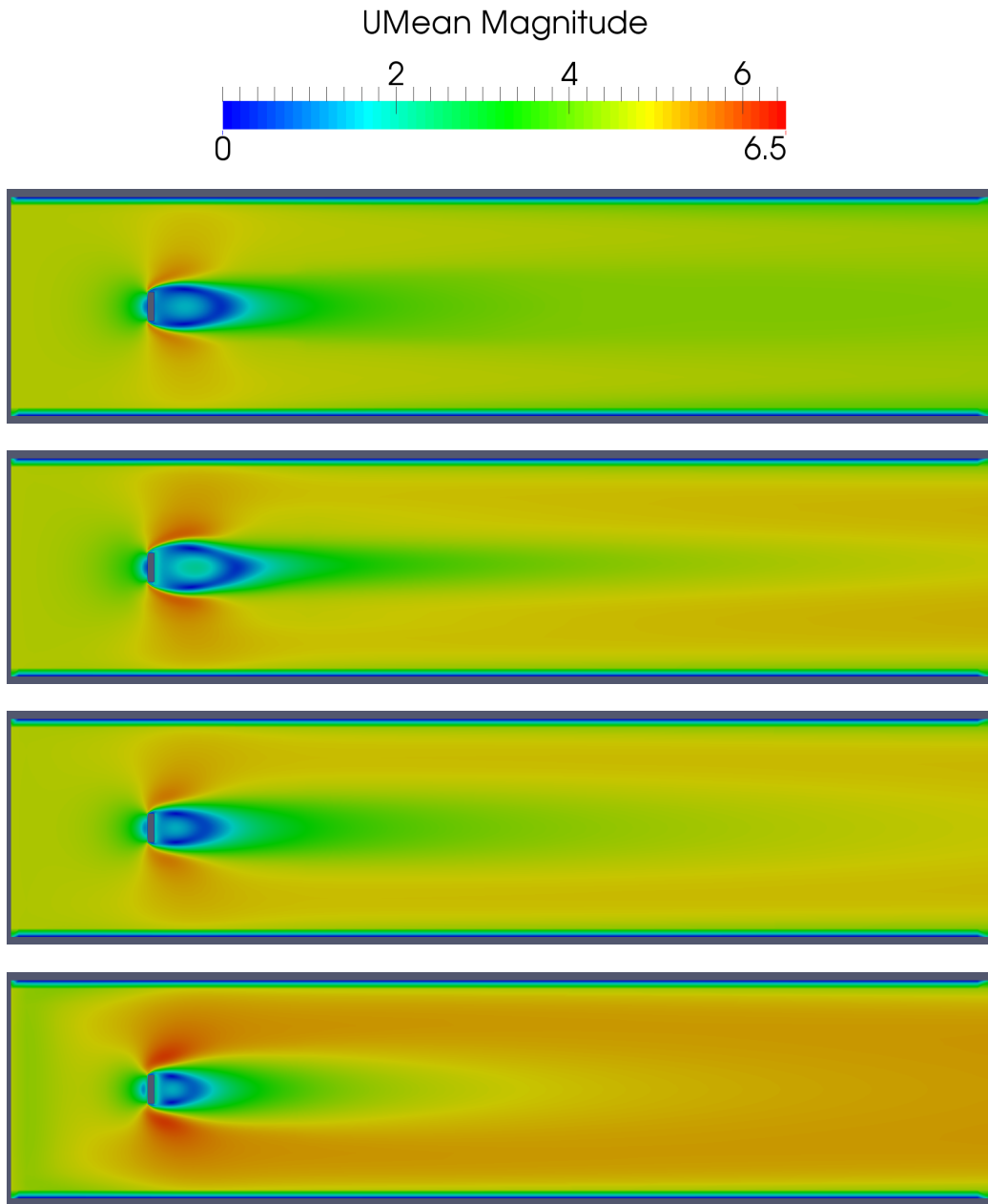


Figure 5.11: Velocity contour of the steady cases, horizontal view at $z=0.1\text{m}$. for the building 1:4:4. In order: comprehensive approach, SST k-omega model, k-epsilon model, k-omega model.

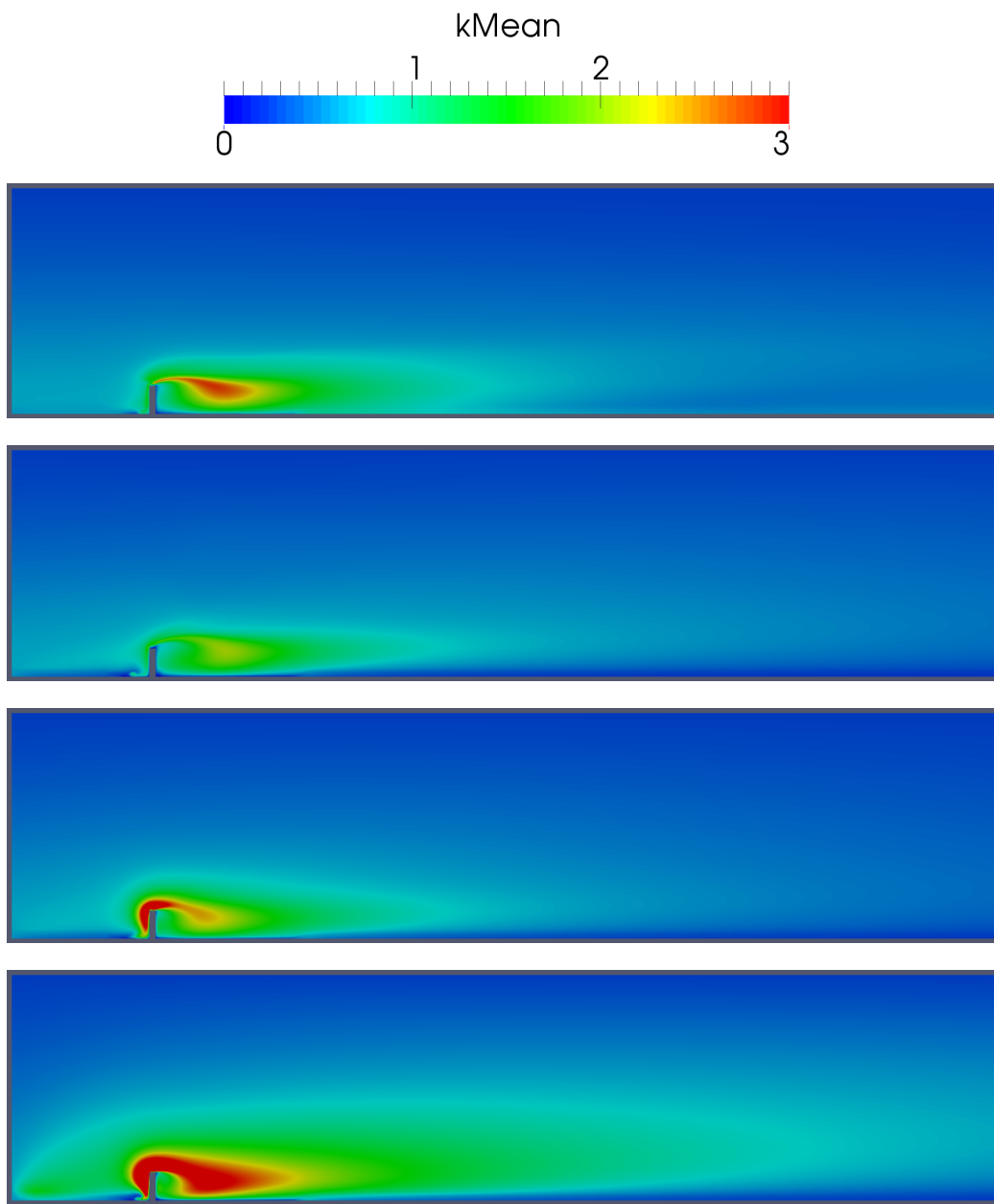


Figure 5.12: Turbulent Kinetic Energy contour of the steady cases, vertical view at $y=0$ for the building 1:4:4. In order: comprehensive approach, SST k-omega model, k-epsilon model, k-omega model.

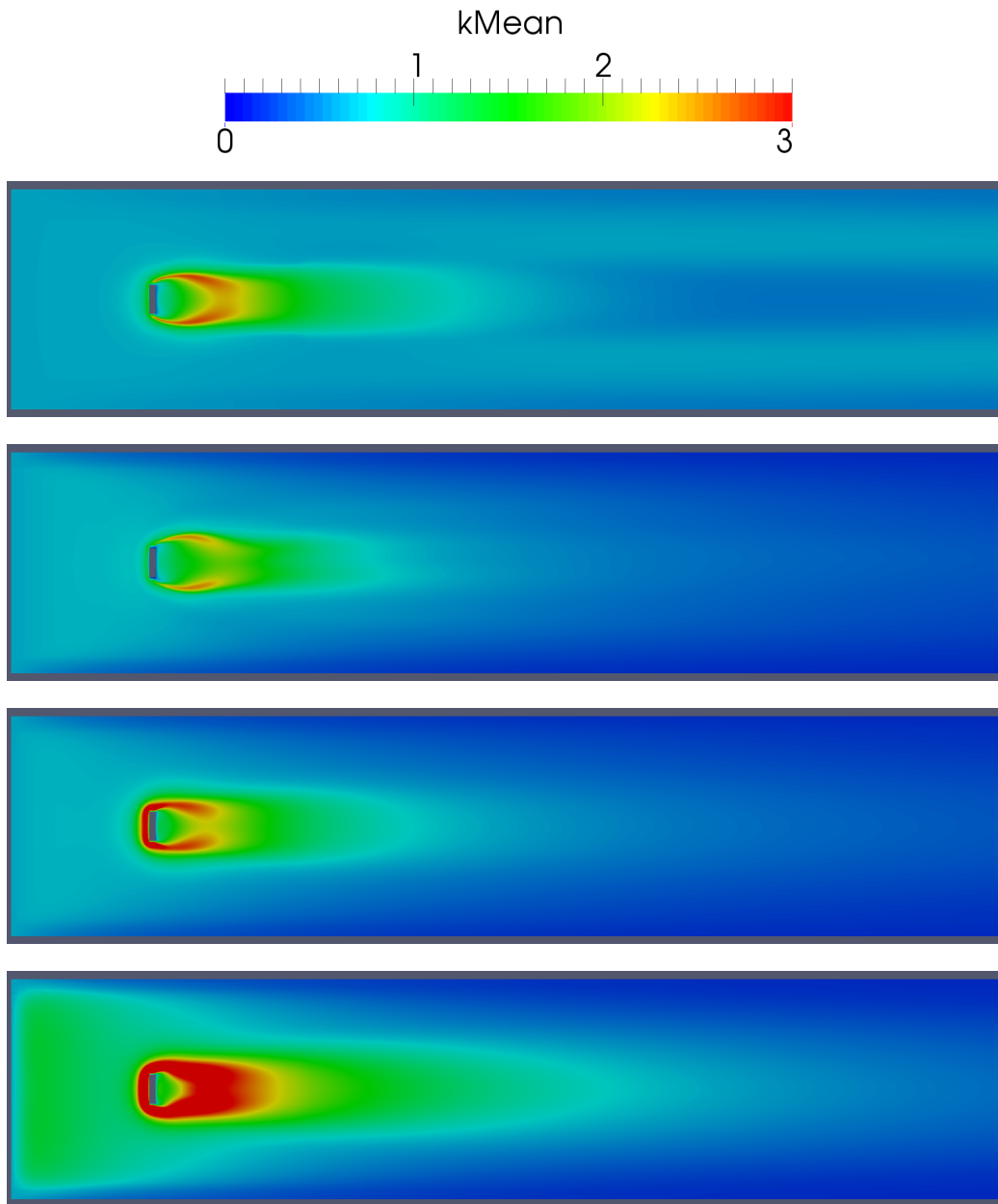


Figure 5.13: Turbulent Kinetic Energy contour of the steady cases, horizontal view at $z=0.1\text{m}$ for the building 1:4:4. In order: comprehensive approach, SST k-omega model, k-epsilon model, k-omega model.

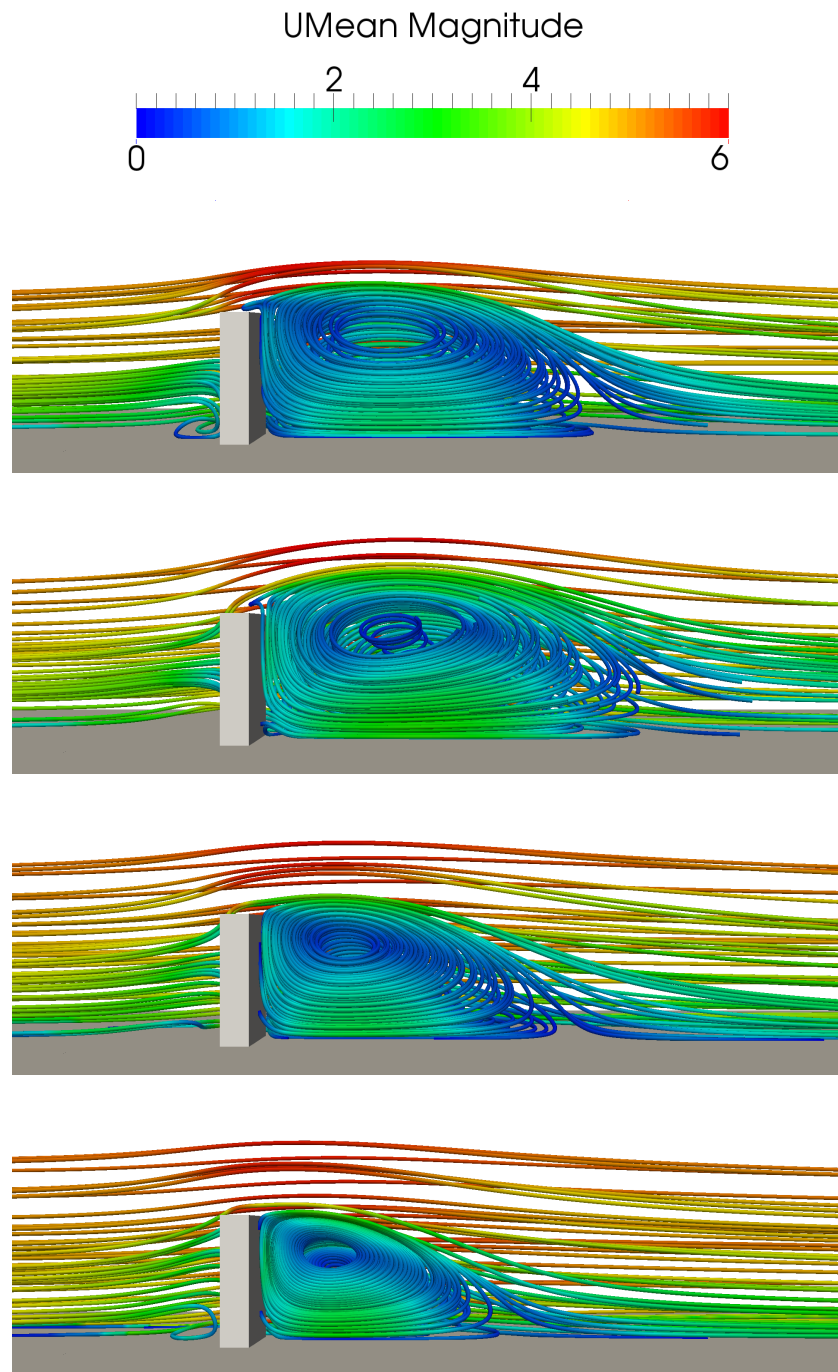


Figure 5.14: Streamlines of the steady cases vertical view for the building 1:4:4. In order: comprehensive approach, SST k-omega model, k-epsilon model, k-omega model.

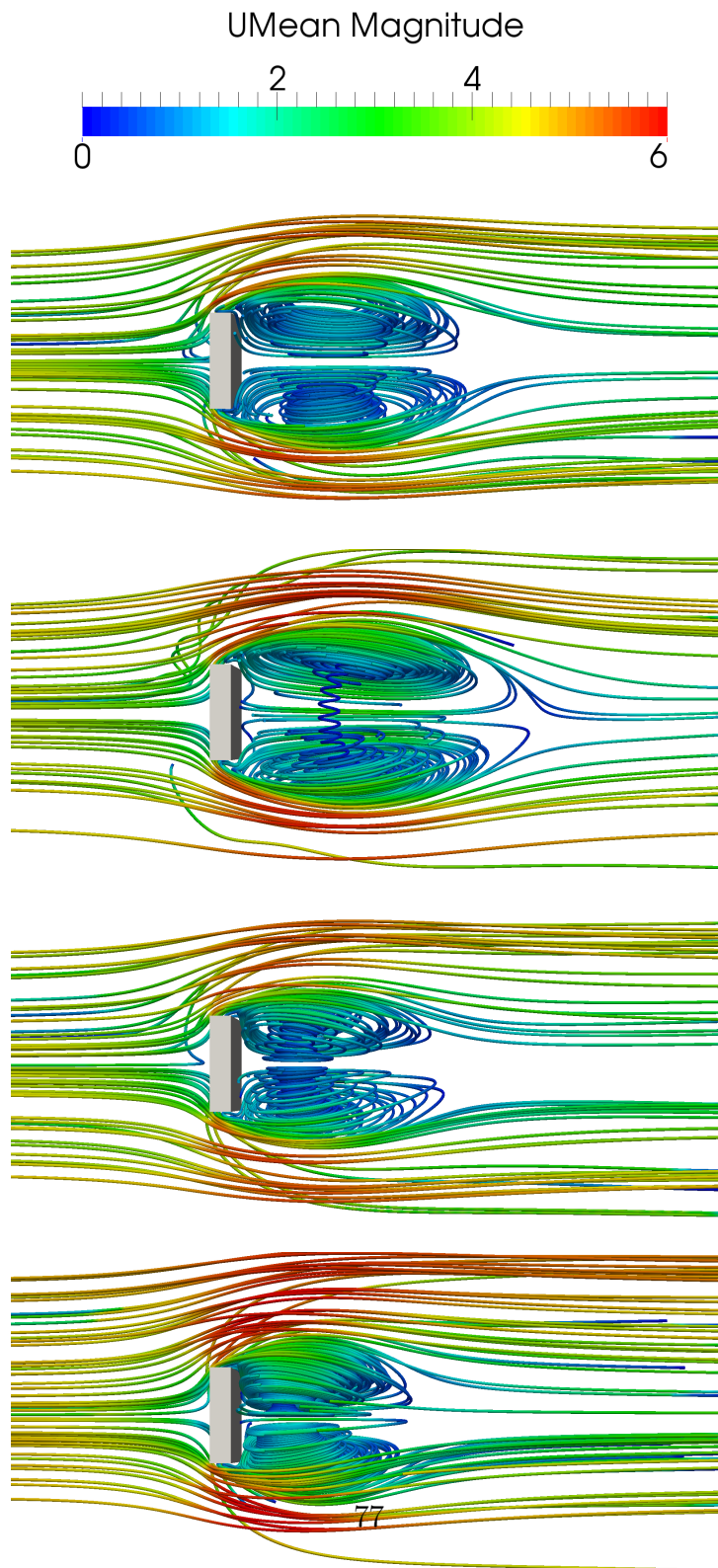


Figure 5.15: Streamlines of the steady cases horizontal view for the building 1:4:4. In order: comprehensive approach, SST k-omega model, k-epsilon model, k-omega model.

Geometry analysis

Post-processing

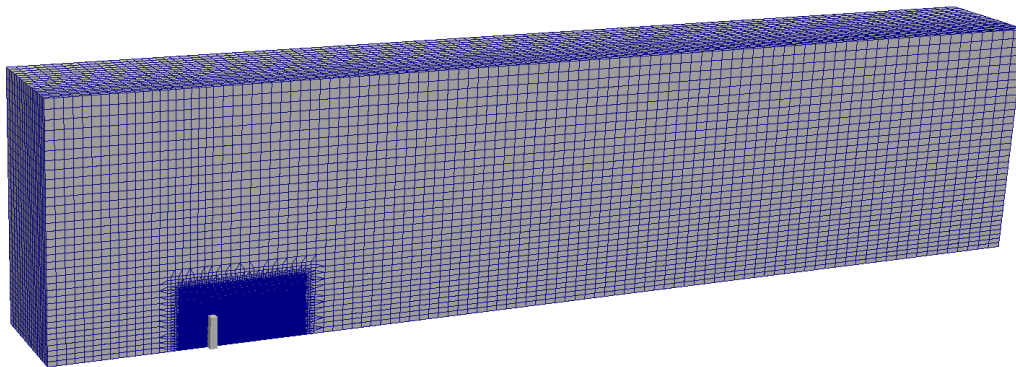


Figure 5.16: View of the mesh for the Building 1:2:4.

The convergence criteria is analogous to the previous case, since the simulation configuration and only the width of the building changes.

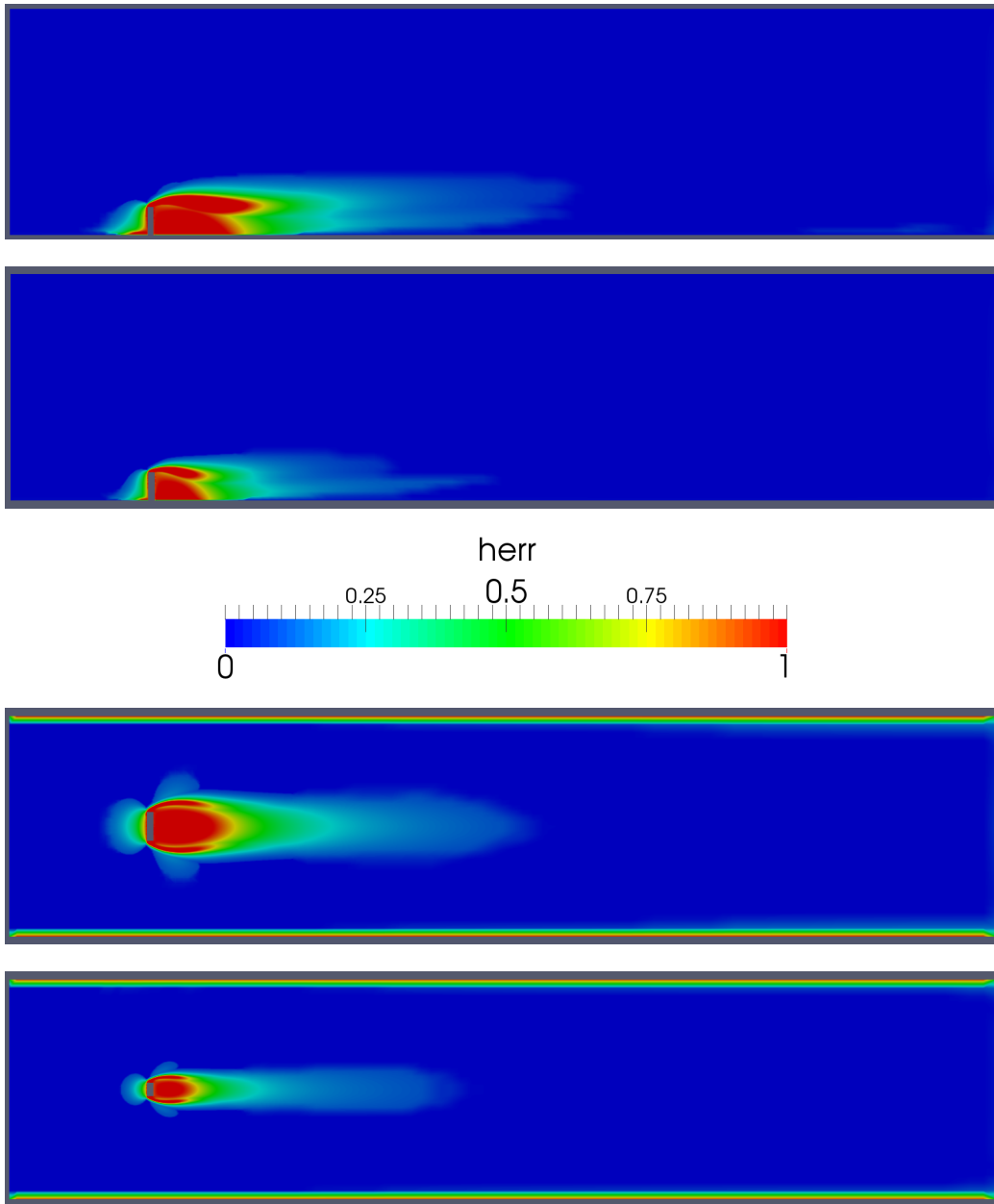


Figure 5.17: BIA of unsteady cases shown with the variable $herr$. Vertical view at $y=0$ (symmetry plane) and horizontal view at $z=0.1\text{m}$. In both views, Building 1:4:4 up and Building 1:2:4 down.

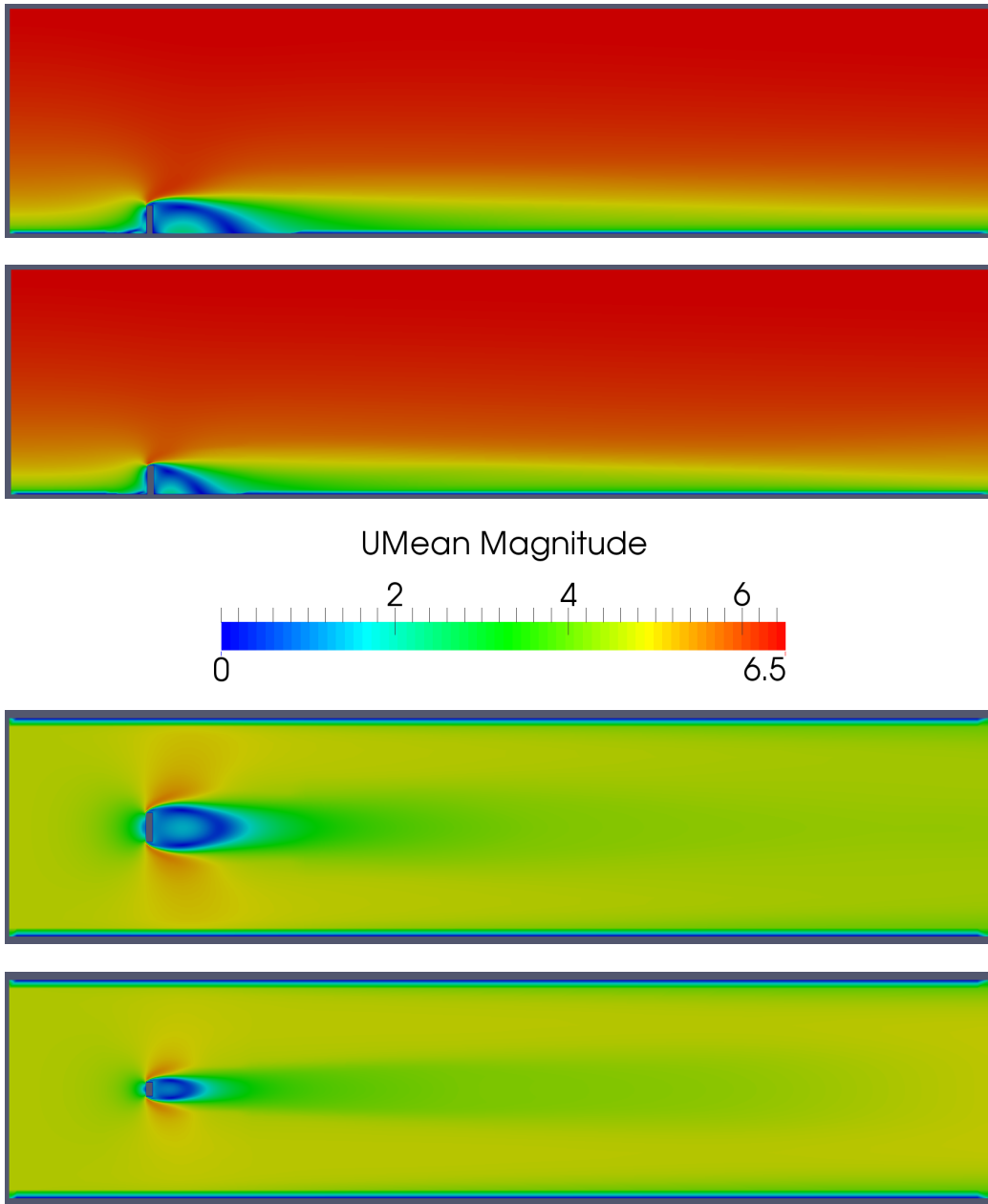


Figure 5.18: Velocity contour of the unsteady cases. In the upper part, the vertical view at $y=0$, and in the lower part the horizontal view at $z=0.1\text{m}$. In both views the up image is the Building 1:4:4 case and the lower one is the Building 1:2:4.

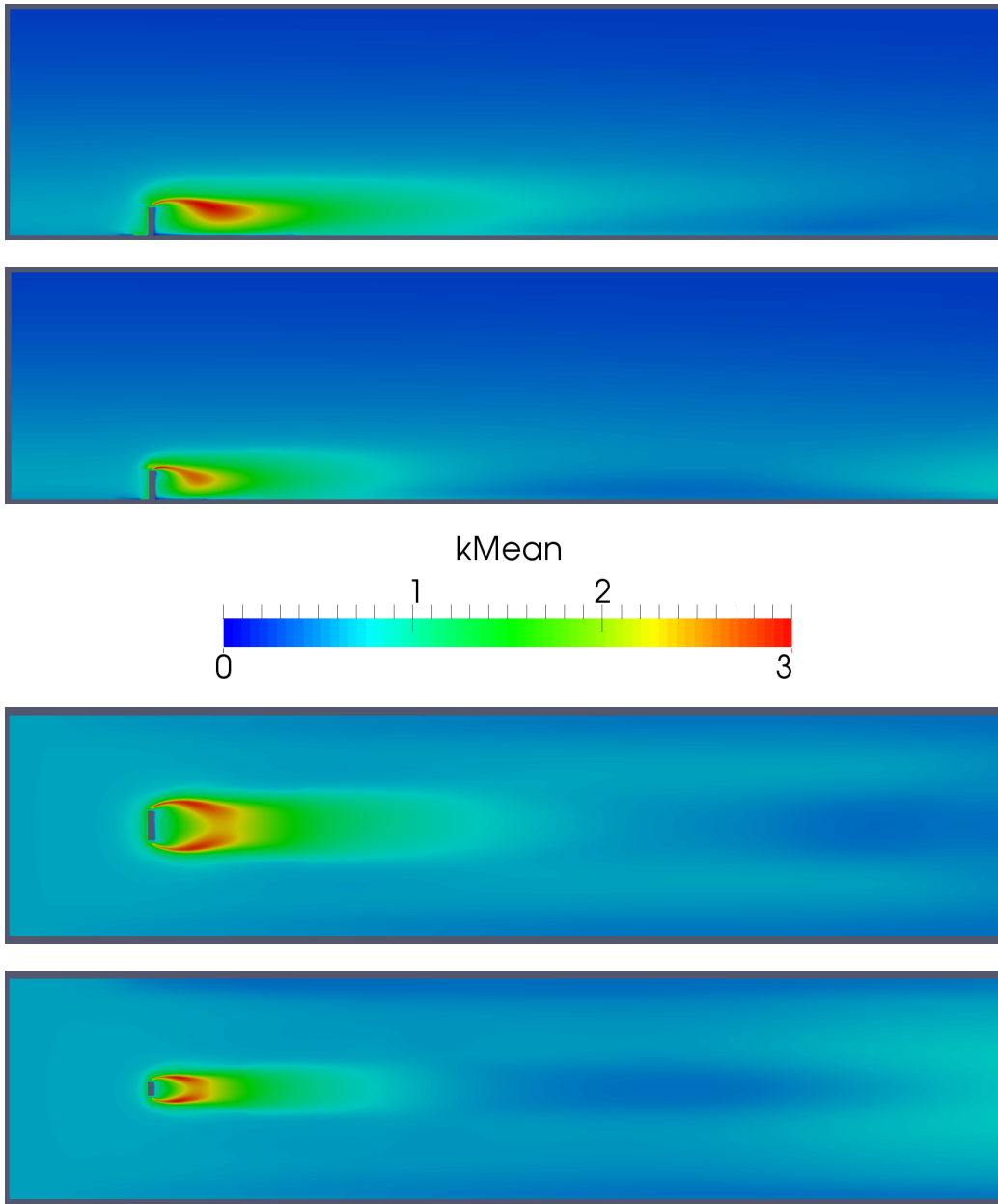


Figure 5.19: Turbulent Kinetic Energy contour of the unsteady cases. In the upper part, the vertical view at $y=0$, and in the lower part the horizontal view at $z=0.1\text{m}$. In both views the up image is the Building 1:4:4 case and the lower one is the Building 1:2:4.

REFERENCES

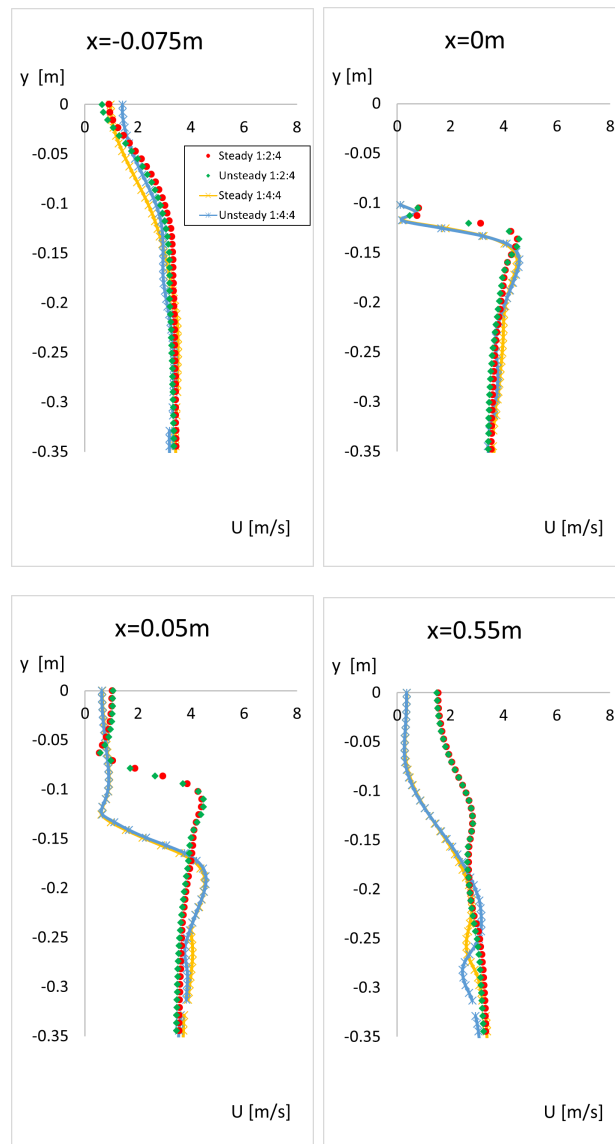


Figure 5.20: Velocity in horizontal lines, at different longitudinal positions. CFD simulations of the steady and unsteady case of the buildings 1:4:4 and 1:2:4.

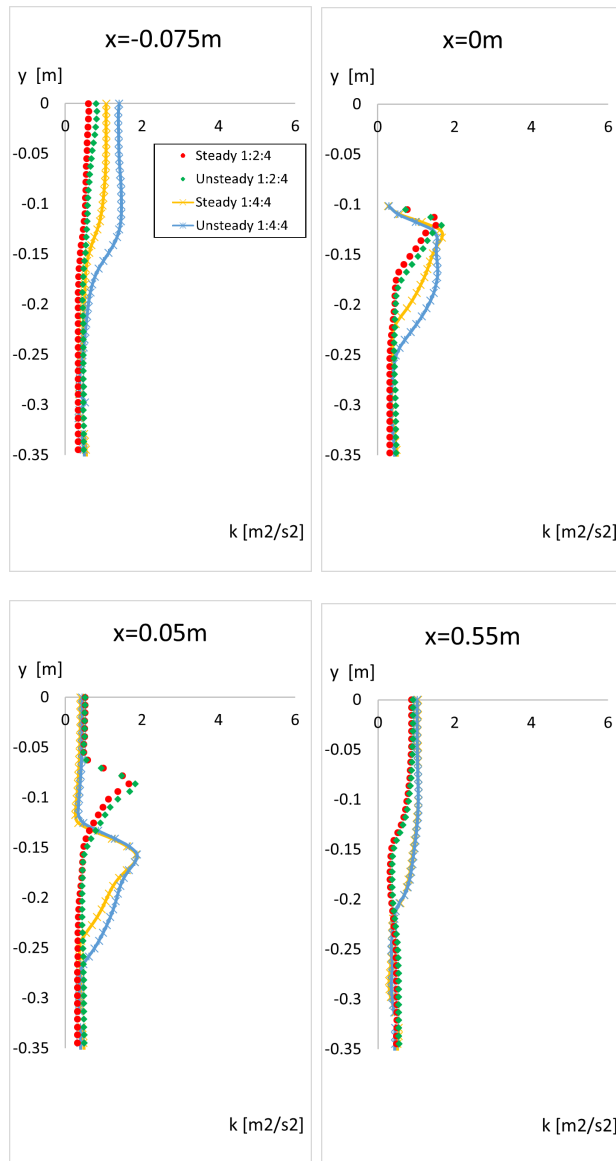


Figure 5.21: Turbulent Kinetic Energy in horizontal lines, at different longitudinal positions. CFD simulations of the steady and unsteady case of the buildings 1:4:4 and 1:2:4.

Application to a high-rise building

Convergence

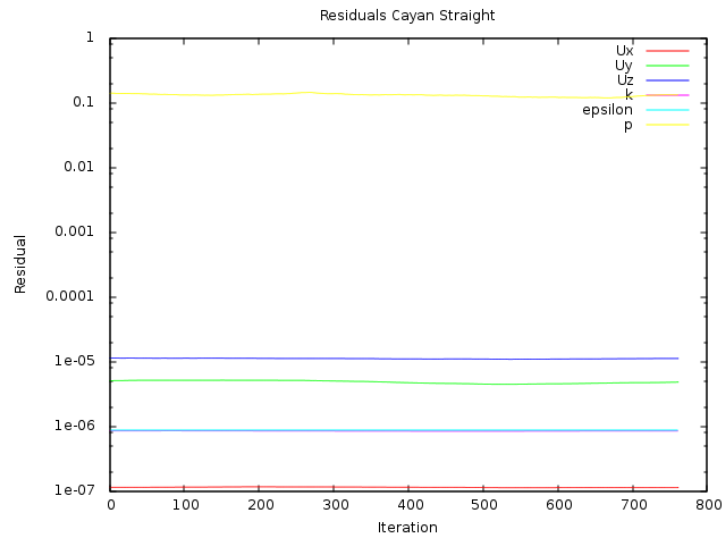


Figure 5.22: Residuals of the steady case of the high-rise building.

Post-processing

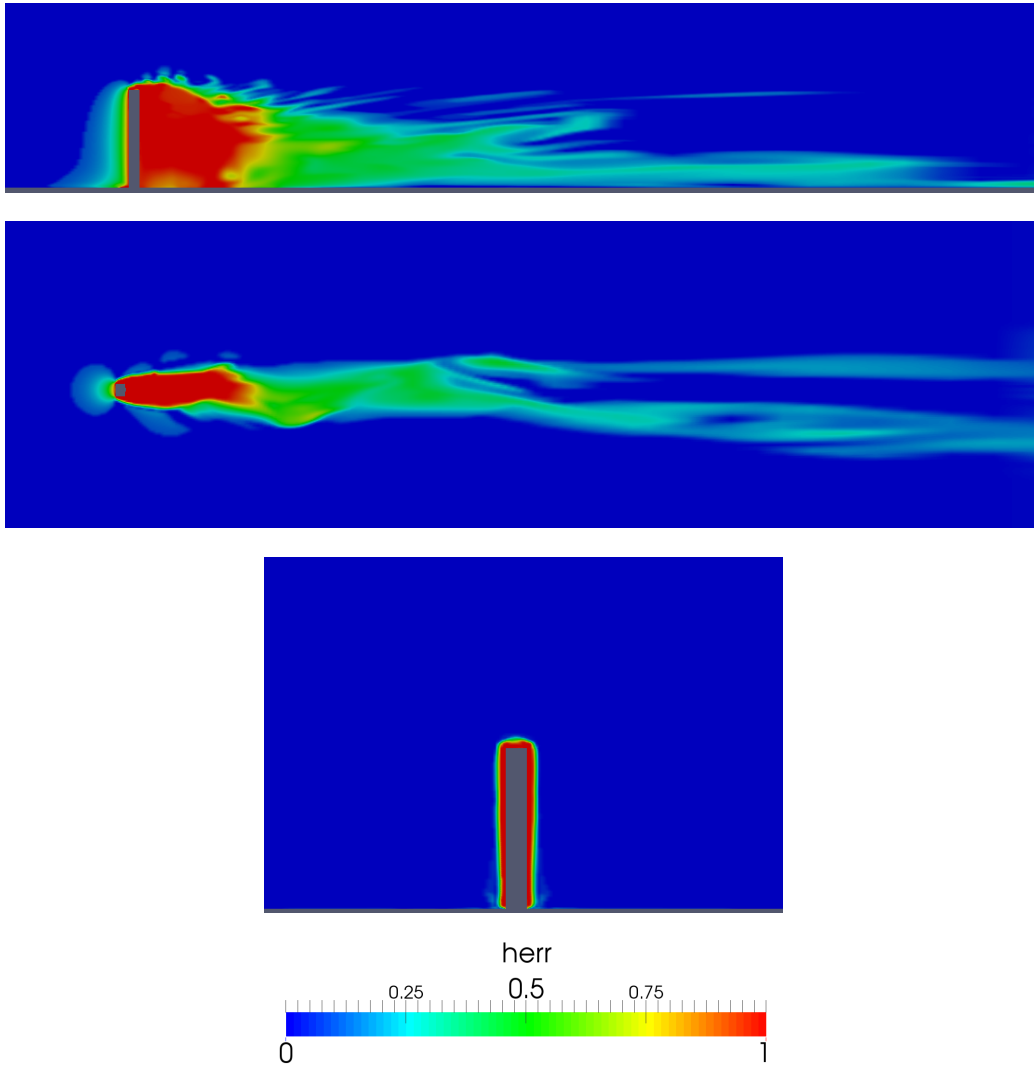


Figure 5.23: Building influence area for the high-rise building. In order, vertical view at $y=0$, horizontal view at $z=150\text{m}$ and front view at $x=0$.

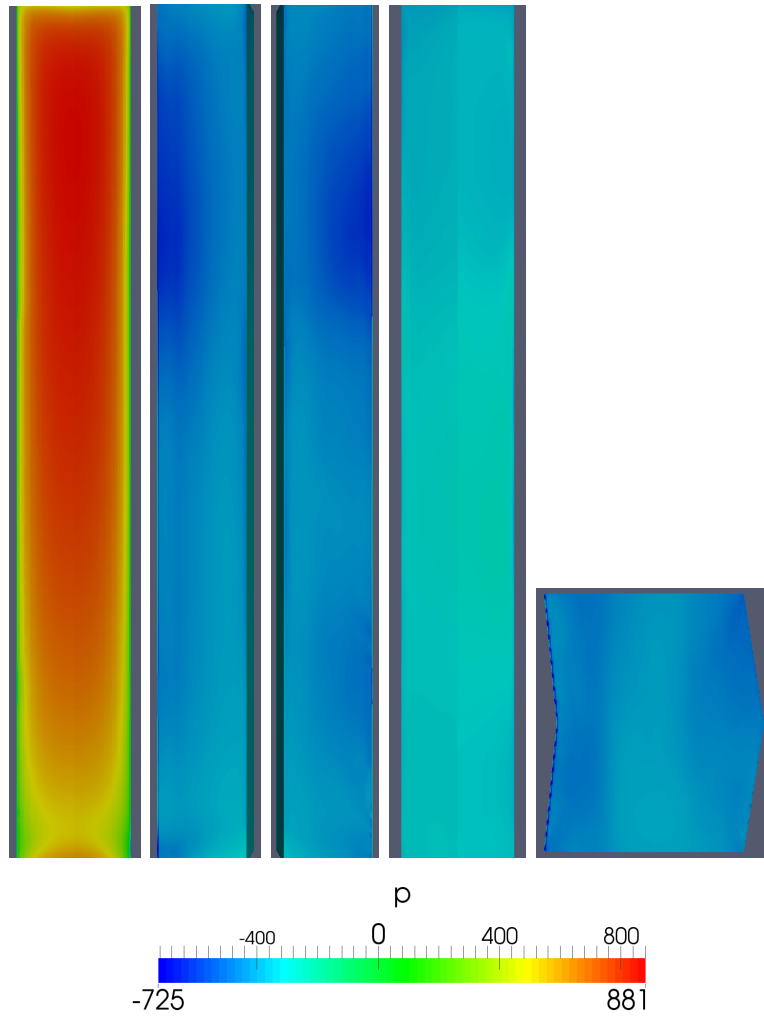


Figure 5.24: .
Pressure distribution on the faces of the building. In order: front, sides,
back and up face.

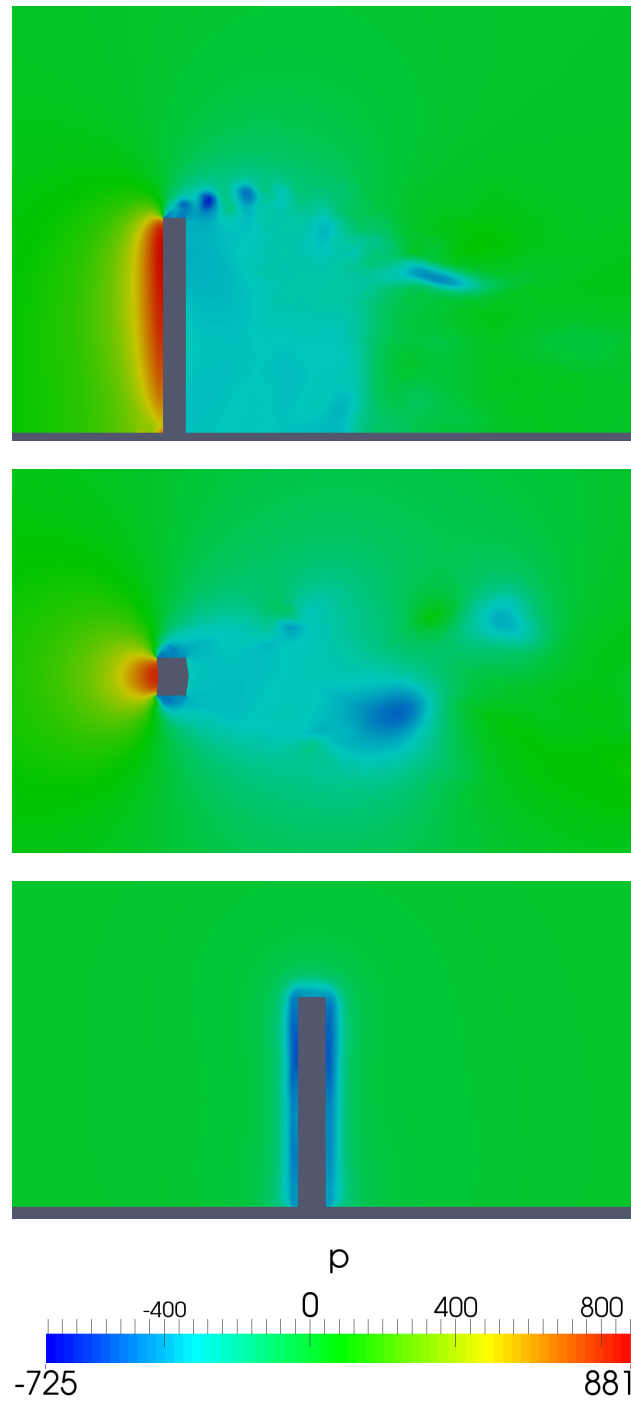


Figure 5.25: Pressure around the high-rise building. In order: vertical view at $y=0$, horizontal view at $z=150\text{m}$, front view at $x=0$.

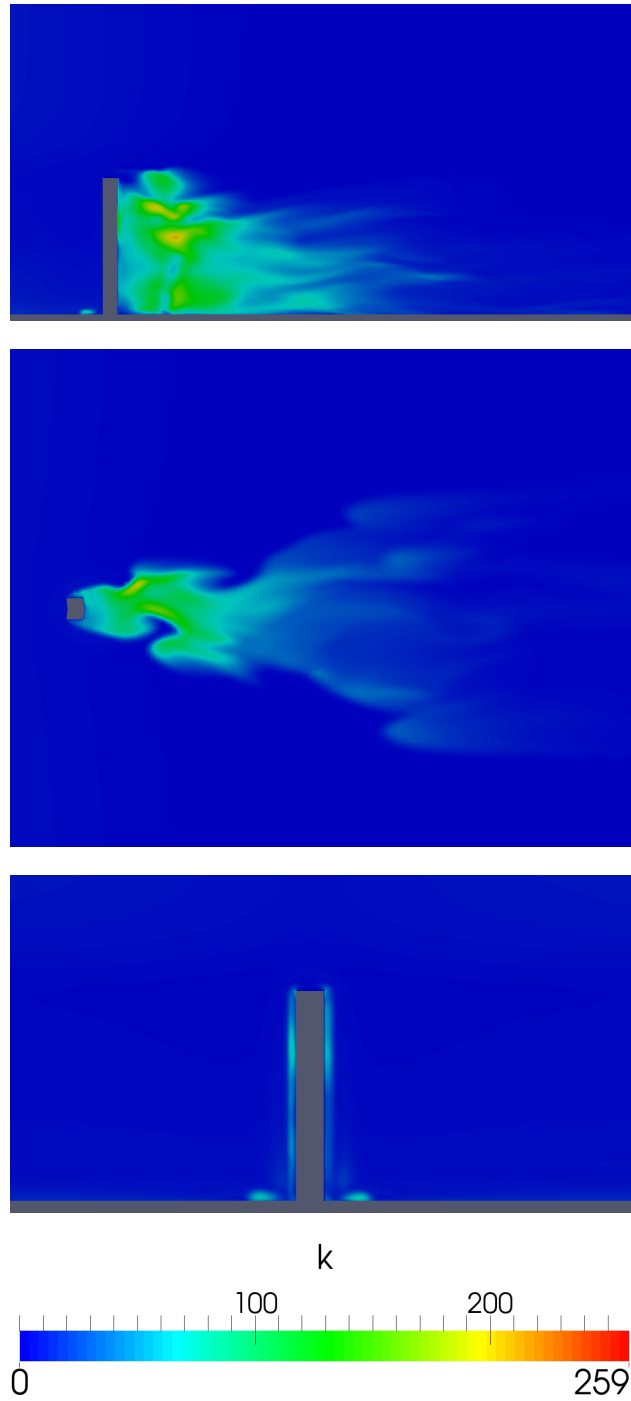


Figure 5.26: Turbulent kinetic energy around the high-rise building. In order: vertical view at $y=0$, horizontal view at $z=150\text{m}$, front view at $x=0$.

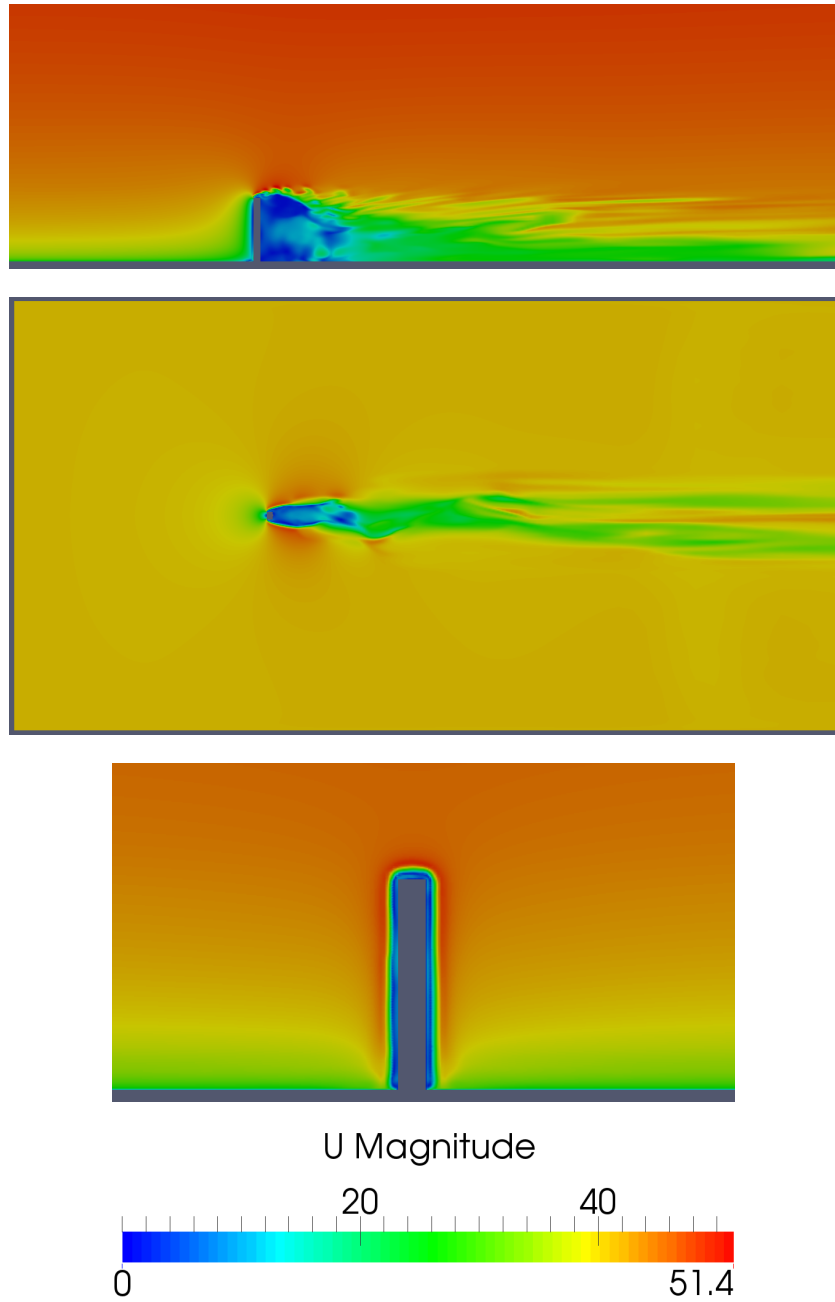


Figure 5.27: Velocity around the high-rise building. In order: vertical view at $y=0$, horizontal view at $z=150\text{m}$, front view at $x=0$.

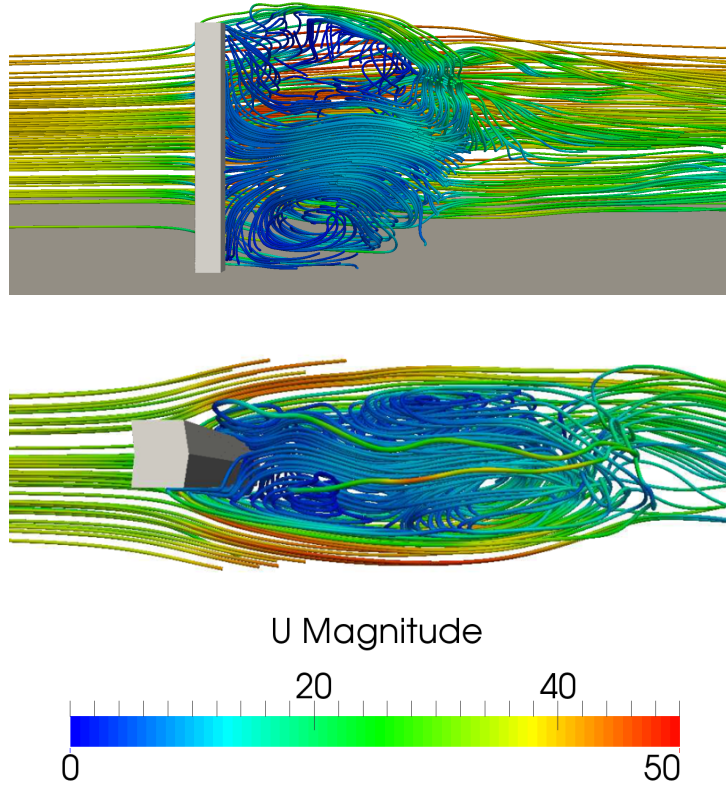


Figure 5.28: Streamlines around the high-rise building. In order: vertical view at $y=0$, horizontal view at $z=150\text{m}$